Development of Astronaut Reorientation Methods: A Computational and Experimental Study

by

Leia Abigail Stirling

B.S., University of Illinois at Urbana-Champaign (2003)
S.M., University of Illinois at Urbana-Champaign (2005)

Submitted to the Department of Aeronautics and Astronautics
in partial fulfillment of the requirements for the degree of

Doctor of Philosophy

at the

MASSACHUSETTS INSTITUTE OF TECHNOLOGY

June 2008

Author .....
Department of Aeronautics and Astronautics
May 23, 2008

Certified by .....
Karen Willcox
Associate Professor of Aeronautics and Astronautics
Thesis Supervisor

Certified by .....
Dava Newman
Professor of Aeronautics and Astronautics

Certified by .....
Emilio Frazzoli
Associate Professor of Aeronautics and Astronautics

Accepted by .....
Prof. David L. Darmofal
Associate Department Head
Chair, Department Committee on Graduate Students

Development of Astronaut Reorientation Methods:
A Computational and Experimental Study

by

Leia Abigail Stirling

Submitted to the Department of Aeronautics and Astronautics
on May 23, 2008, in partial fulfillment of the
requirements for the degree of
Doctor of Philosophy

Abstract

Past spaceflight missions have shown that astronauts adapt their motor-control strategies to the microgravity environment. Even though astronauts undergo hundreds of training hours, the strategies for locomotion and orientation are not specifically prescribed. The majority of an astronaut's motion-control strategies are developed underwater. While underwater training can be beneficial in certain aspects, such as learning which orientations an astronaut will encounter and becoming familiar with task timelines, it is not effective for self-learned motor-control strategies. Further, the development of unfamiliar tasks, such as reorienting without external forces, will most likely not occur naturally. Self-rotations—human-body rotations without external torques—are not only helpful for reducing adaptation time, but can be a crucial safety countermeasure during extravehicular activity.

In this thesis, computational and experimental methods are developed to create and analyze astronaut reorientation methods. The computational development of control methods for human motion planning offers a novel way to provide astronauts with maneuvers that are difficult to obtain experimentally in Earth gravity (1-G). Control of human-body dynamics can be posed as a motion-planning problem for which many different solution methods exist. This research considers two different frameworks—quantized control and optimal control. The quantized control method permits the development of complete maneuvers that are appropriate for humans to perform in high-stress situations by defining a set of specific finite-time trajectories called motion primitives. The implementation of an optimal control method allows for the refinement and further understanding of maneuver characteristics with an emphasis on how the central nervous system controls motion. Human rotation experiments provide further insight into the complexity of self-rotation techniques and a way to study the effects of training in a rigorous and realistic manner.

Thesis Supervisor: Karen Willcox
Title: Associate Professor of Aeronautics and Astronautics

Acknowledgments

Obtaining a Ph.D. at a university such as MIT cannot be accomplished alone. There were many people that helped and guided me along the way and I would like to try my best to thank everyone.

First my advisors. I am not sure which order to thank them in as they were both so helpful in many different ways. So, I will go in order of how I met them. Prof. Dava Newman was the first to help me to apply concepts developed in aeronautics and astronautics to a biomechanical problem. She gave me the freedom to develop my research, but was always there when I had a question or just wanted to discuss the problem. My other advisor, Prof. Karen Willcox, was also outstanding. She took on the role of academic advisor as well as research advisor and helped me map out my research and coursework at MIT. She also provided me with a wonderful balance of support and freedom. Not only have Dava and Karen been helpful with research, but have been helpful in my life outside of MIT. During times of personal hardship, they have given me their full support and have always wished me well. These two women have been wonderful role models for me in their passion for their work and their ability to achieve their goals. In a field where there are few women, I have been very lucky to have two such phenomenal inspirations.

I would also like to thank to the rest of my thesis and defense committee. Prof. Emilio Frazzoli, whom I first met while at the University of Illinois at Urbana-Champaign, offered great insight and first taught me about the field of quantized control. Prof. Larry Young put me in touch with several astronauts, some of whom had attempted to self-rotate while in microgravity. Prof. Mark Drela offered valuable techniques that I couldn't find in any text. For all your valuable help and comments along the way, thank you.

I have been fortunate to be part of two research labs at MIT, the Aerospace Computational Design Lab (ACDL) and the Man-Vehicle Lab (MVL). The people and professors affiliated in both labs have always been so helpful to me. I would especially like to thank Dr. Chuck Oman for providing insight into many space biomedical studies, Dr. Alan Natapoff for teaching me important statistical techniques, and Dr. Bob Haimes for providing insight into scientific visualization methods. The students in both labs have also been wonderful. I thank the ACDL folks for always helping me with computing questions. In MVL, I learned a considerable amount by discussing experimental techniques and biomedical principles with people. I would especially like to thank Dr. Erika Wagner, Dr. Jessica Marquez, and Dr. Philip Ferguson.

To my friends and colleagues that took part in my experimental study, thank you. I know you would have much rather been in parabolic flight than hooked up with harnesses. Just remember you helped me finish my degree and I couldn't have done that without you. I would also like to thank Noah Riskin, the coach of the MIT men's gymnastics team, for allowing me to use their facilities to run these experiments. Thank you to the undergraduates, Micaela Newman and Vicki Stolyar, who worked with me during the experiments in

this thesis and the work we did on translational motion that is not included here. You were both such an excellent help and I was lucky to have you both working with me. Thanks also to Vicki Moorman who gave up her anonymity by letting me use her picture in my thesis.

The assistance I have received from the administrative staff in the department has been invaluable. I don't know what I would have done without Jean Sofronas, Sally Chapman, and Liz Zotos. The three of them made my life so much easier and always had good pointers. I tried my best to make all my forms correct for Ping Lee and she was ready to help when I needed it. In the academic programs office, Barbara Lechner, Marie Stuppard, and Beth Marois have been very helpful in making sure I graduate.

I have always tried to balance my studies with extracurricular activities. To have a balance between working hard and enjoying life has always been important to me. I have enjoyed my lunch breaks with Omar Bashir, Josh Krakos, Laslo Diosady, and JM Modisette. I learned that some days it is better to not sit and eat my lunch while working and that a short break can be better for me mentally in the long run. I also want to thank everyone in the MIT Micropoker group. An evening of fun and games every week made my life far more enjoyable. Thanks to Andrew Takahashi for setting up the group many years ago, Dan Buckland for letting slip to me he enjoyed an occasional game and inviting me to join, and to all you guys for becoming such special people in my life. Thanks also to Kristen Bethke who started the Student Teacher Outreach Mentorship Program (STOMP) at MIT. I have always enjoyed working with students in the community and with your hard work was able to help at the Haggerty School with a wonderful group of students, parents, and teachers.

I would also like to thank my family for their unending support, love, and guidance. To my parents, I don't say thank you enough, you have both always believed in me even when I worried myself. To my siblings—Shoshana, Naomi, and Ari—thanks for putting up with me. Thanks also to my Grandma Doris, who first brought me into her research lab when I was very young and introduced me to the idea that I could get my doctorate. To the many members of my family that have always believed in me and supported me, I wish I could list all your names and am so grateful to have all of you around.

Finally, I would like to thank my husband and best friend, Sebastian Stirling. There are no words that can express my gratitude for all you have done for me. Especially during the past year you have given me your unending support and love and I am so thankful that I met you all those years ago.

Contents

List of Figures

List of Tables

Chapter 1

Introduction

To be productive in a microgravity environment, astronauts must be able to control their orientation and locomotion. However, it is well known that exposure to weightlessness causes changes in the perceived environment. Removal of the 1-G load can cause a perception of inversion upon entering weightlessness [104]. After astronauts acclimate themselves to the absence of the gravitational orientation cue, they still need additional information in order to maintain or modify their body position and orientation. In a study by Manzey et al. [72], a set of cognitive and motor control tasks were performed by astronauts before, during, and after an eight-day space flight. These tasks involved fine manual control of a cursor controlled by a joystick. The authors note that there was a highly significant learning trend seen during the spaceflight that was indicative of an adaptation to the microgravity environment. In a study of dual-task sensorimotor adaptation [21], it was seen that complete adaptation in the microgravity environment required continuous task practice with an increase in resource allocation to the motion control task.

In studies by Newman et al. [78, 79], the effects of astronaut motion on the surrounding environment during intravehicular activity (IVA) were analyzed using force and moment sensors. Over time the astronauts were again seen to adapt their motor-control strategies, including lowering their velocities and reducing the forces necessary for microgravity motion. This adaptation time took four weeks on average during a long-duration space station mission. Part of the adaptation time was due to neuromusculoskeletal alterations between the different gravity environments, while the rest might be attributed to training and longer-term adaptation.

Even though astronauts undergo hundreds of training hours, the strategies for locomotion and orientation are not specifically prescribed. Most of an astronaut's motor-control strategies are developed during training in underwater simulators, the Neutral Buoyancy Lab at NASA's Johnson Space Center and the pool in Russia's Star City complex. One major drawback to underwater training is that the viscous drag of the water leads to the use of larger motions, hence recruitment of larger muscles, both of which are inappropriate for optimal microgravity body motions. Additionally, one can undergo a net rotation in the

microgravity environment without an external moment. Having grown up in a 1-G environment, astronauts are not familiar with reorienting without external forces and will most likely not develop any self-rotation techniques naturally. Several former astronauts mention grabbing anything within reach, such as hand-holds or latches on lockers, in attempts to externally torque themselves to achieve a net rotation. While underwater training can be beneficial in some aspects, such as learning which orientations an astronaut will encounter and becoming familiar with task time lines, it is not effective for self-learned motor-control strategies. With the development of appropriate astronaut maneuvers, a training program can be created such that adaptation time upon entering a microgravity environment is reduced.

Reduction of adaptation time to increase astronaut performance is not the only application of astronaut self-rotation. Another important application is as a safety countermeasure during extravehicular activity (EVA). Consider an astronaut performing an EVA in which the astronaut becomes separated from the spacecraft and the thruster backpack incurs a partial failure. If the astronaut has trained with a simple reorientation methodology, a maneuver can be performed such that the remaining thrusters direct the astronaut back to the spacecraft. While there are no flight data for crew separations, neutral buoyancy simulations have shown periodic separations that can be extrapolated to one every 1000 EVA hours [24].

This research studies astronaut reorientation methods both computationally and experimentally in an effort to reduce astronaut adaptation time and provide for a safety countermeasure during EVA.

1.1 Background

1.1.1 Self-Rotation and Astronaut Motion Studies

The problem of self-rotation has been previously studied in the context of astronaut motion [56, 64, 89], diving and gymnastics [41, 91, 107], and robotic manipulators [53, 54, 84, 105]. It is well known that when no external force is present, conservation of linear momentum shows that no translation is possible when starting from rest. However, when no external moment is present, conservation of angular momentum does not rule out a net rotation. The ability to obtain a net rotation is due to the nonholonomic nature of the system [20]. Since people are not familiar with reorientation without external forces, maneuvers such as these are not likely to be developed efficiently by new astronauts. Kulwicki, Schlei, and Vergamini [64] developed a set of rules governing human self-rotation, forming two possible methods of rotation—limb manipulation and continuous rotary motion. In the continuous rotary motions, some part of the body is rotated about an axis until the desired orientation is reached. In the limb manipulation method, a multi-stage motion is performed where there is an initial state, a twist about the axis of desired rotation, a change of the moment

of inertia, and a return to the initial state. While the maneuvers discussed in [64] would work to rotate the body, the energy to perform these tasks and the stability of the motions were not examined.

Even though there has been limited research into astronaut self-rotation, more extensive data does exist regarding other aspects of astronaut motion control. In studies of arm motions in a microgravity environment, several characteristics were seen to change, including a reduction in response time, a reduction in hand trajectory curvatures, and final hand position in aimed motions [21, 22, 86–88]. Adaptation was also affected by the speed of the motion. Slow movements, which are more dependent on central nervous system (CNS) afferent feedback, were affected to a greater extent than fast movements, which are more dependent on force feedback. This suggests that muscle spindle activity is reduced in microgravity [34], which is consistent with astronaut reports of a reduction in limb position perception [97] and experimental arm motion tests during parabolic flight [90].

In studies of whole body postural control and adaptation, microgravity was seen to affect simple postural motions. When a foot-down stance was requested, the center of mass of the body shifted with respect to the 1-G location [12, 13, 74]. When the foot-down requirement was not included, an even greater shift in posture was observed [2]. These changes in postural control are thought to be due to the reinterpretation of the muscle spindle activity by the CNS [66]. During the trunk-bending motions with the foot-down requirement, a reduction in the center of mass motion similar to a terrestrial environment was seen after an initial adaptation period [13, 61, 73, 90]. Translational motion studies have also shown adaptation to the modified environment [6, 33, 62, 78, 80], including reductions in velocity and applied forces.

1.1.2 Simulation of Human Motion

The study of multibody dynamics has been examined by many researchers and can be separated into Lagrangian, Newton-Euler, and Kane's methods. Asada and Slotine [9] give a detailed description of the methods for determining the equations of motion based on the first two formulations, with Kane's method described by Kane and Levinson [57, 58]. All variants of the equations of motion when developed correctly can be shown to be identical through mathematical manipulation.

The control of human-body dynamics can be posed as a motion-planning problem, for which many different solution methods exist. This research focuses on two of these methods, namely quantized control and optimal control. The use of optimal control to develop motions provides the ability to understand how the CNS plans motion. However, it may be difficult to formulate an objective function that captures all the necessary elements. For example, cognitive complexity of a given motion can be difficult to quantify; yet difficult-to-perform maneuvers could result if the appropriate complexity constraints are not included in the optimal control formulation.

There are many different applications of optimization for human movement simulation, including robotics, computer graphics, and gait analysis. The field of robotics offers many insights into the development of behavior and the different types of control for attaining the desired behavior. For example, studies have examined whole-body dynamic behavior and control of human-like robots in many ways, including posture control, task prioritization, and physiologically-based potential energies [59, 60, 98]; as well as the implementation of optimal control methods for robot path planning in real time operations [70, 109, 110]. In the graphics community, optimization techniques are applied to character motion in order to get a smooth transition between keyframes and to create adaptations to already developed motions [68, 69, 102]. While the graphical methods provide insight into the different techniques available, the results were not always physically realizable as the best graphics were the desired output. In a human motion study by Anderson and Pandy [7], human gait was modeled with a three-dimensional neuromusculoskeletal model of the lower body combined with a minimal metabolic energy optimization. Optimal gait studies with varying complexity models have also been studied by many others, including [47, 50, 76].

The most critical step in developing any optimization problem is determining what the objective function should be, along with what constraints should be included. There have been many theories on whether the CNS codes kinematics or dynamics for motion planning. Studies of planar reaching motions suggest that there is an invariant kinematic plan and a dynamic internal model is learned in order to obtain the desired motion trajectory [19,67,99]. The adaptation to the dynamic environment was dependent on the length of exposure to the environment and the motions made while in the environment. However, the intent of the current optimal control formulation is to predict the steady-state learned behavior. In a study by Flash and Hogan [36] and Hogan [51], planar arm motions were examined using the mean-jerk-squared (a motion smoothness term) of the hand trajectory. They saw that by looking only at the kinematics, the planar motions could be reproduced when the resulting trajectories were used as virtual trajectories in a second order model of the arm. If the arm is instead in a vertical plane, this objective function will not work to capture the resulting hand trajectory. In tests performed by Atkeson and Hollerbach [10], curved hand trajectories were obtained, which is inconsistent with a minimization of motion smoothness in the hand coordinate system. The differing motions in the vertical plane could be due to the increased dynamic information necessary, or due to a difference in the perceived visual information. When analyzing motion strategies it is important to realize that the analysis of these tasks can be coordinate frame dependent [36]. For the motion smoothness term analyzed in the hand frame, a linear profile is obtained for the hand path. However, a linear hand path implies a curved joint path. Had the analysis been performed in the joint space, a linear joint path would have been obtained.

The important parameters for the objective function seem to depend on the environment. In the previously mentioned study by Flash and Hogan [36], the kinematic term was

sufficient to predict the arm trajectories. In a study by Ohta et al. [82], purely dynamic terms were sufficient to model an arm rotating a crank. However, the interaction between the kinematics and dynamics is necessary for certain dynamic environments. In studies by Osu et al. [83] and Franklin et al. [38] two-dimensional planar arm movements were also examined. The arm trajectory and electromyographic (EMG) adaptation in several force fields was examined, with fields that were variable and based on the arm velocity or position. Franklin et al. [38] suggest that the motor control system needs both the kinematic and dynamic information, where an inverse dynamics model was needed to learn the mean dynamics and an impedance controller was needed to generate stability. Further, they saw that different motion planning styles existed depending on whether the motion was dynamically stable or unstable, with the two methods functioning together in parallel for certain scenarios. The need for forward and inverse information was also seen in a study on reaching motions of the arm in and out of a force field by Bhushan and Shadmehr [16]. Since the desire of the current research is to have an objective function in the optimal control formulation that can give information on how the CNS controls motion in a microgravity environment, it seems essential to include a dynamic and kinematic term, or reliance on these terms, since interaction between the two has been shown. Tagliabue et al. [103] have tried several objective functions that attempt to look at the kinematics, dynamics, and combinations thereof to predict astronaut motion for a planar four-element body during bending motions. A single motor-control planning strategy could not be found that correctly predicted the motions, the internal torques, and the external forces.

In cases where it is difficult to capture all the necessary elements in the objective function and constraints, quantized control can be extremely beneficial. The control problem can be formulated using a quantization of motion by defining a set of specific finite-time trajectories called motion primitives. The quantized control method permits the development of complete maneuvers that are appropriate for humans to perform in high-stress situations by incorporating complexity considerations in the definition of the motion primitives. Further, these motion primitives can be refined using the optimization methodology with an appropriate parameterization that maintains the intrinsic characteristics of the maneuver.

One purpose of quantized control is to yield a reduction in the complexity of the control task by splitting the task up in some way [40]. The quantization can occur in time, state, or control input. Quantized control has been applied in many settings [14,17,40] and has been shown to determine appropriate maneuvers in complex dynamical systems. While there is a long history showing that human motions are composed of submovements [31,63,77,81,106], the use of quantization for developing human control tasks is significantly newer. In a study of human drawing [30], the motion was split into "movemes," similar to the motion primitives defined here, that describe the "reaches" and "draws" necessary to produce an image. In a different study that looked at categorizing humanoid motion, motion primitives were developed based on motion capture data [32].

Since it is well known that two rotations can yield any orientation, a quantization for the self-rotation planning problem can be created by defining two motion primitives, which in this case are each a specific finite-time trajectory representing a rotation about a given principal body axis. Using a concatenation of these two motion primitives, the quantized control method admits candidate motions that define all possible orientations. Such an approach will lead to a small number of rotations that need to be learned, which is desirable in situations such as astronaut training for microgravity motions. The concept of motion primitives as building blocks for a maneuver has been examined at the level of neural muscle control for creating elementary motor behaviors [18, 77] and provides a different interpretation as to how the CNS signals coordinated movements.

1.2 Thesis Objectives

The objectives of this research are as follows:

1. Develop an astronaut dynamics model that is appropriate for IVA and EVA motions and incorporates constraints to ensure motion feasibility.
2. Simulate the astronaut dynamics model for several reorientation techniques to determine the resulting off-axis motions, necessary torques, and effects of the space suit.
3. Apply quantized control to the human reorientation problem.
4. Determine an appropriate optimal control formulation to predict human motor control strategies for the microgravity environment.
5. Design and implement a system for performing self rotations in a 1-G environment.
6. Determine the appropriate parameters for investigating the affects of reorientation training.

1.3 Thesis Outline

This thesis presents a research program designed to study self-rotation of astronauts. In Chapter 2, a multibody dynamics model is developed that is appropriate for studying human self-rotations in microgravity conditions. This model was developed for the suited and unsuited configurations so that it would be applicable for intravehicular activity (IVA) and extravehicular activity (EVA) motions. Several scenarios are examined in order to further understand rotations in the microgravity environment and the limitations of the current space suit.

Astronaut self-rotation strategies are developed in Chapter 3 using two different motion control techniques. First the quantized control methodology is presented along with the

concatenation necessary to obtain any reorientation. The optimization methodology is then presented with applications to refining the motion primitives as well as determining self-rotations from more general motion parameterizations.

Chapter 4 presents the experiments that were conducted to further understand astronaut reorientation. Three main hypotheses were studied: (1) Subjects that have had motion strategy training will have a better initial performance with respect to the performance parameters than those that have not received training; (2) Rotations and motions that are common in an Earth environment will yield a lower complexity score than those that are completely unfamiliar; and (3) The variation in performance of a group with less training will be greater than the variation in a group with more training. In addition to detailing the experiment protocols, results are presented that give insight for future training protocols.

Finally, Chapter 5 summarizes this research and discusses ideas for future work.

Chapter 2

Development of the Astronaut Dynamics Model

In developing any computational model there is a balance between including all the parameters that could affect the system and simplifying the model so that it can properly reproduce the needed solution. As the model developed in this research will be implemented in an optimization framework in the following chapter, this model attempts to be of a high-enough fidelity to reproduce the dynamics of the body while simple enough to be efficiently simulated numerous times. In this chapter, the astronaut dynamics model that will be used throughout this research is developed following this ideology and uniquely contributes to understanding both IVA and EVA motions.

The derivation of the equations of motion is developed using conservation of linear and angular momentum, which reduces the complexity of the equations when compared to the derivation using a summation of forces and torques. The human body parameters are then defined for the unsuited and suited astronaut configurations. In order to have a feasible motion, the model includes calculations of the range of motion, possible collisions, and available muscle torque. Following the model development, the single-axis rotations implemented in this research are defined and sample simulations are presented for the unsuited and suited astronaut.

2.1 Deriving the Equations of Motion

The human body can be thought of as multiple interconnected rigid bodies. As previously mentioned, the study of multibody dynamics has been examined by many researchers and can be separated into Lagrangian, Newton-Euler, and Kane's methods. The equations of motion for the current research were developed using a Newton-Euler method, which are written out in a recursive manner.

The equations of motion can be approached in two distinct main ways, forward and

inverse dynamics. They are stated:

Forward Dynamics: Given a set of joint forces and torques, one can determine the motions of the joints and limbs.

Inverse Dynamics: Given a set of joint motions (position, velocity, accelerations), one can determine the joint forces and torques to create the motions.

In certain scenarios a combination of these two approaches is necessary. For example, consider the astronaut performing a self-rotation. While the limb motions can be specified, the motion of the astronaut with respect to the inertial frame (the astronaut's root motion) may not be explicitly known. Thus the root motion should be a function of the astronaut's limbs. Further, since it is possible to calculate the root motion, introducing it as a variable is redundant and would over-parameterize the system. The combination of inverse dynamics with the calculation of the root dynamics will be called modified inverse dynamics and can be formally stated as:

Modified Inverse Dynamics: Given a set of actuated joint motions (position, velocity, accelerations), one can determine the motion of the unactuated joint connecting the body to the inertial frame, as well as the joint forces and torques to create the actuated joint motions.

2.1.1 Geometric and Kinematic Representation

While there are many ways to represent the kinematics of a body, certain methods are more appropriate depending on the application. Since this research is concerned with body rotations, it is important to use a representation that models the rotations efficiently. The use of Euler angles to represent the position and orientation of a body is common in aerospace applications; however, gimbal lock can occur due to singularities in the parameter space leading to problems when defining motions for articulated systems. The concept of gimbal lock is shown schematically in Figure 2-1. When two or three of the rotational axes become

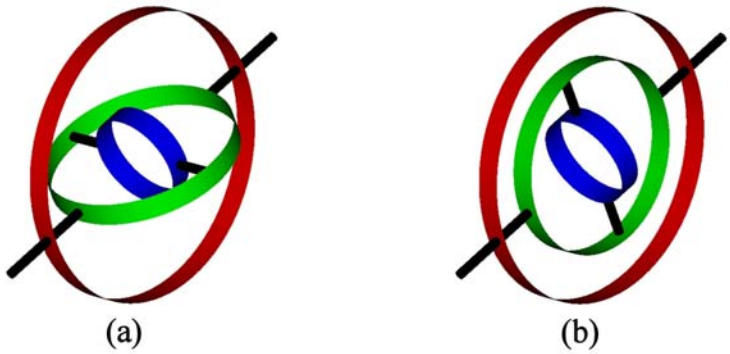

Figure 2-1: A comparison of a gimbal in a (a) non-singular and (b) singular configuration.

parallel, the gimbal is in a singular state and the number of degrees of freedom available is reduced, artificially limiting the available range of motion.

Limitations in the design space are also incurred when using Euler angles as the parameters are cyclical (i.e., 0 is equal to 2π). In addition, it is well known that when Euler angles are used, the order of rotations is important. For example, consider the box shown in Figure 2-2. If the rectangular box is rotated the same amount about the **x** and **y** axes in different orders, the resultant orientation will be different even though the rotation values were the same.

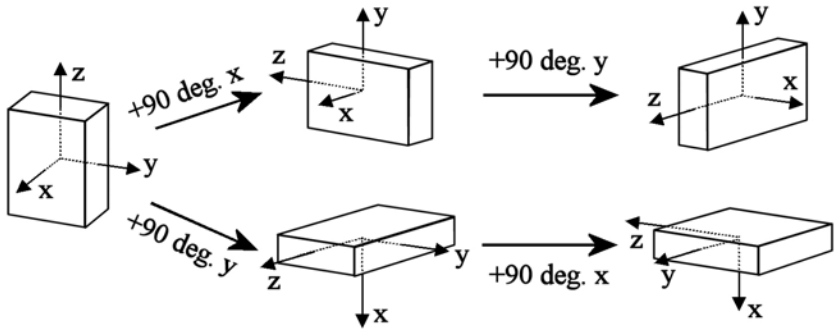

Figure 2-2: Even though the box is reoriented the same amount about the **x** and **y** axis, the final orientation is different, adapted from [9].

A common method to avoid these complications is the use of a quaternion representation. The quaternions span the $\Re^4$ space and can be thought of as a vector with three imaginary parts and one real part, $\mathbf{q} = a + b\mathbf{i} + c\mathbf{j} + d\mathbf{k} = [a\ b\ c\ d]$. The position and orientation can be completely described by two quaternions. The position can be written as a quaternion with a zero real part and the **x**, **y**, and **z** coordinates as the imaginary parts ($\mathbf{q_p} = 0 + x\mathbf{i} + y\mathbf{j} + z\mathbf{k}$). The orientation can be interpreted as a rotation about an axis and can be written as $\mathbf{q_r} = [q_1\ q_2\ q_3\ q_4] = [cos(\theta/2)\ sin(\theta/2)\mathbf{e}]^T$, where θ is the angle of rotation about the axis described by $\mathbf{e} = [e_1\ e_2\ e_3]^T$. The orientation and position of the body can then be fully determined by the vector $\bar{\mathbf{q}} = [q_1\ q_2\ q_3\ q_4\ x\ y\ z]^T$, where the zero real part from the position quaternion has been removed. Since there are only six degrees of freedom in a rigid body and there are seven unique parameters, there is an additional constraint that the orientation quaternion must be of unit length. The angular velocities (ω_x, ω_y, and ω_z) are related to the time rate of change of the orientation quaternion through the matrix equation

$$\begin{bmatrix} \dot{q_1} \\ \dot{q_2} \\ \dot{q_3} \\ \dot{q_4} \end{bmatrix} = \frac{1}{2} \begin{bmatrix} -q_2 & -q_3 & -q_4 \\ q_1 & -q_4 & q_3 \\ q_4 & q_1 & -q_2 \\ -q_3 & q_2 & q_1 \end{bmatrix} \begin{bmatrix} \omega_x \\ \omega_y \\ \omega_z \end{bmatrix}. \tag{2.1}$$

A basic review of quaternion algebra is provided in Appendix A.

2.1.2 Modified Inverse Dynamics

Figure 2-3 shows the representation of the human body and the associated body axes for this research. A tree structure configuration is implemented, formed by joints and links, with a reference frame created at each joint. The reference frame for link i is aligned with joint i and the reference frame for link j is aligned with the reference frame for joint j. In this manner, the number of reference frames is minimized and fewer transformations are needed.

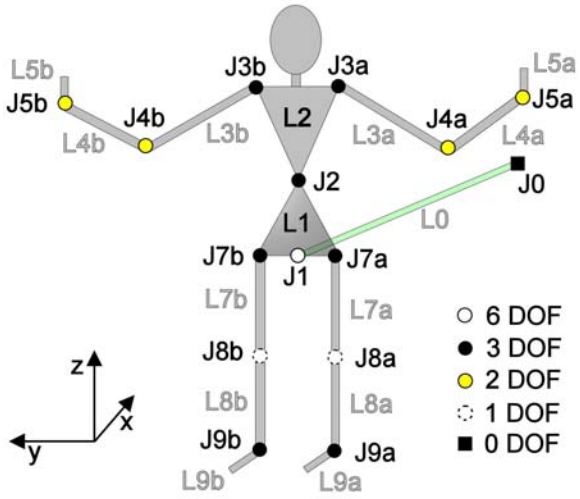

Figure 2-3: The human body configuration with link and joint numbering (a total of 37 DOF). The z-axis is from toe-to-head, the y-axis is parallel to the finger-to-finger vector when the arms are spread, and the x-axis is pointing into the body.

Generally, the root joint of the configuration is defined as the link with no superior link. However, for the human body, the root is defined as the joint that is connected to the inertial system. This connection is made with a virtual link to a virtual joint that is a fixed point in the inertial space. In Figure 2-3, the virtual link is $L0$ and the virtual joint is $J0$, with $J1$ as the root joint of the body. A link is a "parent" to another link if they are connected by a joint, with the parent closer to the root. For example, $L3a$ has $L2$ as a parent and they are connected at $J3a$. A link is a "child" to another link if they are connected by a joint, with the child further from the root. In the case of $L2$, there are two child links, $L3a$ and $L3b$, which are connected by $J3a$ and $J3b$, respectively. Now define B as the set of all links, P_i as the set of all parent links to link i, and C_i as the set of all child links to link i. The position and orientation of all joints in the body are described with quaternions. The state vector describing the position, orientation, and velocity of joint i can be written as $\mathbf{x}_i = [\bar{\mathbf{q}}_i \; \boldsymbol{\omega}_{J_i} \; \mathbf{v}_{J_i}]$, where $\bar{\mathbf{q}}_i$ is the quaternion orientation and position, $\boldsymbol{\omega}_{J_i}$ is the angular velocity, and $\mathbf{v}_{J_i}$ is the linear velocity of joint i. For the current research, it is assumed that $J0$ is fixed, $J1$ has rotational and translational components, and all other joints are purely rotational. The neck and head of the body are considered as part of $L2$.

The total number of degrees-of-freedom (DOF) in the model is 37.

Each reference frame moves with the joint to which it is attached. Thus a transfer from one reference frame to another consists of a rotation based on the joint orientation and a translation based on the link length. The rotation matrix from frame i to j, R_i^j, can be expressed as a function of the quaternion orientation, $\mathbf{q}_{\mathbf{r}j}$. With the four components of the quaternion orientation written as $\mathbf{q}_{\mathbf{r}j} = [q_1\ q_2\ q_3\ q_4]^T$, the rotation matrix representation of this orientation is:

$$R = \begin{bmatrix} 2q_1^2 + 2q_2^2 - 1 & 2q_2q_3 + 2q_1q_4 & 2q_2q_4 - 2q_1q_3 \\ 2q_2q_3 - 2q_1q_4 & 2q_1^2 + 2q_3^2 - 1 & 2q_3q_4 + 2q_1q_2 \\ 2q_2q_4 + 2q_1q_3 & 2q_3q_4 - 2q_1q_2 & 2q_1^2 + 2q_4^2 - 1 \end{bmatrix}. \tag{2.2}$$

Now, following the method of Luh, Walker, and Paul [71], the inverse dynamics can be written recursively for the human body.

Recall for the inverse problem the positions, velocities, and accelerations are specified for each joint in order to obtain the forces and torques. Then by using a forward and backwards recursion at each time increment, the kinematics and dynamics can be calculated. For example, the angular and linear velocities of link i are found with the forward recursion

$$\boldsymbol{\omega}_{L_i} = \sum_{j \in P_i} \left(R_j^i \boldsymbol{\omega}_{L_j} \right) + S_{\omega_i} \boldsymbol{\omega}_{J_i}, \tag{2.3}$$

$$\mathbf{v}_{L_i} = \sum_{j \in P_i} R_j^i \left(\mathbf{v}_{L_j} + \boldsymbol{\omega}_{L_j} \times \mathbf{L}_{ij} \right), \qquad i = 2, \ldots, N, \tag{2.4}$$

where $i = 1$ is the root of the body and N is the number of links. The first term in Eq. (2.3) is the mapping of the angular velocity of the parent links to the current link. The summation is performed only on the set P_i for the given link. The second term is the mapping of the joint angular velocity to the link. The constant matrix S_{ω_i} is the subspace of possible angular joint motions, and defines the angular degrees of freedom of the joint. The linear velocity of link i, Eq. (2.4), is the summation over P_i of the velocity due to the translation and the rotation of the parent frame, where $\mathbf{L}_{ij}$ is the distance from frame i to frame j.

Since the base of the astronaut is floating in the microgravity environment, $\boldsymbol{\omega}_{J_1}$ and $\mathbf{v}_{J_1}$ are not known *a priori*. Thus, the recursion cannot be used to find these parameters. Instead, these velocities are determined with conservation of linear and angular momentum. First, the velocity of the center of mass of link i, $\mathbf{v}_{cm_i}$ is defined as

$$\mathbf{v}_{cm_i} = \mathbf{v}_{L_i} + \boldsymbol{\omega}_{L_i} \times \mathbf{r}_{cm_i}, \tag{2.5}$$

where $\mathbf{r}_{cm_i}$ is the location of the center of mass of link i.

Since there is no net translation and the angular momentum about the center of mass

is zero, Eqs. (2.3)–(2.5) can be used to write conservation of linear and angular momentum as

$$\sum_{i \in B} R_i^0 m_i \mathbf{v}_{cm_i} = \mathbf{0}, \tag{2.6}$$

$$\sum_{i \in B} R_i^0 I_i \boldsymbol{\omega}_{L_i} + \mathbf{r}_{0,cm_i} \times R_i^0 m_i \mathbf{v}_{cm_i} = \mathbf{0}, \tag{2.7}$$

where the summation is performed over all of the links. In Eqs. (2.6) and (2.7), I is the inertia, m is the mass, $\mathbf{r}_{0,cm_i}$ is the distance from the center of mass of the entire body to the center of mass of link i, and R_i^0 is the mapping from frame i to the inertial frame. Eqs. (2.6) and (2.7) give a set of six coupled equations, that are solved for the angular velocity, $\boldsymbol{\omega}_{J_1}$, and linear velocity, $\mathbf{v}_{J_1}$, of the base joint. These coupled equations can be written in a compact form that expresses the rate of change of the quaternion of the base joint, J_1, as a function of the quaternion and velocity values of the joints as

$$\dot{\bar{\mathbf{q}}}_{J_1} = Q(t, \bar{\mathbf{q}}, \boldsymbol{\omega}_J), \tag{2.8}$$

where t is time, $\bar{\mathbf{q}}$ is the vector of all the joint quaternions, and $\boldsymbol{\omega}_J$ is the vector of all joint velocities.

The joint torques, $\boldsymbol{\tau}$, are found using a backwards recursion such that

$$\boldsymbol{\tau}_i = \sum_{j \in C_i} R_j^i \boldsymbol{\tau}_j + \boldsymbol{\tau}_i^* + \boldsymbol{\tau}_{\mathrm{SS},i}, \qquad i = N, \ldots, 1, \tag{2.9}$$

where $\boldsymbol{\tau}_i$ are the torques of joint i. The first term in Eq. (2.9), maps the torques of the child joints, C_i, to the current joint. The second term, $\boldsymbol{\tau}_i^*$, is the torque due to the coupling forces applied to link i by link $i-1$ and $i+1$ and the rotation of the reference frame. This is expressed as

$$\boldsymbol{\tau}_i^* = \mathbf{r}_{i,cm_i} \times \mathbf{f}_{i,i+1} - \mathbf{r}_{i-1,cm_i} \times \mathbf{f}_{i-1,i} - I_i \dot{\boldsymbol{\omega}}_{L_i} - \boldsymbol{\omega}_{L_i} \times (I_i \boldsymbol{\omega}_{L_i}), \tag{2.10}$$

where $\mathbf{r}_{i,cm_i}$ is the distance from the origin of link i to the center of mass of link i and $\mathbf{f}_{i,i+1}$ is the coupling force between link i and $i+1$. The coupling force between link $i-1$ and i is

$$\mathbf{f}_{i-1,i} = \mathbf{f}_{i,i+1} + m_i (\mathbf{g} - \dot{\mathbf{v}}_{cm_i}), \tag{2.11}$$

where $\mathbf{g}$ is the acceleration due to gravity and is assumed to be zero in the microgravity environment. When evaluating Eqs. (2.10) and (2.11), the distances and coupling forces must be expressed in the reference frame for link i.

The final term in Eq. (2.9), $\boldsymbol{\tau}_{\mathrm{SS},i}$, are the torques at joint i due to the space suit. The determination of these values is discussed further in Section 2.6. The system of equations

that is solved to find all joint torques, $\mathbf{\Gamma}$, is written as

$$\mathbf{\Gamma} \quad = \quad T(t, \bar{\mathbf{q}}, \boldsymbol{\omega}_J, \dot{\boldsymbol{\omega}}_J), \tag{2.12}$$

where $\bar{\mathbf{q}}$ is the vector of all joint quaternions and $\boldsymbol{\omega}_J$ is the vector of all joint velocities.

In many multibody dynamics problems, the equations of motion are solved using a forward dynamics approach. Recall in the forward dynamics problem, the forces and torques are specified for each joint in order to solve for the positions, velocities, and accelerations. In this scenario, the angular momentum equations become extremely difficult if not impossible to integrate. Papadopoulos [84] proved that multibody systems with more than two links have no non-trivial solutions. Therefore, one has to write the equations of motion using a summation over the torques and forces. In this latter form, the equations are more complicated than those obtained using conservation of momentum. By using the modified inverse dynamics methodology presented here, the equations are simplified.

2.2 Human Body Parameters

2.2.1 Unsuited Astronaut Configuration

The moments of inertia of a human body are typically generated either by regressions from previous studies or with mathematical models. The regressions are typically developed using methods such as anthropometric measurements, stereophotometric measurements, and analysis of cadavers. The Generator of Body Data (GEBOD) [25], developed at Wright-Patterson Air Force Base, is a common tool to obtain needed body parameters using regression equations and is based on data from measurement surveys [26, 45] and stereophotometric data [75, 108]. An example of a mathematical determination of the body inertias can be found in Yeadon [107]. This research uses GEBOD to determine the unsuited body parameters.

In general, design based on anthropometry involves accommodation of 5th percentile female data to 95th percentile male data. Designing for the 50th percentile is a common mistake since only half the population will be able to use the equipment. However, since this research focuses on the design of motion maneuvers, changing the body parameters will modify the efficacy of the motion, but will not prevent the motion from being performed. The analyses performed in this document are based on a 50th percentile male with regards to weight (parameters shown in Table 2.1). This leads to a 1.77 m (5 ft 9 in) man weighing 78.7 kg (173.5 lb). The methods developed with this research can be reanalyzed using any body configuration desired, from the 5th percentile female to 95th percentile male, as well as personalized data for a specific subject.

Table 2.1: Model masses, lengths, and inertias from GEBOD [25] for a 50th percentile male by weight. Moments of inertia are are given about the center of mass for all body segments except the torso (which includes the head, neck, and upper body), which is given in the body-fixed coordinate frame.

Body Segment	Mass (kg)	Length (m)	COM (%)	Ixx (kg-m^2)	Iyy (kg-m^2)	Izz (kg-m^2)
Torso	31.47	0.71	40.0	3.6587	3.5246	0.3482
Pelvis	11.20	0.22	50.0	0.1028	0.0943	0.1190
Upper Arm	1.90	0.33	43.6	0.0130	0.0026	0.0137
Lower Arm	1.34	0.31	43.0	0.0086	0.0013	0.0088
Hand	0.50	0.19	50.0	0.0013	0.0004	0.0011
Upper Leg	9.57	0.42	43.3	0.1596	0.1680	0.0431
Lower Leg	3.76	0.43	43.3	0.0593	0.0602	0.0068
Foot	0.94	0.27	50.0	0.0008	0.0043	0.0046

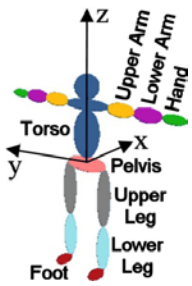

2.2.2 Suited Astronaut Configuration

During EVA, astronauts wear a pressurized space suit called an extravehicular mobility unit (EMU). The EMU is shown in Figure 2-4 and consists of several layers and parts. The body temperature of the astronaut is maintained through the liquid cooling and ventilation garment (LCVG) that is worn under the pressure and gas garment. The LCVG consists of tubing through which cooling water can flow. The lower torso assembly (LTA) consists of the pants and boots, as well as the hip, knee, and ankle joints. The lower torso connects to the hard upper torso (HUT) with a ring-shaped bearing. The HUT has the attachments for a variety of EMU systems, including the display and control module, electrical harness, and primary life support system (PLSS). The arm assemblies, which contain the shoulder joint, elbow joint, and wrist bearing, are also connected to the HUT. The gloves contain the wrist joints and are connected to the arm assemblies. Communication is possible through a microphone and headset commonly referred to as the communications carrier assembly. On top of this, the helmet is worn, followed by the EVA visor assembly. When flight ready, the total weight of the EMU is 126 kg (278 lb) [94]. The majority of this weight is due to the PLSS, which is 72 kg (158 lb). In addition to this gear, the simplified aid for extravehicular activity rescue (SAFER) is attached to the EMU by fitting it over the PLSS, with the majority of the mass just below the PLSS. SAFER was designed as a safety measure for use during EVA, but has no safety countermeasures of its own. With the controls on the SAFER, the astronaut can translate and reorient by expelling nitrogen gas through the appropriate nozzles. The SAFER adds an additional 34 kg (75 lb) to the astronaut's EVA configuration.

The mass and inertial parameters for the EMU were determined based on data from NASA [94]. The mass of the suit was divided between the body segments as shown in Table 2.2. The segment inertias were increased proportionate to the increase in mass of

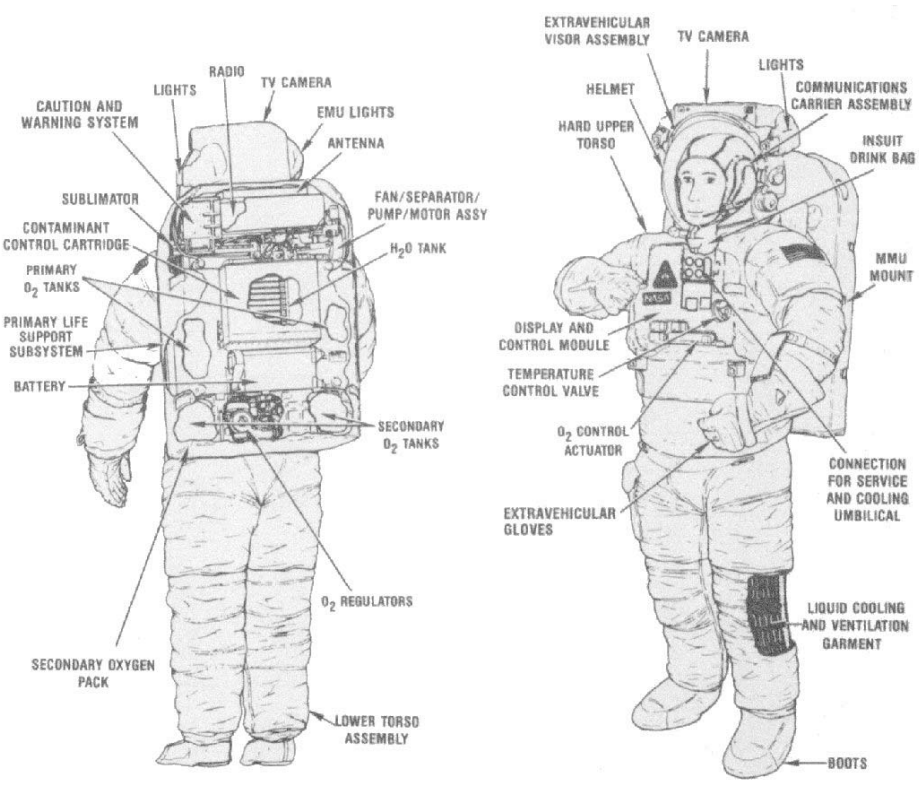

Figure 2-4: The EMU components [3].

the respective segment. The body parameters for the suited astronaut are given in Table 2.3. The center of mass locations were assumed to be in the same location for all segments except the torso segment, which was shifted further to the back and lower down based on the added depth and length of the PLSS and SAFER attachments.

Table 2.2: EMU parts list, based on data from NASA [94].

Part	Mass (kg)	Associated Segments
LCVG	2.94	Arms, Torso, Pelvis, Legs
HUT	12.29	Torso
Arm Assembly	7.87	Arms
LTA	20.72	Legs, Pelvis, Feet
Gloves	2.31	Hands
Helmet	8.23	Head, Neck
PLSS	71.89	Torso
SAFER	34.00	Torso

Table 2.3: The model masses and inertias when the EMU and SAFER are worn. Moments of inertia are are given about the center of mass for all body segments except the torso (which includes the head, neck, and upper body), which is given in the body-fixed coordinate frame.

Body Segment	Mass (kg)	Ixx (kg-m^2)	Iyy (kg-m^2)	Izz (kg-m^2)
Torso	159.84	15.1719	14.4138	1.8893
Pelvis	17.27	0.1585	0.1454	0.1835
Upper Arm	4.27	0.0292	0.0058	0.0308
Lower Arm	3.00	0.0193	0.0029	0.0198
Hand	1.65	0.0043	0.0013	0.0036
Upper Leg	14.75	0.2461	0.2591	0.0665
Lower Leg	5.80	0.0914	0.0928	0.0105
Foot	1.43	0.0012	0.0065	0.0070

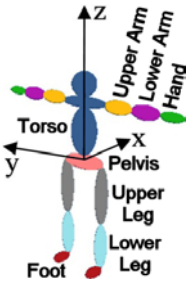

2.3 Model Range of Motion

When performing a motion, a set of boundaries for the range of motion must be considered. Single DOF joints can be constrained by simply setting limits on the angle of the joint. As limits on a quaternion are not readily available, three-DOF joints are more complex. Considering a three-DOF joint as a twist about an axis and a swing in the plane perpendicular to this axis leads to constraints that are more appropriate for realistic human ranges of motion. The limits are then determined by a function that is defined to be negative only for valid orientations [11].

A three-DOF joint can be decomposed from its quaternion orientation, $\mathbf{q_r} = [q_1 \;\; q_2 \;\; q_3 \;\; q_4]^T$, into the swing and twist components as follows. For a **z**-axis twist, T_z,

$$T_z \;\; = \;\; 2\tan^{-1}\left(\frac{q_4}{q_1}\right). \tag{2.13}$$

With intermediate parameters β and γ defined as

$$\beta \;\; = \;\; \tan^{-1}\left(\frac{\sqrt{q_2^2+q_3^2}}{\sqrt{q_4^2+q_1^2}}\right), \tag{2.14}$$

$$\gamma \;\; = \;\; \frac{T_z}{2}, \tag{2.15}$$

the swing components, S_x and S_y, can be written as

$$\begin{bmatrix} S_x \\ S_y \end{bmatrix} \;\; = \;\; \frac{2}{\mathrm{sinc}\beta}\begin{bmatrix} \cos\gamma & -\sin\gamma \\ \sin\gamma & \cos\gamma \end{bmatrix}\begin{bmatrix} q_2 \\ q_3 \end{bmatrix}, \tag{2.16}$$

where sinc is the sine cardinal and is defined as

$$\text{sinc}(x) = \begin{cases} 1, & x = 0 \\ \frac{\sin x}{x}, & \text{otherwise.} \end{cases} \tag{2.17}$$

Then, using the function

$$f(S_x, S_y) = \left(\frac{S_x}{r_x}\right)^2 + \left(\frac{S_y}{r_y}\right)^2 - 1, \tag{2.18}$$

defines a spherical ellipse with swing limits of r_x and r_y. For joints where the twist axis is about $\mathbf{x}$ or $\mathbf{y}$, the quaternion parameters can be modified appropriately in Eqs. (2.13)–(2.16) and (2.18). Figure 2-5 shows an example spherical ellipse region mapped onto a sphere.

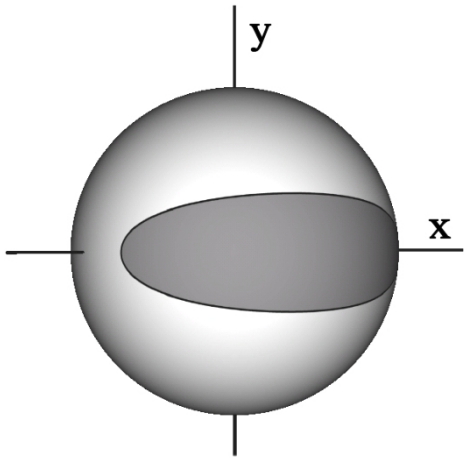

Figure 2-5: The range of motion for a three-DOF joint determined by mapping an ellipse onto a sphere. The inside of the ellipse is the feasible region.

The range of motion limits for this research were determined for both the suited and unsuited configuration. Unsuited range of motion values were determined from the Constellation Program Human-System Integration Requirements (HSIR) when provided [4], otherwise the values were determined from Stubbs et al. [101] and Boone et al. [23]. Range of motion limitations for the suited configuration were determined with the suit pressurized at 30 kPa (4.3 psig) from NASA documentation [2, 4], as well as experimental data from Schmidt [96] and documentation by Harris [48]. The range of motion limits are provided in Table 2.4, with Figure 2-6 detailing these angles. While the range of motion remains unaffected for some joints, as the nominal unsuited range is a subset of the designed suit range, certain joints, such as the shoulder and hip, are limited by the suit range of motion.

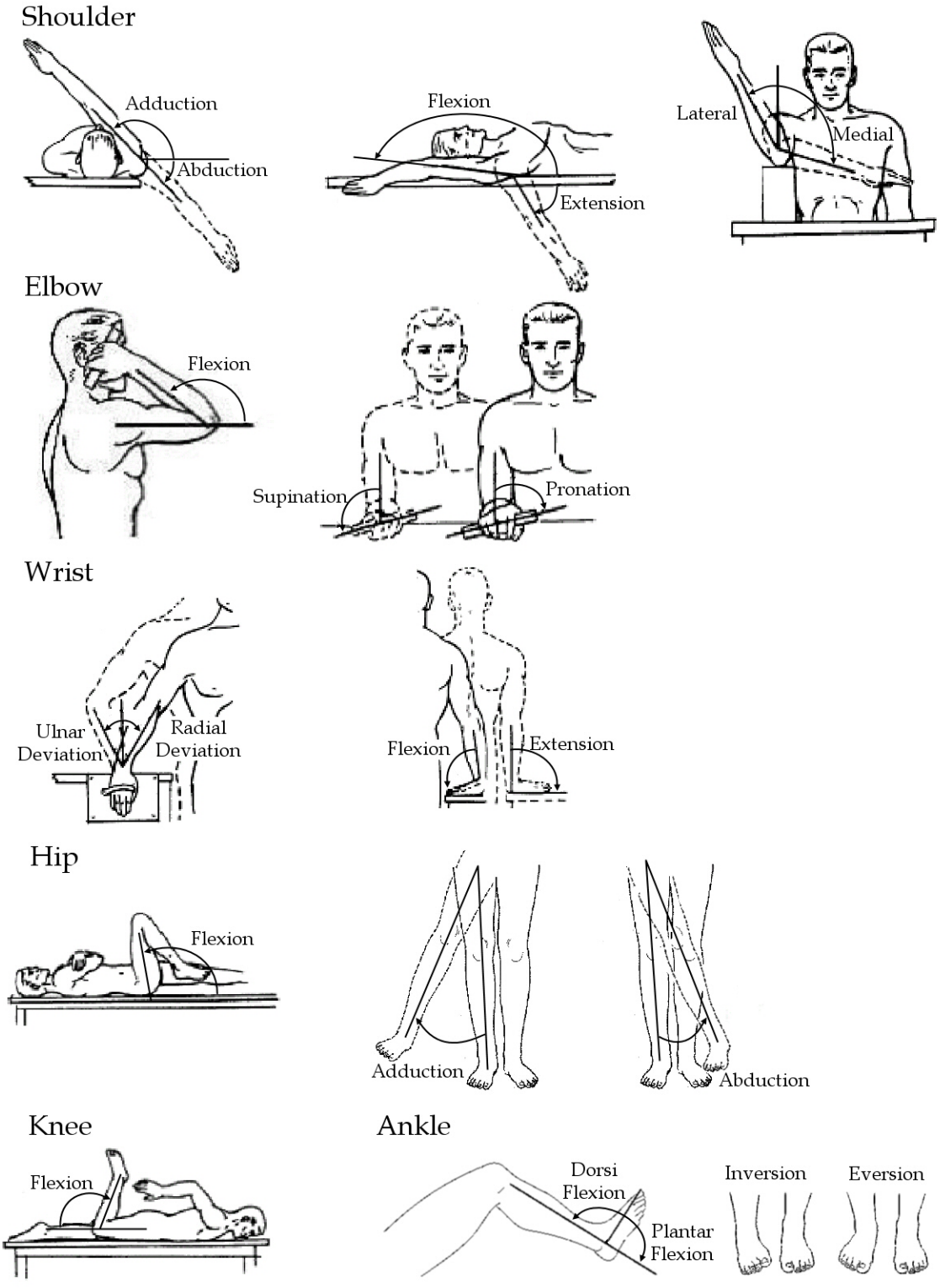

Figure 2-6: Joint movement schematics, adapted from [4].

Table 2.4: Joint range of motion for the suited an unsuited range of motion [2, 4, 23, 48, 96, 101]. All angles are given in degrees.

Shoulder	Unsuited	Suited	Hip	Unsuited	Suited
Flexion	213	180	Flexion	117	70
Extension	35	0	Extension	28	0
Horizontal Abduction	135	150	Abduction	30	0
Horizontal Adduction	45	20	Adduction	35	10
Lateral Rotation	46	90	Inward Rotation	45	20
Medial Rotation	91	90	Outward Rotation	45	20
Elbow			Knee		
Flexion	141	130	Flexion	135	120
Extension	0	0	Extension	0	0
Pronation	78	0			
Supination	83	0			
Wrist			Ankle		
Flexion	62	45	Plantar Flexion	36	40
Extension	40	35	Dorsi Flexion	7	40
Radial Deviation	16	15	Inversion	33	20
Ulnar Deviation	19	25	Eversion	18	20
			Inward Rotation	45	20
			Outward Rotation	45	20
Waist (Lumbar/Thoracic)					
Forward Flexion	123	90			
Backward Extension	30	0			
Lateral Flexion (Left)	33	75			
Lateral Flexion (Right)	33	75			
Rotation (Left)	45	75			
Rotation (Right)	45	75			

2.4 Collision Avoidance

In addition to checking the joint range of motion, a realistic motion must avoid collisions between the limbs. For example, the arms and legs must not penetrate each other or the torso. A collision detection method was implemented to ensure motions were realistic in that there were no inappropriate collisions. Since the model poses an inverse dynamics problem, the motions are known over time and it is possible to determine whether there are any collisions over the entire maneuver. For a rigid body, a collision can be detected by determining the separating axis between object bounding boxes (OBB) [44, 93]. The separating axis theorem test is as follows:

Theorem 2.1. *Given two rigid bodies with OBBs. The first OBB is described by three axes,* $\mathbf{e}_1$,$\mathbf{e}_2$, *and* $\mathbf{e}_3$, *a center* $\mathbf{T}_A$, *and half-sizes along its axes* a_1, a_2, *and* a_3. *The second*

OBB is described by three axes, $\mathbf{f}_1$,$\mathbf{f}_2$, *and* $\mathbf{f}_3$, *a center* $\mathbf{T}_B$, *and half-sizes along its axes* b_1, b_2, *and* b_3. *An axis,* $\mathbf{s}$, *separates the OBBs if and only if*

$$|\mathbf{s} \cdot \mathbf{T}_A\mathbf{T}_B| > \sum_{i=1}^{3} a_i|\mathbf{s} \cdot \mathbf{e}_i| + \sum_{i=1}^{3} b_i|\mathbf{s} \cdot \mathbf{f}_i|. \tag{2.19}$$

The sufficient set of fifteen axes to test are $\{\mathbf{e}_i, \mathbf{f}_j, \mathbf{e}_i \times \mathbf{f}_j, 1 \leq i \leq 3, 1 \leq j \leq 3\}$.

Proof. See references [44, 93]. □

Figure 2-7 shows a two-dimensional example of the separating axis theorem. The two ellipses, A and B, have OBBs that are projected onto the $\mathbf{f}_1$ axis. Since the distance between the center of the OBBs is larger than the projected radii of the OBBs, $\mathbf{f}_1$ is a separating axis and there is no collision. For each test between the body segments, there are fifteen equations, with all fifteen needing to be violated for a collision to occur.

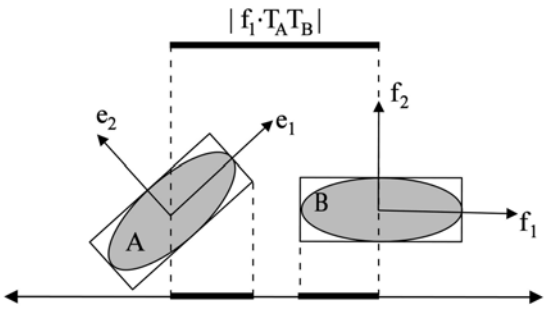

Figure 2-7: Ellipsoid A and B are shown with their bounding boxes in two dimensions. The projected difference between the centers of the OBBs and the radii of the OBBs are shown with respect to the f_1 axis. This figure has been adapted from [93].

2.5 Muscle Model

As the goal of the current research was to develop astronaut self-rotations techniques, a skeletal model of the body was developed as described in Section 2.1.2. While this model determines the total body orientation based on the body segments, it does not include the muscle parameters directly. Instead, the torques necessary to achieve the prescribed motions were calculated through Eq. (2.9). Then the question becomes whether the motions are feasible based on the human muscular system.

To determine the available limb torques at each joint, a muscle model was created in the Software for Interactive Musculoskeletal Modeling (SIMM) environment [1] for the upper and lower body based on experimental data from Delp [29] and Holzbaur et al. [52]. Available torques from the waist were determined from Kumar [65]. In SIMM, the muscle geometry is specified by origin and insertion points, with intermediate position points during

a joint motion so that the muscle does not pass through bone. The physical properties of the muscle are specified by the force-length curve of the tendon, the active and passive force-length curves of the muscle fibers, and the excitation pattern of the muscle. A normalized muscle excitation is a function of time and varies between zero and one. When the excitation is zero, the muscle does not produce any force and when the excitation is one, the muscle produces the maximum available force. To calculate the total available torque, all muscles were fully activated (i.e., all excitation patterns were set to one over the entire time frame).

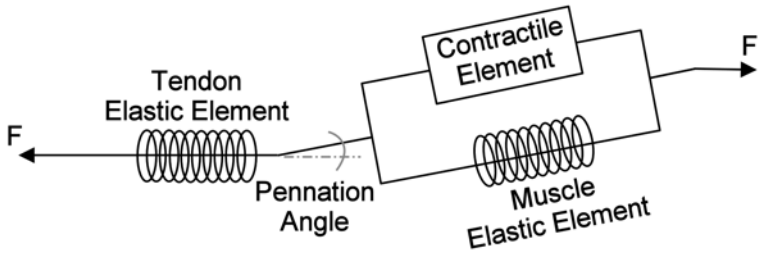

Figure 2-8: A schematic of the musculotendon actuator model, figure adapted from [29].

The musculotendon actuators are characterized using a Hill-based model [29] with parameters of tendon slack length (the length beyond which force develops), maximum isometric force (the force generated without muscle change in length), optimal fiber length (length of maximum force generation), pennation angle (angle between the tendon and muscle), and activation level. In this model, shown in Figure 2-8, the tendon is represented as a nonlinear elastic element in series with the muscle, which is represented as a contractile element in parallel with a passive elastic element. The contractile element is composed of the passive and active muscle forces.

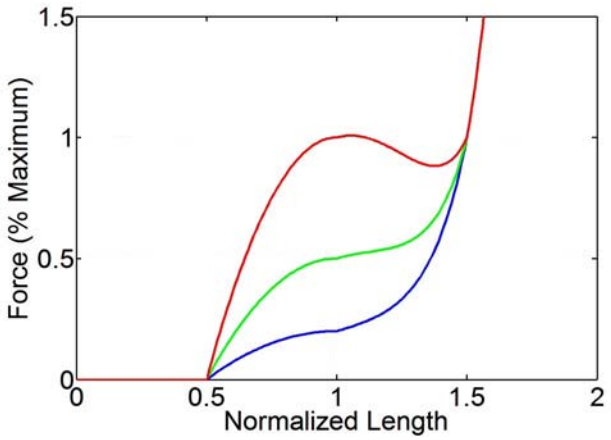

Figure 2-9: A few characteristic musculotendon force-length profiles. The normalization in length is performed with respect to the unstretched actuator length.

The maximum torque available due to a given muscle is a function of the force available and the moment arm between the muscle and selected joint. The available force is specified

by the musculotendon force-length profile. Figure 2-9 shows a few characteristic force-length profiles for the musculotendon actuator. While some muscles have a local maximum in the force-length curve, other muscles have profiles that are purely monotonic. The muscle torques acting on each joint were summed to obtain the maximum available torque. It is important to note that the torque provided by a given muscle can be negative due to the sign of the muscle moment arm. Therefore the maximum positive and negative torque that can be produced at each joint are calculated to get the range of torques available.

In this muscle model, the effect of muscle contraction velocity in the evaluation of the joint torques is not included. This approximation was made since astronauts have been observed to adapt their motor-control strategies to lower their velocities and reduce their applied forces [78]. Thus, the muscle velocities are also assumed to be low and the effect of velocity on the force can be neglected.

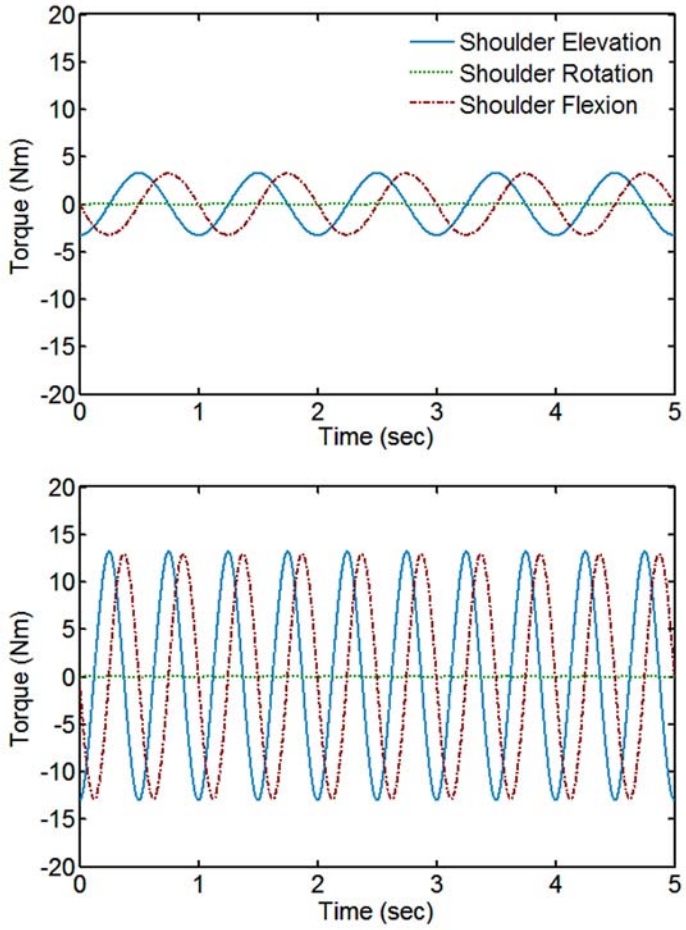

Figure 2-10: The actual torques necessary to perform an arm rotation about **z** with a semi-vertex angle of 10 deg. as calculated by the simulation dynamics for a rotation speed of one cycle/second (upper) and two cycles/second (lower).

To understand this assumption further, consider the shoulder rotating about the offset

z-axis with a semi-vertex angle of 10 degrees at a rate of one and two cycles/second. We define a rotation about the shoulder **x**, **y**, and **z** axes as the elevation, rotation, and flexion, respectively. Figure 2-10 gives the necessary torques based on the simulation dynamics, which were defined in Eq. (2.12). If a full muscle activation is assumed, then the range of torques available for this rotary motion without any velocity corrections are −155–82 Nm for shoulder elevation, −23–78 Nm for shoulder rotation, and −94–120 Nm for shoulder flexion. If we were to include the effects of velocity, we would need to modify the available forces. Figure 2-11 shows the characteristic effect that velocity has on the available force. In this figure, a negative velocity is muscle shortening and a positive velocity is muscle lengthening. When a muscle is shortening, it produces less force than when the muscle is contracted isometrically (zero muscle velocity motion). Therefore, if the muscle moves near its maximum speed, the available force goes to zero. If, like in the current example, the muscle moves at speeds less than 80 percent of the maximum value, then the force available is not reduced to a value that would cause the velocity effects to be significant. The magnitude of the actual torques in this example are quite low. Even the higher velocity motion has magnitudes that remain below 16% of the maximal available torque. Therefore, even though the model does not account for the velocity effects, it appears that the required torques are in range of what the muscles realistically produce.

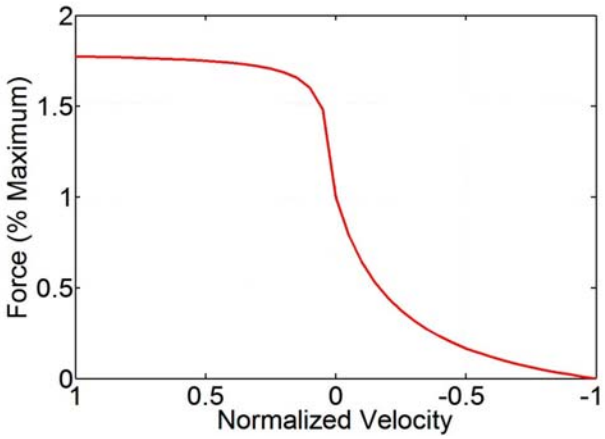

Figure 2-11: A characteristic force-velocity curve for a typical muscle. The normalization in velocity is performed with respect to the maximum shortening velocity.

2.6 Space Suit Torque Measurements

A critical requirement of the space suit is to provide an adequate partial pressure of oxygen required for breathing [5]. However, if the suit is pressurized such that the total pressure is one atmosphere, the joints would become extremely difficult to bend. If the pressure is too low, the astronaut can experience decompression sickness. Clearly there is a trade-off

in the design to allow for ease of mobility while still providing a safe environment for the astronaut. To reduce the effort required by the astronaut and increase the range of motion, bearings and bending joints are installed in the suit. Bearing joints are located at the interface between the HUT and the upper arm, on the upper arm, at the wrist, and at the waist. Bending joints are located at the shoulder, elbow, wrist, hip, knee, and ankle.

The suit-induced torques, which are mainly caused by volume changes in the multi-layer fabric suit, create a resistance torque that the astronaut has to overcome to bend a joint. The determination of these torques was performed by Schmidt [96] and Frazer [39] by outfitting an instrumented robot with an EMU and pressurizing the suit to 30 kPa (4.3 psig). The robot used to obtain the torque data is located at MIT and is a 12-joint hydraulic humanoid robot built by Sarcos, Inc. (Salt Lake City, UT) for the purpose of space suit mobility testing. At each actuated joint, potentiometers measured joint deflection and strain gauge load cells measured torque. The actuated joint locations are shown in Figure 2-12. Notice that only one half of the robot is actuated, while the other side is passive. The spacesuit used in the experiment was a class III EMU provided by Hamilton Sundstrand (Windsor Locks, CT).

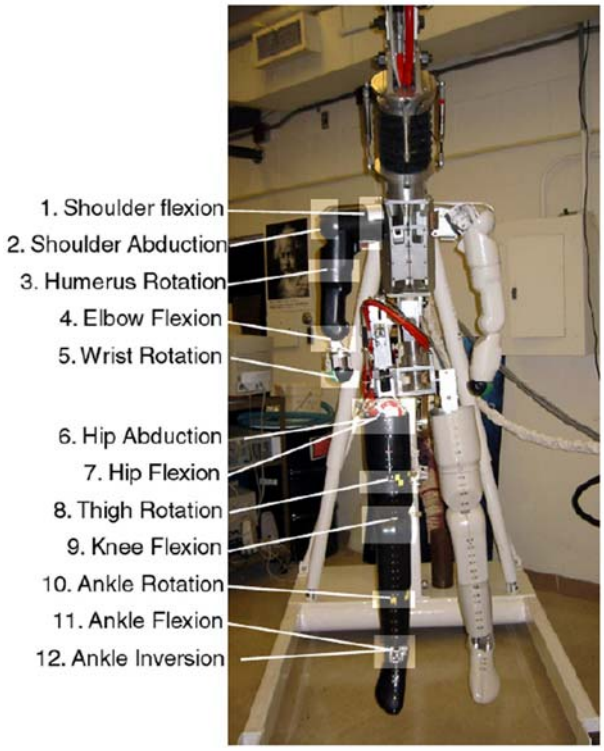

Figure 2-12: Robotic space suit tester used to obtain space suit joint torques.

Torques were measured at seven of the twelve joints during the experiments of Schmidt [96] and Frazer [39]. While these data showed hysteresis with regards to the angle input, the current research implemented a polynomial fit that approximated the data. Figure 2-13

shows an example of the polynomial fit and measured data for the knee flexion. As most joints were not pushed to the torque saturation limit, the polynomial fit is only accurate in the angle range for which data was recorded and should not be extrapolated beyond this range. The entire data set for the joint torques is provided in Appendix B. Since data was not available to determine the space suit torques at all joints (for example the wrist and waist were not available), care was taken to analyze torques and energies in the suited configuration only when appropriate.

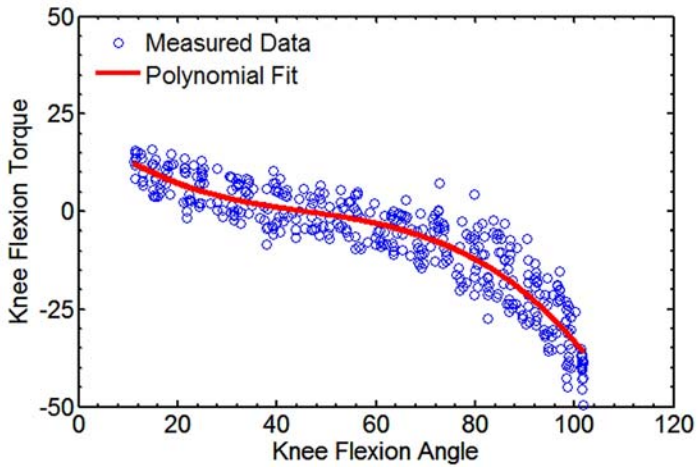

Figure 2-13: The measured data and implemented polynomial fit for the knee flexion. Writing the knee flexion torque as τ and the knee flexion angle as θ, the polynomial fit is expressed as $\tau = -1.5 \times 10^{-4}\theta^3 + 0.02\theta^2 - 1.1\theta + 22.4$.

2.7 Definition of Single-Axis Self-Rotations

In this section, the single-axis rotations used for this research are defined. All definitions assume that the astronaut begins in some neutral position prior to performing the reorientation and returns to this position after the rotation. Positive rotations are defined as right-handed rotations about the desired axis.

Definition 2.1 (Arm Rotation about **x**)**.** *This maneuver is shown in Figure 2-14 and is performed as follows:*

1. *From the neutral position, place the arms at one's sides, one arm up and one arm down, and draw the legs into a tuck position.*
2. *Rotate the raised arm outward to the side in the coronal plane and down to the side of the body. At the same time rotate the other arm outward to the side in the coronal plane until it is overhead.*
3. *Return the arms to their respective positions of step two by bending the elbows and moving the hands along the torso while keeping the hands and arms as close to the*

body as possible. The arms will need to be rotated about the body **z** *in order to begin the cycle again.*

4. *This cycle can be repeated until the desired rotation is reached, at which point the legs and arms are returned to the neutral position.*

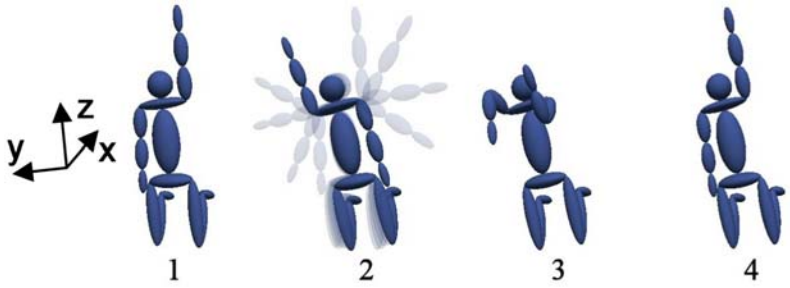

Figure 2-14: An approximation to a continuous rotary motion about **x**.

This maneuver was originally defined by Kulwicki et al. [64] and is the simplest single-axis rotation about **x**. Since it is not possible for an arm to rotate continuously about **x**, the maneuver is simply an approximation to a continuous rotation. Tucking the legs increases the net rotation achieved with each cycle since it reduces the body's moment of inertia with respect to the axis of rotation. When the motion begins with the right arm raised and left arm lowered, the arms rotate in a clockwise manner yielding a counterclockwise rotation of the body due to the conservation of angular momentum. If the motion begins with the left arm raised and the right arm lowered, the arms rotate in a counterclockwise manner leading the body to rotate clockwise.

Definition 2.2 (Leg Rotation about **y**)**.** *This maneuver is shown in Figure 2-15 and is performed as follows:*

1. *From the desired neutral position, move the limbs such that the arms are next to the body and the legs are bent such as when on a bicycle.*
2. *The legs are then pedaled about the offset* **y** *until the desired net rotation is obtained.*
3. *The limbs are returned to the chosen neutral position.*

A forward pedaling of this maneuver will cause the body to pitch backwards and a backwards pedaling will cause the body to pitch forwards. This motion is conceptually easy to perform as most people are familiar with riding a bicycle. To increase the net rotation achieved with this maneuver, one can modify the manner in which one pedals. This will be examined in more detail in Chapter 3. The next maneuver also yields a net rotation about **y**, but is performed with the arms as opposed to the legs.

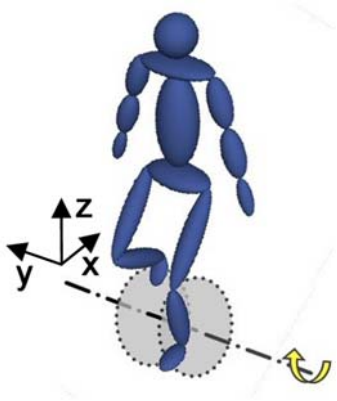

Figure 2-15: A continuous rotary motion about **y** implemented with a pedaling motion of the legs.

Definition 2.3 (Arm Rotation about **y**)**.** *This maneuver is shown in Figure 2-16 and is performed as follows:*

1. *From the desired neutral position, move the limbs such that the arms are equally inclined from* **y***. The legs can be outstretched or tucked.*
2. *The arms are rotated about* **y** *until the desired net rotation is obtained.*
3. *The limbs are returned to the chosen neutral position.*

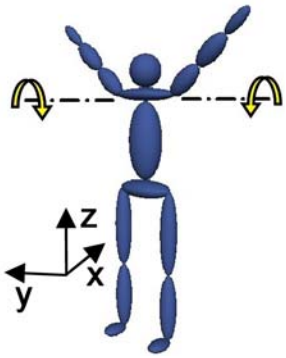

Figure 2-16: A continuous rotary motion about **y** implemented by rotating the arms.

When forward arm circles are performed, the body rotates backwards and when backwards arm circles are performed the body will rotate forward. In the following section the effect of tucking the legs will be presented. Notice that when the arms are rotated about the indicated axis, a cone is traced and that varying the inclination of the arms will modify the cone semi-vertex angle. For rotating about **z**, motions using the legs and arms are considered.

Definition 2.4 (Leg Rotation about **z**)**.** *The maneuver is performed as follows:*

1. *From the desired neutral position, move the limbs so that the arms are next to the body and the legs are at an angle from the body's* **z***-axis as shown.*
2. *The legs are then rotated about the offset* **z***, such that one leg is 180 degrees out of phase with the other, until the desired net rotation is obtained.*
3. *The limbs are returned to the chosen neutral position.*

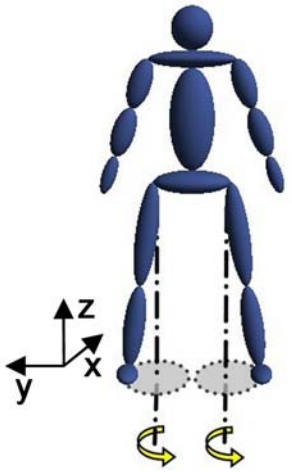

Figure 2-17: A continuous rotary motion about **z** implemented by rotating the legs.

A positive rotary motion of the legs about **z** will yield a negative rotation of the body, while a negative rotary motion of the legs will yield a positive rotation of the body. The rotation with the arms is similar to that performed by the legs.

Definition 2.5 (Arm Rotation about **z**)**.** *This maneuver is shown in Figure 2-18 and is performed as follows:*

1. *From the desired neutral position, move the limbs such that the arms inclined from* **z***. The legs can be outstretched or tucked.*
2. *The arms are rotated about the offset* **z** *in the same direction until the desired net rotation is obtained.*
3. *The limbs are returned to the chosen neutral position.*

Just as for the legs, a positive rotary motion of the arms yields a negative rotary motion of the body. This rotation will be explored with the arms both in-phase and out-of-phase. The final rotation that will be examined is a four-part limb manipulation motion originally developed by Kulwicki et al. [64].

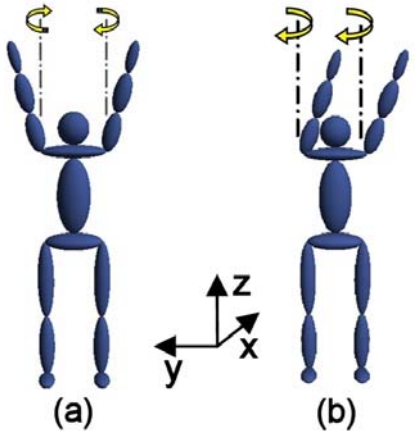

Figure 2-18: A continuous rotary motion about **z** implemented by rotating the arms (a) out-of-phase and (b) in-phase.

Definition 2.6 (Limb Manipulation Rotation about **z**)**.** *The maneuver is performed as follows:*

1. *In the initial stage, the body is straight, arms down, and legs spread to the side.*
2. *The torso is twisted about the axis of intended rotation.*
3. *The moment of inertia is increased at the top of the body by spreading the arms and decreased in the lower part of the body by closing the legs.*
4. *In the final stage, the body is untwisted at the waist and the arms are lowered.*

These steps can be repeated until the desired net rotation is achieved.

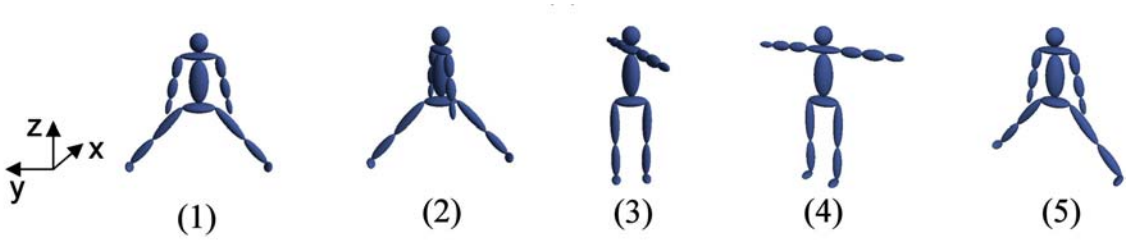

Figure 2-19: A limb manipulation rotation about **z**.

By modifying the ratio of the inertia of the upper body with respect to the lower body between the twist and untwist, a net body rotation is possible. While this maneuver does not have significant off-axis rotations, its complexity increases due to the increased number of steps. During the experimental stage of this research, motion complexity issues were considered and are discussed in Chapter 4.

2.8 Sample Model Implementation

2.8.1 Unsuited Astronaut Analysis

In a study by Kane [56] and Scher and Kane [95], continuous rotary motion self-rotations were examined for the pitch, roll, and yaw axes (**y**, **x**, and **z**, respectively). The pitch rotation was obtained as in Definition 2.3. As the cone semi-vertex angle was increased, the net pitch rotation increased. To further increase the rotation, the inertia was modified by tucking the legs and holding weights with the hands. Simulations of the rotary arm motion about **y** for the model developed herein are shown in Figure 2-20. Notice that tucking the legs is seen to increase the net rotation, which is consistent with the results in Kane [56]. The increase in rotation is due to the decrease in body inertia, while the inertia of the arms was kept constant. Increasing the cone semi-vertex angle also predicted an increase in the net rotation obtained per cycle. This follows physically as an increase in angular momentum for the arms occurs while the inertia of the rest of the body remains constant. The oscillations seen in Figure 2-20 arise since the lower body is held rigid and varies position based on the orientation of the arms.

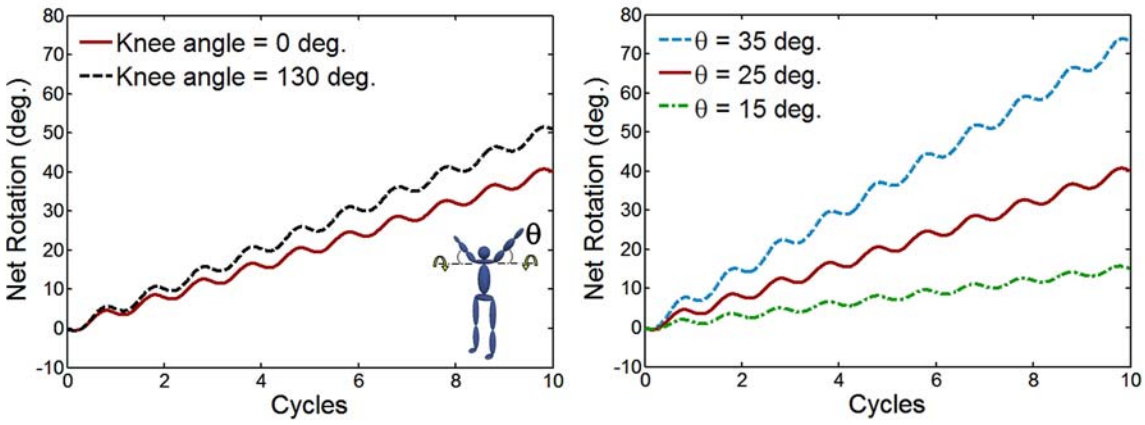

Figure 2-20: The net rotation about **y** when modifying (a) the knee angle for a cone semi-vertex angle, θ, of 25 deg. and (b) the cone semi-vertex angle for a knee angle of 0 deg.

Modifying the rotary motion about **z** using in-phase arm cycles for the model developed here showed similar results in that as the number of cycles was increased, the net rotation increased and as the cone semi-vertex angle was increased, the net rotation increased. It is important to note that as the cone semi-vertex angle was increased, the magnitude of the coupled off-axis oscillations also increased, which could lead to implementation difficulties. However, the off-axis components can be eliminated with a simple and easy modification to the rotation strategy. Instead of rotating the arms in-phase as shown in Figure 2-18(b), simply rotate the arms in the same direction, but 180 degrees out-of-phase, as shown in Figure 2-18(a). When rotating the left and right arms in the same direction, but out-of-phase, the off-axis rotations do not arise.

An important consideration that was not examined previously was that arm rotations may not be the most efficient way to obtain a net rotation. As the legs have a greater mass and moment of inertia than the arms, a greater net rotation in a similar amount of time can be obtained with leg motions. Consider Definitions 2.4 and 2.5. When the legs/arms are inclined 8 degrees from the body and rotated at 2 cycles/sec, the net rotation is 31 degrees and 12 degrees after one second for the legs and arms, respectively. As expected, motion of legs produces a greater net rotation than motion of the arms for similar speeds and orientations, as the legs have a greater inertia and mass. While it would take less time to reorient a given amount with the legs, a greater energy would be necessary. This aspect of net rotation versus energy consumption was examined when developing the control methods (Chapter 3) as well as during the experimental phase (Chapter 4).

2.8.2 Suited Astronaut Analysis

Since the EMU does not have hip extension, hip adduction, shoulder extension, or shoulder flexion past 180 deg., neither the arm nor leg cyclical motions can be performed as defined when suited. If these rotations are modified such that the limbs rotate about an axis slightly shifted but performable in the EMU, then off-axis rotations are generated as components of the traced circles project into the off-axis planes. The inability to bend any part of the body behind the center of mass eliminates cyclical motions about **z** from being performed in the suited configuration if single-axis rotations with minimal off-axis rotations are desired. To have a rotation about **z**, a limb manipulation method is necessary for the suited configuration. One disadvantage to the limb manipulation motions is that they are at minimum a four part motion and must be performed in the correct order to obtain the desired rotation. This makes them more difficult to learn and perfect than the continuous rotary motions. A limb manipulation rotation about **z** was previously given in Definition 2.6 and shown in Figure 2-19.

When this maneuver is performed with the legs going from a 0 to 10 degree adduction, the arms going from a 20 to 90 degree adduction, and the waist twisting 45 degrees, the net rotation is 18 and 12 degrees per cycle for the unsuited and suited cases, respectively. While this cycle can be completed in about 3–6 seconds, the equivalent rotation is obtained much quicker with the continuous rotary motions of the arms or legs. While the complexity has been reduced by removing off-axis rotations, the complexity has increased as the motion is a multi-step method, plus the time to perform the rotation has increased.

Similar to the issues seen when rotating about **z**, the limited mobility of the arms affects the rotation given in Definition 2.3. Although a rotation about **y** can still be performed with the method given in Definition 2.2. When rotating at 2 cycles/second, tracing a circle of radius 0.13 m located 0.7 m below the hip joint, and the waist bent forward 60 degrees, the net rotations are 11 and 7 degrees after three seconds for the unsuited and suited astronaut, respectively. By increasing the radius, the net rotation of the body will increase.

The selection of this radius and location below the hip joint for the example was not limited by range of motion or the necessary joint torque, but by the data available experimentally for the space suit torque. While the hip can freely rotate up to 70 degrees when suited, the experimental data only exist up to 52 degrees.

The addition of the space suit increases the mass of the body to a greater degree than the associated increase leg mass; thus there is a decreased net rotation after a given time for the suited astronaut with respect to the unsuited astronaut. Based on the SIMM muscle model, the feasible range of torques for the knee and hip are −146–248 Nm and −262–107 Nm, respectively. Figure 2-21 shows the actual torque required for this motion at the knee and hip as determined by the dynamics model. During this motion, the knee flexion angle oscillates between 95–20 degrees, resulting in a −26 to 7 Nm change in the required torque. (The neutral position of the knee is approximately 46 degrees for the implemented space suit torque polynomial fit.) The added torque necessary at the hip is more significant. This maneuver has a hip flexion angle ranging between 52–9 degrees, with a corresponding torque change of 121 to −20 Nm. The hip flexion neutral position is approximately 13 degrees and yields positive torques above this angle and negative torques below this angle. Thus, when the hip extends from 52–13 degrees or flexes from 13-52 degrees, a positive torque is added yielding the reduced torque magnitude for the suited configuration seen in Figure 2-21.

The maximum percentage increases in the torques for the given motion in the suited configuration with respect to the unsuited configuration were 46% and 53% for the knee and hip torque, respectively. The design of the current space suit yields high torques whenever the hip is moved as it was designed to use the legs for stabilization and not mobility. This particular motion at the given speed would put the astronaut near his/her hip torque limit. However, modifications to the speed and geometry of the motion could be made to reduce the torques generated at the hip.

As these motions can become tiresome to perform during EVA, they are suggested for use in emergency situations when the SAFER is not working properly. However, during IVA, these motions provide an easy, low-energy way to reorient. While the current EVA suit was designed to have the legs immobile while the upper body was mobile, future suit designs are looking at increasing mobility of all the joints while decreasing suit mass [15,55]. These changes will make EVA self-rotation more effective in cases when the SAFER has limited functionality.

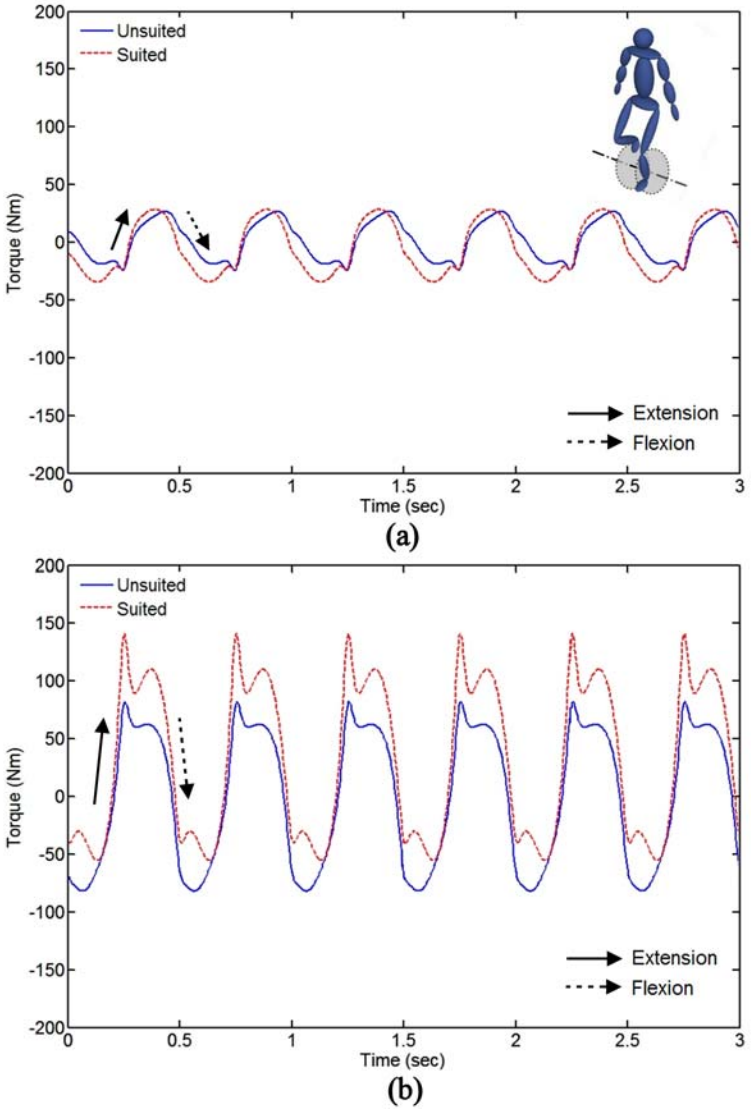

Figure 2-21: Comparison of the torque at the (a) knee and (b) hip when the legs are pedaled for the suited and unsuited astronaut.

Chapter 3

Development and Application of the Control Methods

The computational development of engineering control methods for human motion planning offers a novel way to provide astronauts with maneuvers that are difficult to obtain experimentally in a standard 1-G environment. In this Chapter, two control methodologies are presented and analyzed—quantized control and optimal control. The quantized control method permits the development of complete maneuvers that are appropriate for humans to perform in high-stress situations by defining a set of specific finite-time trajectories called motion primitives. A benefit to quantized control is that motion constraints are naturally incorporated into the motion primitive definitions. The implementation of an optimal control method allows for the development and refinement of maneuvers based on general motion parameterizations. Additionally, the use of optimization can provide insight into many different maneuvers that are possible when trying to reorient and can yield information on how the central nervous system controls body motion.

3.1 Quantized Control Methodology

By quantizing the system dynamics, the complexity of motion planning for the astronaut reorientation problem, which is constrained and nonlinear, is reduced. Quantizing the system dynamics means restricting the feasible system trajectories to a set of predetermined finite-time trajectories that are termed motion primitives. Maneuvers are then developed by the concatenation of these primitives. Thus, the complexity of the motion planning problem is simplified by quantizing the possible primitives that can be implemented at each decision step. These primitives are then characterized to capture the relevant characteristics of the system dynamics and to allow for the creation of complex behaviors. Further, the minimal set of key primitives are identified.

When forming self-rotation methods, it is important to have a rotation that requires

a low workload so that the astronaut can still perform other tasks. Workload, as defined by the NASA-TLX [49], is the cost incurred by a human to achieve a particular level of performance and is composed of mental, physical, and temporal demand along with perceived effort, performance, and frustration. Using these criteria, the motion primitives that should be selected and discarded were determined. A lower mental demand was obtained by eliminating all rotations that were not about the primary axes of the body, i.e., the motion primitives selected are pure rotations about the primary body axes, such as those defined in Section 2.7.

To examine the effect of rotation sequences, two sample single-axis rotations were selected that are about $\mathbf{y}$ and $\mathbf{z}$ as these are the least cognitively complex motions for a trained astronaut (see Section 4.5.4 for a discussion of motion complexity). The set of motion primitives $\mathcal{Y}$ are maneuvers that rotate about $\mathbf{y}$ and the set of motion primitives $\mathcal{Z}$ are maneuvers that rotate about $\mathbf{z}$. As will be seen shortly, only these two classes of rotations are necessary for any orientation to be achieved. For the following analysis, motion primitives $\mathcal{A} \in \mathcal{Z}$ and $\mathcal{B} \in \mathcal{Y}$ are given by Definition 2.4 and 2.2 with Figs. 2-17 and 2-15, respectively. To combine these motion primitives into a feasible maneuver, it is important that they begin and end with the same neutral position, otherwise there will be a discontinuity in the motion. The determination of the neutral position is not fixed and is up to the user to select.

The reachability of all orientations of the body with respect to the environment is shown using Poincaré's realization of $SO(3)$ as given in Figure 3-1. With this construction, an astronaut can reach any configuration using only two rotational motion primitives. In order to develop the motion trajectory framework, the geometry must be formalized.

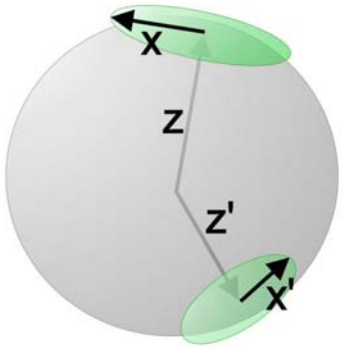

Figure 3-1: SO(3) mapping using Poincaré's realization.

Consider a sphere S^2 of unit radius, fix a point p on it, and consider the tangent plane to the sphere at this point, usually indicated with T_pS^2 [46]. Inside this tangent plane, consider a circle of unit radius centered at p. Instead of the whole tangent plane at p to S^2, we consider just the unit circle within T_pS^2 centered at p. This circle with point p is called

$T_{p,S^1}S^2$. Now consider the union of all such $T_{p,S^1}S^2$ where p varies over S^2, and call it $T_{S^1}S^2$. This is known as the *unit circle bundle* over S^2. If instead of taking just the circles, one takes all the tangent planes, one gets the tangent bundle TS^2 to the sphere. Since circles are included in the appropriate tangent spaces, it is clear that $T_{S^1}S^2$ is a subset of TS^2. The following proposition gives a global geometric picture of $SO(3)$.

Proposition 1 (Poincaré's realization)**.** *The group $SO(3)$ can be identified as the* unit circle bundle *$T_{S^1}S^2$ inside the tangent bundle TS^2 of the two-sphere S^2.*

Proof. Since elements of $SO(3)$ are in one-to-one correspondence with orientation-preserving rotations, they can be identified with oriented orthonormal frames in $\mathbb{R}^3$, i.e. with ordered triples of orthonormal vectors $(\mathbf{x}, \mathbf{y}, \mathbf{x} \times \mathbf{y})$. The third unit vector $\mathbf{x} \times \mathbf{y}$ is redundant since it can always be reconstructed using the other two unit vectors. Therefore, triples of the form $(\mathbf{x}, \mathbf{y}, \mathbf{x} \times \mathbf{y})$ are in one-to-one correspondence with the pairs $(\mathbf{x}, \mathbf{y})$. Similarly, using the body axes previously defined in Figure 2-3, there is a one-to-one correspondence of the triple $(\mathbf{x}, \mathbf{y}, \mathbf{z})$ with the pair $(\mathbf{z}, \mathbf{x})$. The first unit vector $\mathbf{z}$ can be chosen arbitrarily, so it can be thought of as describing a sphere S^2 of unit radius inside $\mathbb{R}^3$, centered at the origin, in such a way that the tail of $\mathbf{z}$ begins at the origin, and its head describes S^2 as was seen in Figure 3-1. Once $\mathbf{z}$ has been chosen, the unit vector $\mathbf{x}$ is chosen in the normal plane to $\mathbf{z}$, so $\mathbf{x}$ can be thought of as describing a circle inside the tangent space to the sphere at the point prescribed by $\mathbf{z}$, that is inside $T_{\mathbf{z}}S^2$. Thus $SO(3)$ can be identified with the unit circle bundle $T_{S^1}S^2 \subset TS^2$. □

With the result of Proposition 1, a simple and effective motion trajectory for astronaut reorientation is possible using only two rotation primitives.

Theorem 3.1 (Motion Trajectory)**.** *Let the set $\mathcal{N}$ be the neutral positions of the astronaut, with the astronaut modeled as a rigid body having configuration space $SO(3)$. Then it is possible to reach any configuration starting and ending with an orientation in $\mathcal{N}$. Moreover, the sequence of motion primitives to complete such a task is always of the form $\mathcal{A} \circ \mathcal{B} \circ \mathcal{A}$.*

Proof. Define the initial orientation $i \in \mathcal{N}$, described by $(\mathbf{x}, \mathbf{y}, \mathbf{z})$, and the desired ending orientation $f \in \mathcal{N}$, described by $(\mathbf{x}', \mathbf{y}', \mathbf{z}')$. While the limb positions of i and f are the same, the orientation of the entire body with respect to the inertial reference frame is different. Then the sequence is:

1. $\mathcal{A}$ is performed, leading to a new configuration described by $(\tilde{\mathbf{x}}, \tilde{\mathbf{y}}, \mathbf{z})$. During this primitive, $\mathbf{x}$ is moved into the plane Π, generated by $\mathbf{z}$ and $\mathbf{z}'$.

2. $\mathcal{B}$ is performed to send $\mathbf{z}$ to $\mathbf{z}'$. The orientation after performing $\mathcal{B}$ is given by $(\tilde{\mathbf{x}}', \tilde{\mathbf{y}}', \mathbf{z}')$.

3. To complete the motion trajectory, it is sufficient to apply a motion primitive of class $\mathcal{A}$ in such a way as to rotate $\tilde{\mathbf{x}}'$ about $\mathbf{z}'$ to obtain the final configuration $(\mathbf{x}', \mathbf{y}', \mathbf{z}')$.

□

We formalize the magnitude of the rotations in this sequence in the following definition.

Definition 3.1 (Rotation Magnitudes)**.** *Given the motion plan $\mathcal{A}_1 \circ \mathcal{B}_2 \circ \mathcal{A}_3$, with initial orientation $(\mathbf{x}, \mathbf{y}, \mathbf{z})$, intermediate orientations $(\tilde{\mathbf{x}}, \tilde{\mathbf{y}}, \mathbf{z})$ and $(\tilde{\mathbf{x}}', \tilde{\mathbf{y}}', \mathbf{z}')$, and final orientation $(\mathbf{x}', \mathbf{y}', \mathbf{z}')$, the angle by which each primitive must rotate can be expressed as:*

1. $|\mathcal{A}_1| = \angle(\mathbf{x}, \Pi)$,
2. $|\mathcal{B}_2| = \angle(\mathbf{z}, \mathbf{z}')$,
3. $|\mathcal{A}_3| = \angle(\tilde{\mathbf{x}}', \mathbf{x}')$,

where the notation $|\mathcal{A}_1|$ implies the net rotation attained by performing $\mathcal{A}_1$, $\angle(\mathbf{x}, \Pi)$ implies the angle between $\mathbf{x}$ and Π, and Π is the plane generated by $\mathbf{z}$ and $\mathbf{z}'$.

Using this concatenation technique any orientation can be attained by rotating about $\mathbf{z}$ with $\mathcal{A}_1$, then rotating about $\mathbf{y}$ with $\mathcal{B}_2$, and finally rotating about $\mathbf{z}$ with $\mathcal{A}_3$.

3.2 Quantized Control Results

3.2.1 Implementation of the $\mathcal{A} \circ \mathcal{B} \circ \mathcal{A}$ Motion Trajectory

An example of a motion trajectory using the $\mathcal{A} \circ \mathcal{B} \circ \mathcal{A}$ sequence is given in Figure 3-2(a). From the initial orientation, the legs are rotated in a conical motion about axes parallel to $\mathbf{z}$, in the set of $\mathcal{A}$ motion primitives. Once the $\mathbf{x}$-axis of the body is in the desired Π plane, this rotation stops. The next stage in the sequence is to rotate about $\mathbf{y}$ until the body has the correct $\mathbf{z}'$. Finally, rotate about $\mathbf{z}$ one last time to achieve the desired orientation. While this method is not direct, it is simple and the sequence is the same regardless of final orientation. Consider the astronaut in Figure 3-2(b); the same procedure performed with different rotation magnitudes yields a very different final orientation.

3.2.2 Center of Mass Location

It is important to note that Proposition 1 assumes that the position of the total body center of mass with respect to the reference frame attached to the body, i.e., $J1$ from Figure 2-3, is the same for all motion primitives. While the total body center of mass oscillates during the defined rotations, the center of mass will be the same upon completion of the rotation if a full cycle of the motion is performed before it is stopped. In general, it is important to note that the center of mass of the body as a whole *cannot* move through the world reference frame. This means that if the total body center of mass was calculated with respect to $J0$,

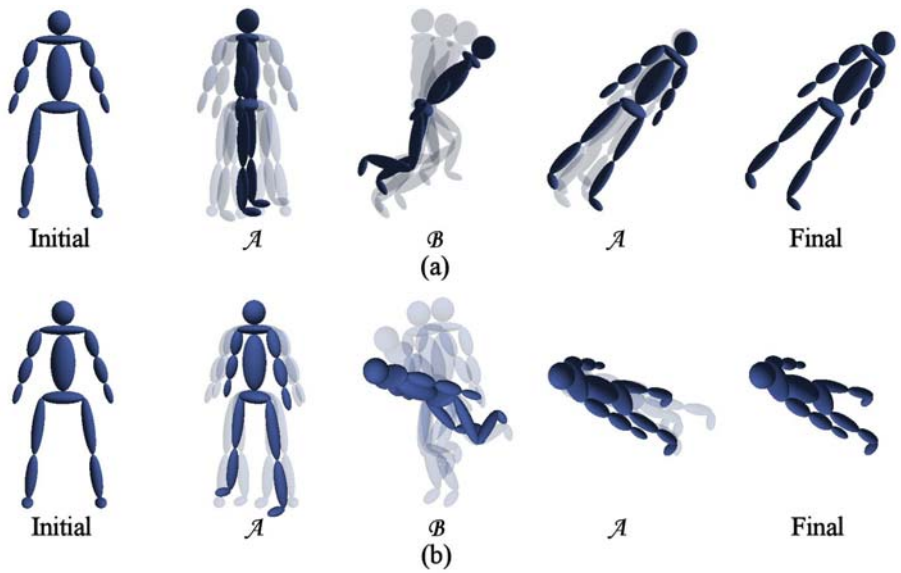

Figure 3-2: Two example trajectories using the sequence $\mathcal{A} \circ \mathcal{B} \circ \mathcal{A}$. The magnitudes of the rotations in (a) are $|\mathcal{A}_1| = 90$ degrees, $|\mathcal{B}_2| = 45$ degrees, and $|\mathcal{A}_3| = 30$ degrees, while in (b) are $|\mathcal{A}_1| = 45$ degrees, $|\mathcal{B}_2| = 70$ degrees, and $|\mathcal{A}_3| = 60$ degrees.

the joint representing the inertial frame, it would remain constant for the entire maneuver. This directly follows from conservation of linear momentum.

If one were to stop a rotation before a full cycle was completed and return to the neutral position, a slight difference in the orientation of the body would result depending on where in the cycle the rotation was stopped. An analysis of the resulting off-axis rotations was performed for $\mathcal{A}$ and $\mathcal{B}$. The change in the off-axis rotations was determined using a neutral position with the arms down near the body and the legs straight. A dynamic simulation was performed with the body moving from the neutral orientation to that of the rotation. One cycle of the rotation was performed, followed by a return to the neutral position. The motion from the neutral position to the initial orientation was calculated using a spherical linear interpolation, generally referred to as slerp (additional information about slerp is given in Appendix A). For motion primitive $\mathcal{A}$ with legs inclined 8.5 degrees from the vertical, the off-axis rotations, i.e., those that create pitch and roll motions, varied less than a degree from those seen when a full cycle was performed. For motion primitive $\mathcal{B}$, the off-axis rotations, which in this case consist of roll and yaw, were larger than seen for $\mathcal{A}$. This is because the leg motions for this maneuver are less symmetric about the principal axes of the body. However, the off-axis rotations were still not significant, with all varying less than three degrees from those seen when a full cycle was performed.

3.2.3 Comparison of x Rotations

The single-axis rotation given in Definition 2.1 and Figure 2-14 was selected as the simplest single-axis roll ($\mathbf{x}$) maneuver. This primitive is significantly more complicated to perform than the pitch ($\mathbf{y}$) or yaw ($\mathbf{z}$) motion primitives. Fortunately a roll rotation can also be achieved using the $\mathcal{A} \circ \mathcal{B} \circ \mathcal{A}$ sequence of motion primitives. If a positive 90-degree roll is desired, the astronaut would perform $\mathcal{A}$ until s/he has rotated a positive 90 degrees, then perform a 90-degree rotation using $\mathcal{B}$, and finally another 90-degree rotation using $\mathcal{A}$. The concatenation of motion primitives yields a maneuver that is mentally and physically easier to perform.

The question becomes, how do the times to perform the rotations compare? In order to have a comparison under realistic conditions, the rotational speeds for each motion primitive were estimated from the experiments as 2 cycles/sec for $\mathcal{A}$ and $\mathcal{B}$ and 1 cycle/sec for $\mathcal{C}$. The simulation dynamics were then used to determine the overall maneuver time. Performing $\mathcal{C}$ at 1 cycle/second yields a 90-degree rotation in 12 seconds. Performing $\mathcal{A}$ at 2 cycles/second with the legs inclined 8 degrees away from the body yields a 90-degree rotation in 3 seconds. Performing $\mathcal{B}$ at 2 cycles/second with a rotational diameter of 0.54 meters yields a 90-degree rotation in 6 seconds. This results in a total maneuver time of 12 seconds to perform a 90-degree roll using the $\mathcal{A} \circ \mathcal{B} \circ \mathcal{A}$ concatenation. Thus, the concatenated rotation time is comparable to that of the single-axis rotation, while being simpler to perfect.

3.2.4 Robustness of Motion Plans

Perfect performance cannot always be expected by the astronaut executing the maneuvers. Therefore, it is important to discuss perturbations to the motion primitives. Since there are no external torques, when the rotation ceases no additional motion will be present. If at any time the astronaut feels unstable or unsure, or the perturbation to the motion maneuvers are large, there is no risk of an uncontrolled divergence from the desired trajectory. In these cases, the motion plan can be restarted based on the actual orientation. Consider an error in the performance of $\mathcal{A}$ of size ϵ and call the perturbed rotation $\mathcal{A}_\epsilon$. If the astronaut becomes aware of this error upon completion of $\mathcal{A}_\epsilon$, the error can be removed by performing a correction rotation, $\mathcal{A}_{\text{corr}}$, and then completing the rest of the maneuver. In this situation the sequence becomes $\mathcal{A}_\epsilon \circ \mathcal{A}_{\text{corr}} \circ \mathcal{B} \circ \mathcal{A}$. If the error is not sensed until the completion of $\mathcal{B}$, then one simply has to restart the sequence with modified rotation magnitudes as shown in Figure 3-3.

The motion sequences obtained through this method are robust to errors as long as the appropriate sensory feedback is obtained and correctly interpreted by the central nervous system. A schematic of this feedback loop is shown in Figure 3-4. The observability of the output is determined by the sensory signals available. If there are problems in this feedback loop, then the propagation of the errors can be found by evaluating a metric that determines the difference between two rotations. An example of such a metric would be to

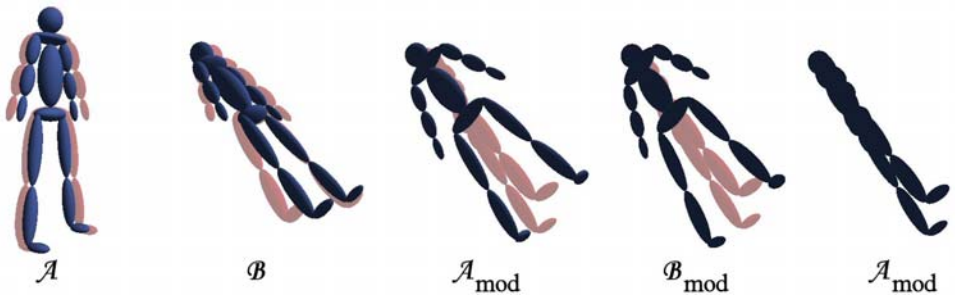

Figure 3-3: An example trajectory of the form $\mathcal{A}_\epsilon \circ \mathcal{B} \circ \mathcal{A}_{mod} \circ \mathcal{B}_{mod} \circ \mathcal{A}_{mod}$. The desired magnitudes (shadows) were $|\mathcal{A}_1| = 45$ degrees, $|\mathcal{B}_2| = 45$ degrees, and $|\mathcal{A}_3| = 45$ degrees. The actual magnitudes were $|\mathcal{A}_1| = 60$ degrees, $|\mathcal{B}_2| = 45$ degrees, $|\mathcal{A}_3| = 84.7$ degrees, $|\mathcal{B}_4| = 10.6$ degrees, and $|\mathcal{A}_5| = 50.3$ degrees.

determine the rotation matrix for the desired orientation, R_d, and the rotation matrix for the actual orientation, R_a, and calculate the difference between the two as

$$d(R_d, R_a) = \sum_{i=1}^{3} \sum_{j=1}^{3} |R_d(i,j) - R_a(i,j)|\,, \tag{3.1}$$

where the notation (i, j) indicates the entry in row i and column j. This metric leads to bounded errors when ϵ is small [8].

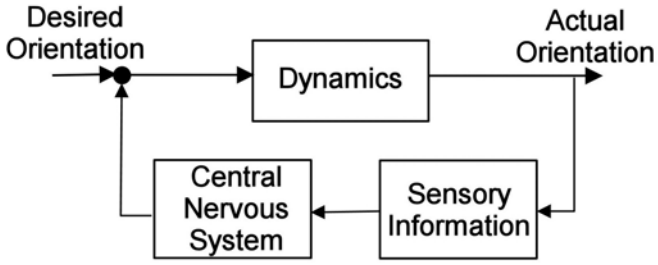

Figure 3-4: A schematic of the motion planning feedback loop.

3.2.5 External Spin Control

The rotations considered to this point have had the astronaut start and end with zero angular velocity. Now consider the case where the astronaut finds him/herself spinning out of control. The problem is now to bring the astronaut to a spin that is about a primary axis, or if possible, the complete removal of the spin. In Equation (2.7), zero initial angular moment was assumed. This equation must be modified such that

$$\sum_{i \in B} R_i^0 I_i \boldsymbol{\omega}_{L_i} + \mathbf{r}_{0,cm_i} \times R_i^0 m_i \mathbf{v}_{cm_i} \quad = \quad \mathbf{H_{init}}, \tag{3.2}$$

where $\mathbf{H_{init}}$ is the initial angular momentum of the system. For simplicity, the zero translational motion assumption is maintained. $\mathbf{H_{init}}$ can be written as

$$\mathbf{H_{init}} = \sum_{i \in B} R_i^0 I_i \boldsymbol{\omega}_{ext}, \tag{3.3}$$

where $\boldsymbol{\omega}_{ext}$ is the external angular velocity of the system.

Given an initial spin composed of a single angular velocity, it is simple for the astronaut to determine his/her spin direction if appropriate visual stimuli are available, or vestibular stimuli if the spin has not exceeded approximately 10 seconds. If the rotation is about $\mathbf{z}$ or $\mathbf{y}$, then $\mathcal{A}$ or $\mathcal{B}$ can be performed at a rate that will eliminate the external spin. If the rotation is about $\mathbf{x}$, then one solution is to perform $\mathcal{A}$ until the astronaut has rotated 90 degrees. The resulting external spin yields a rotation about $\mathbf{y}$ that can be eliminated using the motion primitive $\mathcal{B}$.

If the initial spin is composed of angular velocities about multiple axes, there are several possible solutions depending on the complexity of the spin. If the astronaut senses a rotation about $\mathbf{y}$ and $\mathbf{z}$, $\mathcal{A}$ can be performed to remove the $\mathbf{z}$ rotation, then only a $\mathbf{y}$ rotation remains. However, if the astronaut combines an arm rotation about $\mathbf{y}$ with the leg rotation about $\mathbf{z}$, then s/he can completely remove the spin.

The removal of any external spin depends highly on the astronaut's ability to sense the motion. Otherwise the needed corrections are unknown. For these techniques to be applicable to complex uncontrolled spins, it would be recommended that at a minimum astronauts receive training on the removal of simplified spins.

3.3 Optimization Methodology

Thus far the derivation of the motion primitives has been based on obtaining simple-to-perform motions that yield a reorientation of the astronaut. In this section an optimization method is presented that allows the motion primitives to be evaluated in a formalized manner. The optimization methodology also permits a more generalized motion parameterization that can be implemented to obtain astronaut self-rotations.

3.3.1 Optimization Formulation

The structure of the optimization is shown schematically in Figure 3-5. Given a set of parameters that define the motion, which will be discussed in more detail shortly, the kinematics and dynamics, and thus the objective function and constraints, can be calculated. If the stopping criteria are not met, then the parameters that define the motion are modified and the cycle repeats. The stopping criteria and update method depend on how the optimization is implemented. This analysis solves the optimization problem using a Sequential Quadratic Programming (SQP) method.

The development of an appropriate objective function is key to obtaining realistic rotations. A kinematic objective function that minimized the jerk squared of the hand trajectory was shown to accurately predict several testable characteristics of point-to-point motion in two-dimensional planar arm movements [35], and provides a good starting point for the kinematic term in the objective function. There are several dynamic properties that have been implemented in motion planning, including minimizing the joint torque, the square of the torque, and the change in torque over time. If a minimization of energy is considered for obtaining the astronaut maneuvers, then the torque squared appears to be the natural choice for an initial dynamics term. The problem statement can be formalized as

$$\min_{\mathbf{c}\in\mathcal{C}} J = \underbrace{\frac{1}{2}w_1 t_f^2}_{\substack{\text{final time}\\ \text{penalty}}} + \frac{1}{2}\int_0^{t_f} \left[\underbrace{w_2 \mathbf{\Gamma}^T \mathbf{\Gamma}}_{\substack{\text{dynamics}\\ \text{penalty}}} + \underbrace{w_3 \ddot{\boldsymbol{\omega}}_J^T \ddot{\boldsymbol{\omega}}_J}_{\substack{\text{kinematic}\\ \text{penalty}}} \right] dt \tag{3.4}$$

such that:

$$\dot{\bar{\mathbf{q}}}_{J_1} = Q(t, \bar{\mathbf{q}}, \boldsymbol{\omega}_J), \tag{3.5}$$

$$\mathbf{\Gamma} = T(t, \bar{\mathbf{q}}, \boldsymbol{\omega}_J, \dot{\boldsymbol{\omega}}_J), \tag{3.6}$$

$$\bar{\mathbf{q}}_{J_1}(0) = \bar{\mathbf{q}}_{J_{1,init}}, \tag{3.7}$$

$$\Theta_{min} \leq \Theta(t_f) \leq \Theta_{max}, \tag{3.8}$$

$$\Psi_{min} \leq \Psi(t_f) \leq \Psi_{max}, \tag{3.9}$$

$$\Phi_{min} \leq \Phi(t_f) \leq \Phi_{max}, \tag{3.10}$$

$$\bar{\mathbf{q}} \in \mathcal{Q}, \tag{3.11}$$

$$\angle\mathcal{L} \neq \pi, \tag{3.12}$$

$$\mathbf{\Gamma}_{min} \leq \mathbf{\Gamma} \leq \mathbf{\Gamma}_{max}. \tag{3.13}$$

The objective function is defined as an integral over a time horizon, t_f, of a dynamic and kinematic penalty with a final time penalty. These terms are weighted with respect to each other with the scalars w_1, w_2 and w_3. The optimization is performed over the parameterization variables $\mathbf{c} \in \mathcal{C}$, which are defined in Section 3.4. The initial orientation of the body with respect to the inertial frame, $\mathbf{q}_{J_{1_{init}}}$, is specified through Eq. (3.7).

The first and second constraints, Eqs. (3.5) and (3.6), are the equations representing the dynamics and torques, respectively, and were defined in Section 2.1.2. In solving the optimization, these two constraints were eliminated by incorporating them into the objective function. Equations (3.8)–(3.10) are the limitations on the final orientation of the body with respect to the inertial frame. While the quaternion parameterization is a good choice for evaluating the dynamics, the final orientation is easier to interpret if the Euler angle representation is used. The pitch (Θ), yaw (Ψ), and roll (Φ) of the body are defined as

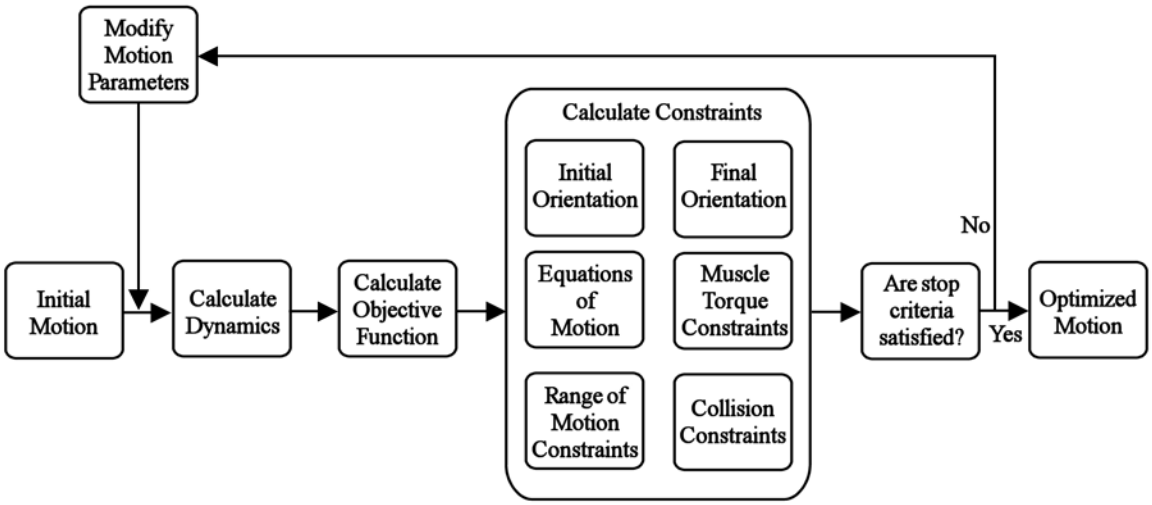

Figure 3-5: The structure of the astronaut motion control optimization problem.

rotations about $\mathbf{y}$, $\mathbf{z}$, and $\mathbf{x}$, respectively, and can be found from the quaternion orientation of the root joint, $\mathbf{q}_{\mathbf{r}J_1} = [q_1\ q_2\ q_3\ q_4]$, as

$$\Theta = \sin^{-1}\left(-2\left(q_2 q_4 - q_1 q_3\right)\right), \tag{3.14}$$

$$\Psi = \tan^{-1}\left(\frac{2\left(q_2 q_3 + q_1 q_4\right)}{q_1^2 + q_2^2 - q_3^2 - q_4^2}\right), \tag{3.15}$$

$$\Phi = \tan^{-1}\left(\frac{2\left(q_3 q_4 + q_1 q_2\right)}{q_1^2 - q_2^2 - q_3^2 + q_4^2}\right). \tag{3.16}$$

The limitation on the quaternion orientations, given by Eq. (3.11), is equivalent to setting the range of motion of the joints. While limiting one-DOF joints can be expressed as an inequality constraint, limiting the three-DOF joints is expressed as a limit on the swing and twist components of the joint orientation [11]. The decomposition of the quaternion to the swing and twist components was presented in Section 2.3. To ensure that there are no collisions between the links, constraints are defined as in Eq. (3.12). This equation represents a modification to the object bounding box method presented in Section 2.4 such that the constraint is differentiable (discussed further in Section 3.3.2). The final constraint, Eq. (3.13), is the limitation on the joint torques and is determined by the available muscle torques, which were found using the Software for Interactive Musculoskeletal Modeling (SIMM) environment [1]. The implementation of the muscle model is described in Section 3.3.3.

3.3.2 Collision Constraints

As discussed in Section 2.4, collisions can be detected using the OBB method, where all fifteen equations expressed by Eq. (2.19) must be violated for a collision to occur. As

currently posed, this is not a differentiable constraint. To improve the optimization design space, all constraints should be differentiable. This quality can be obtained by formulating the collision equations in the complex plane.

If we rearrange Eq. (2.19), we obtain

$$\mathcal{L}_k \equiv |\mathbf{s} \cdot \mathbf{T}_A \mathbf{T}_B| - \sum_{i=1}^{3} a_i |\mathbf{s}_k \cdot \mathbf{e}_i| - \sum_{i=1}^{3} b_i |\mathbf{s}_k \cdot \mathbf{f}_i| > 0, \qquad k = 1, ..., 15. \tag{3.17}$$

These fifteen equations must be combined so as not to lose the information about the sign of the equation for this to become differentiable. In the complex plane each equation has a magnitude and an angle. Since the value of Eq. (3.17) yields a real number, the angles will either be 0 or π. Now define

$$\mathcal{L} \equiv \prod_{k=1}^{15} (\mathcal{L}_k)^{1/15}. \tag{3.18}$$

By taking the fifteenth root, sign information is retained about each of the fifteen equations. If a collision occurs, the angle for all fifteen equations is π, which means that the angle of $\mathcal{L}$ is π. If there is one constraint that has a positive value, then the angle of $\mathcal{L}$ will be a value other than π. Then the collision constraint becomes

$$\angle \mathcal{L} \neq \pi, \tag{3.19}$$

as shown in Eq. (3.12). As the angles range from 0 to π, this constraint was implemented computationally as

$$\pi - \angle \mathcal{L} > \epsilon, \tag{3.20}$$

where ϵ is small.

3.3.3 Muscle Torque Constraints

While the muscle model developed in Section 2.5 was initially included in the constraints, typical solutions yielded torques much smaller than the maximal torques available. A savings in computational time during each iteration of the optimization process was obtained by removing the muscle model from the run-time constraints. The muscle torques were checked prior to and after each complete optimization to verify that they were in range and that the force-velocity assumption was still valid.

3.3.4 Scaling the Optimization Problem

The relative scaling between the optimization design variables can have a significant effect on the outcome of the optimization when implementing a gradient-based algorithm. The

optimization problem should be scaled with respect to its variables so that they have similar magnitudes, as large differences in their order of magnitude will result in ill-conditioning of the Jacobian and Hessian, which can make algorithmic calculations unstable or inefficient [43,85]. The simplest method to improve the conditioning of the Hessian is to use a diagonal scaling of the design variables based on the Hessian evaluated at the initial design point. As the best-conditioned matrix is the identity, selecting $H^{1/2}$ as the scaling, where H is the Hessian, will yield the identity for the initial step of the optimization. This is shown for the current problem by defining the scaled design variables, $\bar{\mathbf{c}}$ as

$$\bar{\mathbf{c}} = \Lambda \mathbf{c}. \tag{3.21}$$

where Λ is a diagonal matrix. The gradient of the objective function with respect to the unscaled parameters is then

$$\frac{dJ}{d\mathbf{c}} = \frac{dJ}{d\bar{\mathbf{c}}}\Lambda, \tag{3.22}$$

where J is the objective function defined in Eq. (3.4). The Hessian of the objective function is

$$\frac{d^2J}{d\mathbf{c}^2} = \Lambda^T \frac{d^2J}{d\bar{\mathbf{c}}^2}\Lambda. \tag{3.23}$$

Thus the diagonal components of Λ are the square-root of the unscaled Hessian's diagonal. While this is not an optimal strategy for rescaling the problem, it is commonly recommended [85].

3.4 Motion Parameterization

The implementation of the optimization methodology requires the determination of control parameters that define the astronaut motion over time. There are many examples of B-Spline parameterization of joint angles, velocities, and accelerations in the computer graphics community for motion development [68,69,102]. However, certain motions, such as the continuous rotary motions, can be difficult to obtain with these methods. Additionally, if the spline control points are not selected properly, unrealistic motions can result.

In this section, parameterizations that are appropriate for the self-rotation maneuvers are presented. The first two parameterizations are general and permit motions that fall under the category of continuous rotary and limb manipulation motions. These parameterizations were selected to be continuous functions so that the derivatives could be taken to obtain the velocity, acceleration, and jerk. Developing these parameterizations also involves understanding the structure of the quaternions. Recall that the quaternion can be interpreted as $\mathbf{q} = [\cos\left(\frac{\theta}{2}\right) \ \sin\left(\frac{\theta}{2}\right)\mathbf{e}]^T$, where θ is the angle about the fixed unit-axis

$\mathbf{e} = [e_1\ e_2\ e_3]^T$. The implementation of a one-DOF joint is simple; the parameterization is performed on θ. For a three-DOF joint, the parameterization is defined over each component of the quaternion, $\mathbf{q} = [q_1\ q_2\ q_3\ q_4]^T$, and then the resulting vector is normalized. The final parameterization is more restrictive of the design space in that it characterizes the motion primitives such that the essential features of the rotation are the control parameters. The quaternion orientations are then calculated for the selected control parameters.

3.4.1 Continuous Rotary Motion

The natural choice for approximating a periodic motion is a sine curve. With this form, a repetitive motion can occur over time with a minimal number of control parameters. The parameterization is then

$$P = C_1 \sin(C_2 t + C_3) + C_4, \tag{3.24}$$

with $\mathbf{c} = [C_1\ C_2\ C_3\ C_4]$ the vector of independent constants that define the motion over time, t. For a one-DOF joint, $\theta = P$, and there are four independent constants. Each three-DOF joint has 16 independent constants and is expressed as

$$\mathbf{q} = \frac{[P_1\ P_2\ P_3\ P_4]}{\sqrt{(P_1^2 + P_2^2 + P_3^2 + P_4^2)}}, \tag{3.25}$$

where the four parameters P_1, P_2, P_3 and P_4 are each represented with a function of the form Eq. (3.24). When parameterized in this form, the model has 152 control parameters.

3.4.2 Limb Manipulation Motion

A limb manipulation is performed by moving the limb from the original position to a modified orientation and then back to the original position. Figure 3-6 shows an example of this type of motion for elbow flexion, with the angle starting at zero degrees, increasing to 45 degrees, and then returning to zero degrees. The continuous function that represents this three-part motion is now developed.

The joining of several functions together, while maintaining continuity, can be attained with the log function. The curve resulting from joining functions will be termed the blend. In general, two blends are possible when combining curves, an upper blend and a lower blend. Figure 3-7 shows an example of the upper and lower blend when combining $y_1 = x$ and $y_2 = -x$.

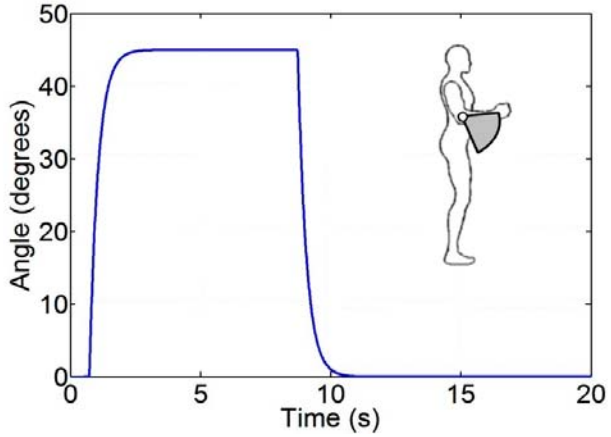

Figure 3-6: An example of the limb manipulation parameterization for a one-DOF joint.

The upper curve is obtained with the equation

$$B_u = \log\left(e^{y_1} + e^{y_2}\right) \tag{3.26}$$

and the lower curve is obtained with the equation

$$B_l = -\log\left(e^{-y_1} + e^{-y_2}\right). \tag{3.27}$$

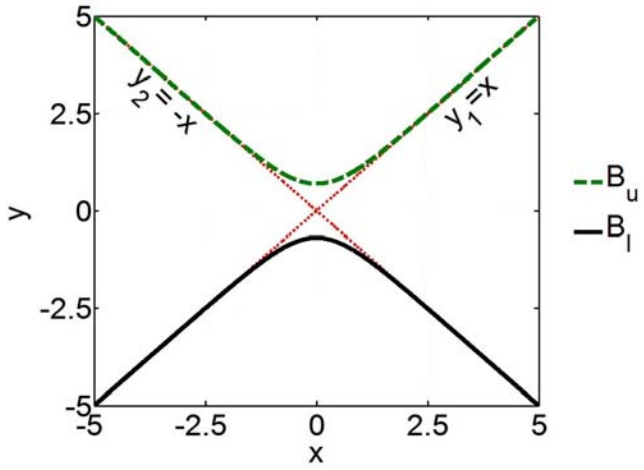

Figure 3-7: An example of two curves ($y_1 = x$ and $y_2 = -x$) being joined using the log function.

For the limb manipulation motions, the three functions joined were a constant, an exponential increase from the initial value, and an exponential decrease back to the initial value. The blending technique is different depending on whether the function increases or decreases from the initial condition. This change occurs because of the blends needed to join the functions. For a motion that increases from the initial condition, the first two curves are

combined using an upper blend. Then the final curve is obtained using a lower blend. For a motion that decreases from the initial condition, the first two curves are combined using a lower blend first, followed by an upper blend. If the curves to be blended are defined as x_1, x_2, and x_3, the first blend as B_1 and the second blend as B_2, then for a motion that has an increase from the initial condition,

$$\begin{aligned} x_1 &= C_{10}, \\ x_2 &= C_{20} - C_{21}e^{-C_{22}t}, \\ x_3 &= C_{30} + C_{31}e^{-C_{32}t}, \\ B_1 &= \log\left(e^{x_1} + e^{x_2}\right), \\ B_2 &= -\log\left(e^{-B_1} + e^{-x_3}\right) + A, \end{aligned} \tag{3.28}$$

and for a motion that decreases from the initial condition,

$$\begin{aligned} x_1 &= C_{10}, \\ x_2 &= -C_{20} - C_{21}e^{-C_{22}t}, \\ x_3 &= C_{30} - C_{31}e^{-C_{32}t}, \\ B_1 &= -\log\left(e^{-x_1} + e^{-x_2}\right), \\ B_2 &= \log\left(e^{B_1} + e^{x_3}\right) + A. \end{aligned} \tag{3.29}$$

The value A is calculated such that the initial and final value are equivalent to C_{10}; and the value C_{30} is calculated such that the initial and final value are equivalent. The vector of independent constants that specifies this motion over time is $\mathbf{c} = [C_{10}\ C_{20}\ C_{21}\ C_{22}\ C_{31}\ C_{32}]$. The determination of whether a motion is an increase or decrease from the initial condition comes from the sign of C_{21}. Then, the parameterization equation is expressed as

$$P = \begin{cases} -\log\left(e^{-B_1} + e^{-x_3}\right) + A, & \text{if } C_{21} > 0 \\ \log\left(e^{B_1} + e^{x_3}\right) + A, & \text{if } C_{21} < 0 \end{cases} \tag{3.30}$$

Again, we have that each one-DOF joint is specified as $\theta = P$, and each three-DOF joint is specified as given in Eq. (3.25). In this parameterization, each one-DOF joint has six control parameters and each three-DOF joint has 24 control parameters, for a total of 228 control parameters. An example trajectory with this parameterization was shown in Figure 3-6. The properties desired in the function are apparent—the initial and final condition are the same, there is an exponential rise, a hold of position, and an exponential decrease.

3.4.3 Motion Primitive Parameterization

The final parameterization examined characterizes the important features of a motion primitive. With this parameterization, the motion primitives can be brought into the optimiza-

tion framework. For this analysis consider the primitives implemented in Section 3.1. Then, the parameters that can be varied in the motion primitives, $\mathcal{A}$ and $\mathcal{B}$, are defined in Figure 3-8. For $\mathcal{A}$, the parameterization contains the leg inclination angle (the angle the leg is inclined away from the body), leg rotational velocity (the velocity at which the leg rotates about the offset **z**-axis), and arm inclination angle (the angle the arm is inclined away from the body). Since the leg inclination angle can be positive or negative, the initial leg position can be into or away from the body. Further, since this parameter is defined for each leg, motions that are in-phase and out-of-phase are possible to analyze. For motion primitive $\mathcal{B}$ the control parameters are the pedal radius (the radius of the imaginary circle the feet trace), pedal offset (the location of the center of imaginary circle with respect to the hip location), and pedal velocity (the velocity at which the feet trace the circle). The legs are assumed to be 180 degrees out-of-phase as is typical when riding a bicycle.

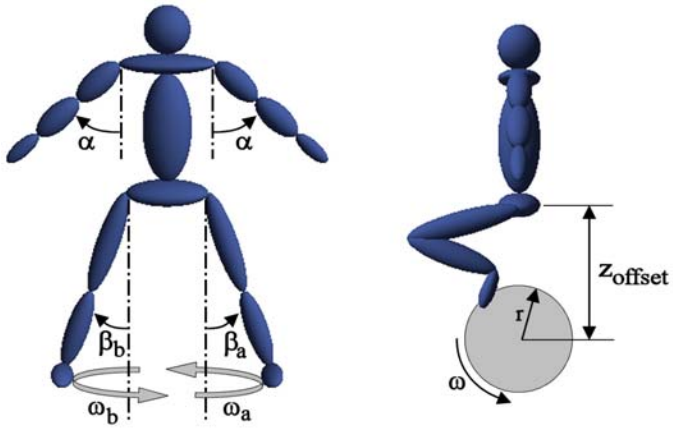

Figure 3-8: Motion primitive parameterization for use in the optimization framework.

3.5 Optimization Results

When implementing the motion parameterizations presented in the previous section, a balance needs to occur between allowing a general motion and constraining the motion complexity of the solution. With a general parameterization, such as that for creating the continuous rotary and limb manipulation rotations, solutions that are cognitively complex to perform can result. With a restricted design space more information can be gained on specific motion maneuvers, but the ability to achieve qualitatively unique motions is lost. This section will first present results from the more restrictive parameterization, followed by the more general parameterizations.

3.5.1 Motion Primitive Parameterization

Motion Primitive $\mathcal{A}$

The effects of the penalty terms in the objective function on the solution were determined by varying the weighting parameters. Figure 3-9 shows the variation in the dynamic and kinematic penalty term of the objective function for motion primitive $\mathcal{A}$. The dynamic penalty was found by varying w_1 and w_2 with w_3 set to zero in Eq. (3.4). The kinematic penalty was found by varying w_1 and w_3 with w_2 set to zero in Eq. (3.4). The desired net rotation was a positive 90 degrees about **z**.

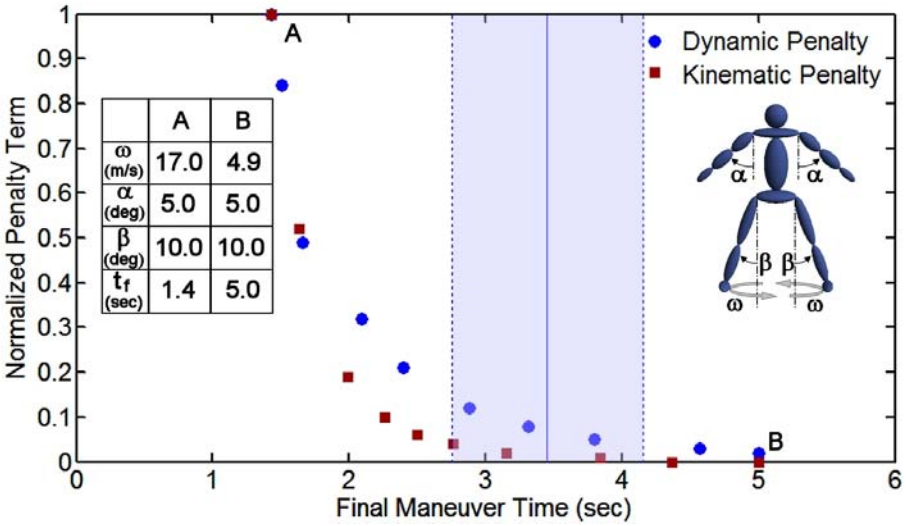

Figure 3-9: Effect of modifying the weighting parameters on the kinematic and dynamic penalty terms for motion primitive $\mathcal{A}$. The shaded region indicates results obtained from actual human reorientation experiments.

In this formulation, both the dynamic and kinematic penalty led to solutions that have the arms close to the body with out-of-phase leg motions that have the maximum allowable leg angle such that there were no collisions. The differences between the solutions when varying the weighting parameters were the leg velocity and final motion time. As w_1 was increased with respect to w_2 or w_3, the final performance time decreased, with an increase in the penalty term of the objective function. These results follow as in-phase motions yield greater off-axis rotations, which require larger torques to stabilize the joints. Similarly, holding the arms close to the body reduces the total body inertia with respect to the axis of rotation, yielding a lower energy. The original selection of an out-of-phase leg motion for the primitive is supported by the current optimization. It is important to note that while all the solutions presented in Figure 3-9 are feasible to perform based on the model assumptions, the solutions found approaching minimum time also approach the limit of the available muscle torque and the effects of muscle velocity could become significant.

By breaking down the components of this motion primitive, the similarity of the kinematic term to the dynamic term can be considered in more detail. For a given rotational velocity without any final orientation constraints, the minimum jerk solution yields a minimum leg inclination angle. However, when the leg inclination angle decreases, the net rotation also decreases. Therefore, when the final orientation constraint is included, the velocity would have to increase. The increase in the kinematic term is greater with an increase in velocity than it is for a decrease in leg inclination angle. Thus in this environment, with this parameterization, the salient features of the motion are the same whether a dynamic or kinematic function is implemented.

While the characteristic of the solutions are similar, the balance with the final time penalty differed. The dynamic penalty with respect to the final time showed a gradual increase as w_1/w_2 was increased and the kinematic penalty showed a more pronounced bend in the curve as w_1/w_3 was increased. As the solutions are the same between the two methods, the difference was not due to the optimized solution, but to the normalization of the penalty terms. The ratio of the maximum to minimum kinematic penalty was greater than the ratio of the maximum to minimum dynamic penalty.

The solution implemented in a real scenario can be determined by experiment. In Chapter 4, the average steady state performance time for a 180-degree rotation for the group trained with this maneuver was 6.9 $\pm$ 1.4 sec. The subjects were instructed to perform the rotations at a comfortable pace. The corresponding final times for a rotation of 90 degrees are shown as the shaded region in Figure 3-9. The rotations implemented by the subjects yielded times that were prior to the large penalty increase seen in Figure 3-9.

Motion Primitive $\mathcal{B}$

For motion primitive $\mathcal{B}$, two additional constraints were added to the problem formulation given by Eqs. (3.4)-(3.13). The first new constraint enforced that the motion be feasible based on the respective leg length. This was written as

$$r + z_{\text{offset}} \leq L, \tag{3.31}$$

where r and z_{offset} are the radius and offset of the traced circle defined in Figure 3-8 and L is the total leg length. The second new constraint simplifies the SIMM evaluation for Eq. (3.13) as this constraint cannot only be examined prior to and after each run for this primitive. All of the geometric constraints affect the generation of torque at the joints. The torques increase with an increase in radius, increase in rotational velocity, and decrease in offset (i.e., as the rotation gets closer to the center of mass). To incorporate these trends without using SIMM during runtime, a linear fit was implemented relating the maximum allowable speed, the pedal radius, and the pedal offset as

$$\omega + Ar + Bz_{\text{offset}} \leq C, \tag{3.32}$$

where A, B, and C were found with SIMM and the dynamics model.

Unlike motion primitive $\mathcal{A}$, the dynamic and kinematic penalty terms yielded different solutions as shown in Figure 3-10. While both the minimization of the dynamic and kinematic penalty imply increasing the pedal offset, decreasing the pedal velocity, and decreasing the pedal radius, the balance between these parameters is slightly different. The dominant parameter in the dynamic penalty was the pedal velocity. The dynamically optimized solutions reduced this parameter and extended the legs as far as possible. However, the kinematic penalty was influenced by the pedal radius to a greater extent than the dynamic penalty. Consequently, the kinematically optimized solution had a smaller radius and an increased velocity when compared to the dynamically optimized solution. When w_1 was zero, the dynamic and kinematic solutions both used the maximum allowable performance time as this admitted solutions with lower pedal velocities.

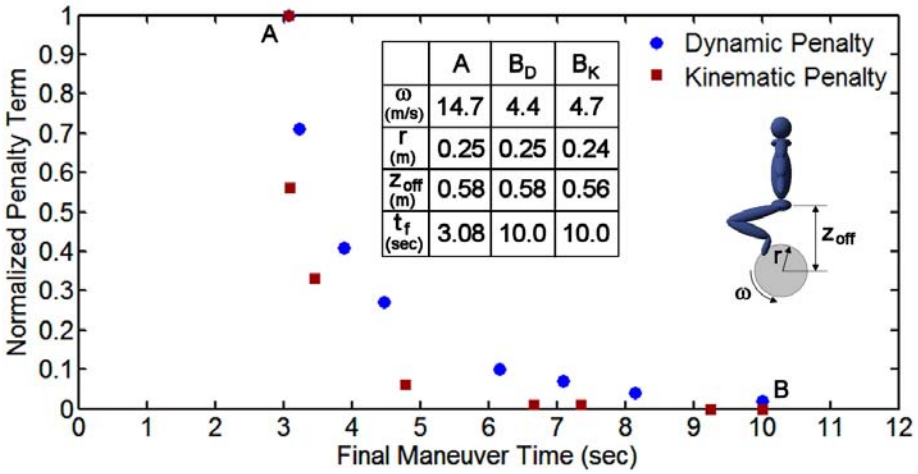

Figure 3-10: Effect of modifying the weighting parameters on the kinematic and dynamic penalty terms for motion primitive $\mathcal{B}$. ($\mathrm{B_D}$ implies point B for the dynamic penalty and $\mathrm{B_K}$ implies point B for the kinematic penalty.)

If the constraint defined in Eq. (3.32) had been removed, the solution would have maximized the velocity and the radius parameters and minimized the pedal offset as w_1/w_2 or w_1/w_3 were increased. With the inclusion of this constraint, the maximum radius cannot be implemented with the maximum attainable velocity and minimum pedal offset. Thus, the optimized solutions balance increasing the velocity with increasing the radius and decreasing the pedal offset. The radius design variable is also highly dependent on the knee's range of motion—as the radius increases, the knee angle must increase. The design variable z_{offset} was also limited by the knee's range of motion. While the dynamic and kinematic penalty could be reduced by increasing z_{offset}, the length of the leg limited how far it could extend. Similarly, the radius of the rotation coupled with the available knee's range of motion limited how close to the body the motion could be performed. The effect of the

weighting parameters for motion primitive $\mathcal{B}$ are shown in Figure 3-10.

These results cannot be as easily compared to the experimental results as done for $\mathcal{A}$. The main reason is that the constraint on the knee's range of motion, which was based on NASA's Constellation program requirements, is more restrictive than seen during the experiments. As shown in Figure 3-11 for the dynamic penalty term, the penalty curve with respect to the final maneuver time changes when the knee range of motion was increased. The difference between curves was not just a shift over time, but a difference in the optimized solution design variables. The increase in the knee's range of motion makes the constraint on the knee angle less restrictive than the constraint given by Equation (3.32). This leads to a minimum maneuver time solution for the increased range of motion that has a lower speed, greater final radius, and decreased pedal offset. As the ratio $w1/w2$ was varied, the increase in maximum knee angle permitted a slower motion for all weighting ratios yielding a reduction in the torque and a delay in the rise of the penalty term.

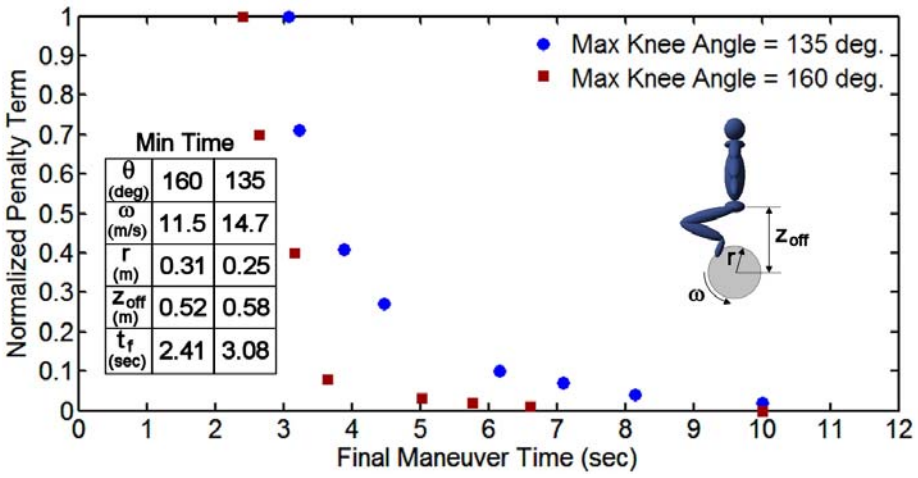

Figure 3-11: Effect of modifying the knee range of motion and the weighting parameters for the dynamic penalty term for motion primitive $\mathcal{B}$.

In addition to having an increased knee range of motion, subjects tended to perform the maneuver by tracing a more elliptical than circular shape. This natural modification allowed for a greater inertia change, making each cycle more effective. This execution style allowed the subjects to trace larger areas than they could have naturally performed with the circular implementation of the motion primitive.

3.5.2 Alternative Parameterizations

The importance of rotation complexity becomes a dominant factor in whether or not the maneuver is feasible when a more general parameterization is implemented as there are fewer restrictions in the design space. For example, Figure 3-12 shows a solution that was obtained using the continuous rotary motion parameterization examining only the dynamic

penalty, i.e., with $w_1 = 0$, $w_2 = 1$, and $w_3 = 0$. The initial motion was that given in Definition 2.5 and the final desired rotation was 90 degrees about $\mathbf{z}$. The off-axis rotations were limited to be ± 5 degrees from the nominal orientation. This problem statement led to a solution with the arms rotating at different frequencies, about different axes, and in different rotational directions. The optimized motion reduced the dynamic penalty by rotating the right arm at an offset axis, with the left arm rotating to correct for the off-axis motions. While this solution solves the given problem, it is not feasible for a person to perform. One way to avoid this problem is to add constraints such that motion complexity is reduced; but care must be taken as the addition of too many constraints will lead to a solution where only an adaptation of the initial motion is obtained.

Figure 3-12: An example of an optimized motion using the continuous rotary motion parameterization.

Yet certain solutions obtained from the more general parameterizations can yield results that offer insight into motion control strategies. Figure 3-13 shows an example of the initial and optimized motions when examining the dynamic penalty term for the motion described in Definition 2.6. The desired orientation was 20 degrees about $\mathbf{z}$ with off-axis rotations limited to be ± 5 degrees. There are several important characteristics of minimum energy motion that can be obtained from these results. For this particular motion, the angle of the hip was decreased and the angle of the knee was slightly increased. These changes decrease the inertia of the lower body, thus requiring less torque when the rotation about the waist is performed. During the optimized solution, the arms also do not fully extend when lifted and there is always a bend at the elbow and wrist. The torque required to lift the arms to a fully extended orientation is larger than the torque required to partially extend the arms. Another factor that led to the reduction of torque in the optimized solution was the decrease in speed and accelerations of the motions. These changes all reduced the torque that the joints needed to generate. While the net rotation of the optimized motion was decreased when compared to the initial motion, it still met the final orientation criteria and the solution reduced the value of the objective function by 74%. Even though this optimization implemented a more general parameterization, the solution was feasible to

perform; however the characteristics did not change significantly from the initial motion.

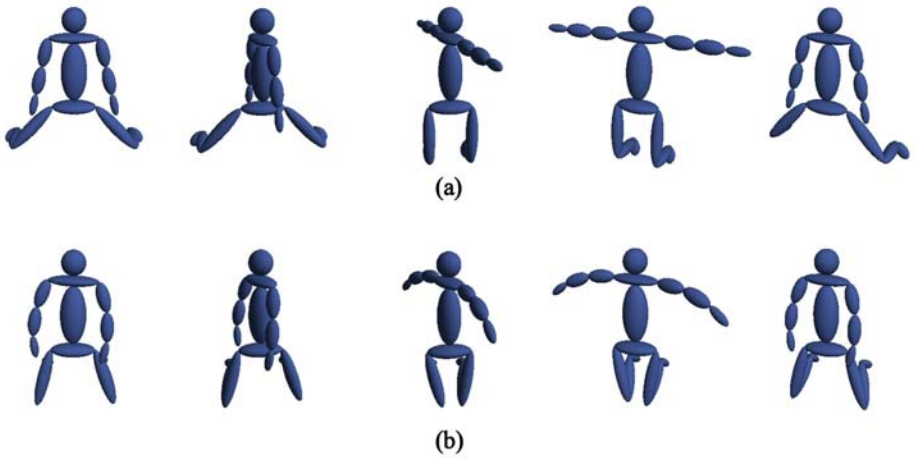

Figure 3-13: An example of an (a) initial motion and (b) optimized motion using the limb manipulation parameterization.

3.6 Summary of Control Methods

When developing motion training strategies, it is important that the motions be straightforward to perform, so that in a high-stress scenario the maneuver can be performed efficiently. The quantized control method permitted the development of complete maneuvers that naturally incorporated motion complexity constraints into the motion primitives. By concatenating the motion primitives $\mathcal{A}$ and $\mathcal{B}$ as $\mathcal{A}\circ\mathcal{B}\circ\mathcal{A}$, any orientation could be obtained. As long as astronauts can rotate about two axes of their bodies, they will be able to achieve any orientation after three rotations. In cases where there is no initial spin, no additional motion will be present when the astronaut ceases to perform the rotations. If at any time the astronaut feels unstable or unsure, or the perturbation to the motion maneuvers are large, there is no risk of an uncontrolled divergence from the desired trajectory.

An optimal control methodology was presented to evaluate the motion primitives in a formalized manner. The optimization methodology also permitted a more generalized motion parameterization that could be implemented to obtain astronaut self-rotations. While there has been significant debate in the motion control literature as to whether kinematics or dynamics are controlled by the CNS, the motions analyzed here show that certain parameterizations yielded similar solutions regardless of whether a kinematic or dynamic term was implemented, while other parameterizations yielded differences in the solution. With the inclusion of experimental data, comparisons can be made between the actual methods implemented and the simulated dynamics. In the following chapter, a human reorientation experiment is presented that will lead to a more detailed understanding of the motion control methods selected in real-time scenarios.

Chapter 4

Human Reorientation Experiments

The computational portion of this research provides a large knowledge base on what can be expected when motions are performed, such as whether maneuvers will have off-axis rotations and how much physical effort they incur. The inclusion of experiments provides the ability to obtain detailed information that cannot be obtained computationally. The results from the optimization were dependent on the parameterization, as well as the type of motion desired. While the quantization method allows for the replacement of complex rotations with simpler ones, this selection needs to be made in a rigorous manner. Prior to performing human experiments, three hypotheses were made:

Hypothesis 1 Subjects that have had motion strategy training will have a better initial performance with respect to the performance parameters than those that have not received training.

Hypothesis 2 Rotations and motions that are common in an Earth environment will yield a lower complexity score than those that are completely unfamiliar. Further, in cases when no technique is provided, familiar motions will be implemented.

Hypothesis 3 The variation in performance of a group with less training will be greater than the variation in a group with more training.

Through these experiments, the hypotheses are examined in order to obtain a better understanding of rotational motion control.

4.1 Testing Environment

There have been several different methods for simulating microgravity in a 1-G setting, including air-bearing floors, underwater scenarios, and body suspension configurations. Each simulation method has its advantages and disadvantages. In the underwater scenario one can move about all the rotational and translational axes; however, the viscous effects of the

water are significant and yield different motion control strategies than would be experienced in microgravity [33]. When using an air-bearing floor, rotations can only be performed about one axis, but there is little friction with the ground so motion control is not as affected as seen underwater. Yet the use of the floor adds mass and inertia to the body, minimizing the effect of the limb motions toward producing a net rotation, and is not ideal for performing self-rotations. When using a body suspension configuration, the subject is still limited in that only rotations about one axis can be performed during each trial; however, there is a negligible addition to the body mass and inertia.

The experiments performed for this research used a suspension system, with the subjects suspended in three different configurations so that a rotation about each body axis could be performed. A body harness was attached via rope to a gymnastics still rings apparatus as shown in Figure 4-1. A typical climbing harness was used for rotations about **x** and **z**, with the carabiner hooked onto the belay. For the rotation about **x**, the harness was worn in the opposite direction so that the subject would be horizontal to the ground. During the experiments, the harness buckles were always double passed for safety. To perform rotations about **y**, a sling harness was constructed in which the subjects would lay on their sides.

For rotations about **z**, the subjects were not aligned with a perfectly vertical posture. Instead, the subjects were instructed to be in a comfortable position in the harness so that the neutral body position found naturally in the microgravity environment would be mimicked, shown in Figure 4-2.

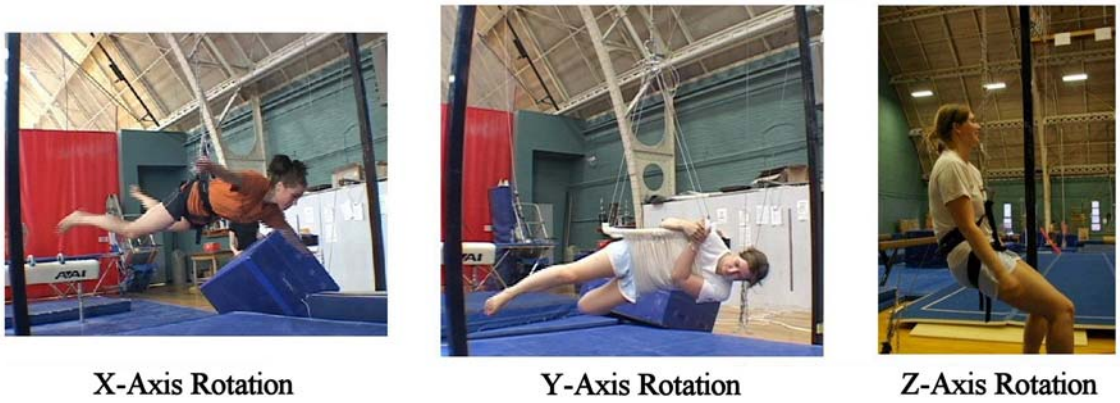

Figure 4-1: Harness arrangements for rotations about the three axes.

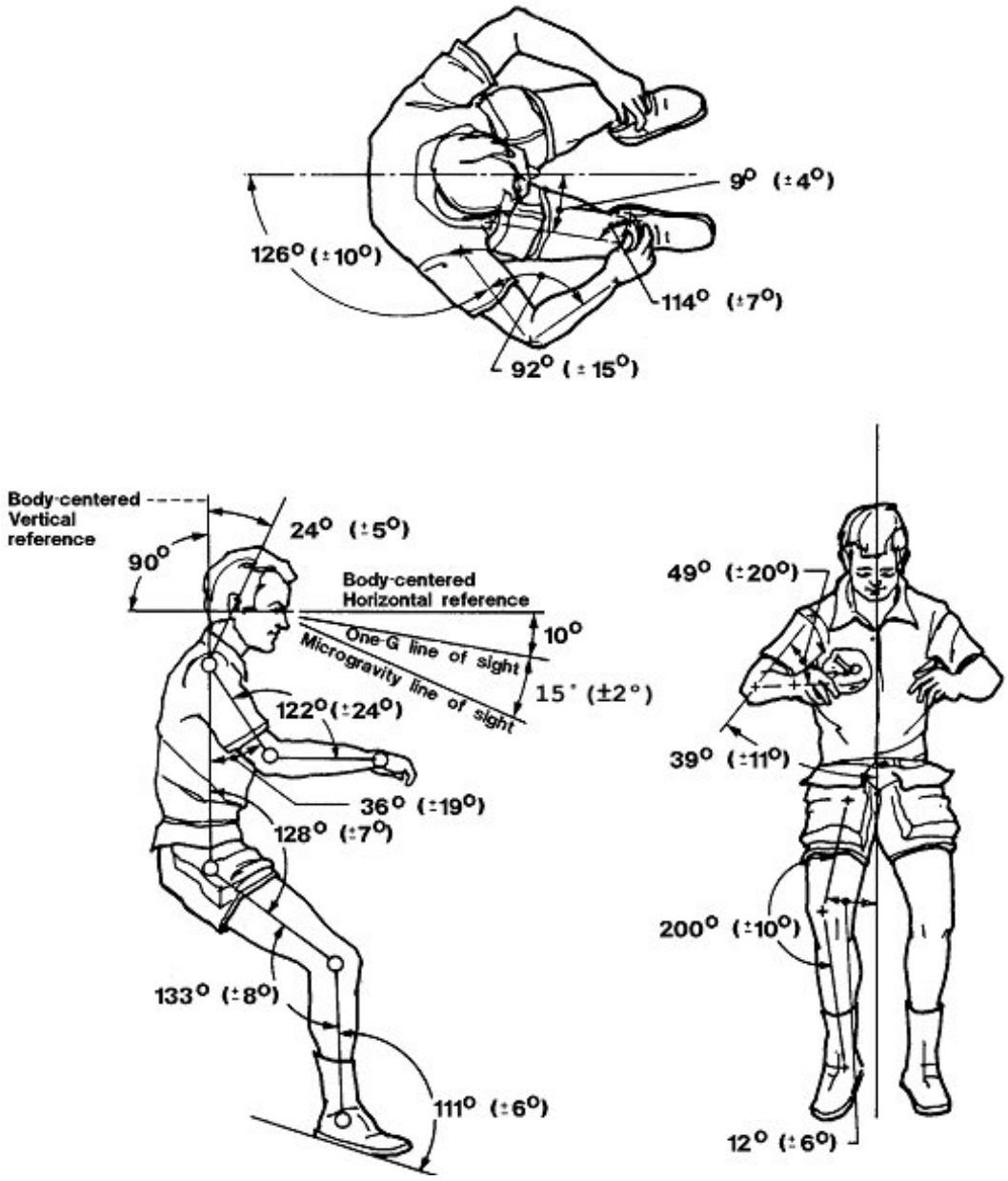

Figure 4-2: Mean neutral body posture as seen in microgravity conditions in Skylab with segment angles and standard deviations given, schematic from NASA [2].

4.2 Training Methodology

Hypothesis 1 stated that trained subjects would have better initial performance than untrained subjects. Yet it was determined that all subjects should receive at least some form of minimal training so that they could have a starting point from which to perform the rotations. Thus, there was a fully and minimally trained group. The minimal training did not include any motion strategies. The subjects in this group received a theoretical description

of momentum conservation. The full training consisted of this conceptual information along with a motion strategy for each rotation and computer visualizations of the rotations. At the completion of the training, the fully trained subjects were asked to explain and show the rotation strategies while unharnessed to ensure their understanding.

There is a great deal of literature defining three types of learners—visual, verbal, and kinesthetic [27]. The visual learners prefer to see what they are learning and benefit from visualizations of the material. The verbal learners, sometimes called auditory learners, benefit by reading to themselves and discussing the topic aloud. Kinesthetic learners need to be active and learn by carrying out the task. Providing visual information and then asking the subject to explain and show the motion covers all types of learning and the results should not be biased due to the training methodology. The minimally trained subjects were not given any strategies and had to interpret conceptual information to create a motion strategy, which will be more difficult for any learning type.

4.3 Pilot Study Results

Prior to conducting the study, a pilot study was performed to determine the best harness configurations, as well as to fine tune the experimental procedure. The selection of the harnesses was based on balancing range of motion with body stability. The harness, procedure, and training provided varied between subjects, as each subsequent subject had an improved version based on previous subjects' comments.

In total, six subjects participated in the pilot study. After the subjects completed the pilot study, they were interviewed so that improvements could be made to the quality of the instructions, comfort of the subject, etc. The following improvements were made during the pilot test.

4.3.1 Variation of Subject Performance

It was seen that some subjects, regardless of training method, were better at learning motions than others. Therefore, in order for the main study to be balanced between the groups, there needed to be a way to determine the subjects' motor ability. The *Ability Requirements Approach*, as presented by Fleishman and Quaintance [37], describes tasks in terms of the human abilities to perform them effectively. The approach relies on using known parameters of human performance as a basis for describing and classifying tasks, and further by giving a way to rate each parameter. Of the 37 human ability definitions, two were selected as being crucial for self-rotation tasks. They were:

Gross Body Coordination The ability to coordinate movements of the trunk and limbs. This ability is most commonly found in situations where the entire body is in motion or being propelled.

Gross Body Equilibrium The ability to maintain the body in an upright position or to regain body balance especially in situations where equilibrium is threatened or temporarily lost. This ability involves only body balance; it does not extend to the balancing of objects.

The ability to keep oneself in balance while performing a complex motion describes a self-rotation maneuver. Fleishman and Quaintance [37] also provide tasks that effectively represent these ability categories as well. For example, gross body coordination can be determined by obstacle courses, jumping rope without tripping or stopping, or skilled ballet dances, while gross body equilibrium can be determined by standing on a ladder, walking on ice, or riding a surfboard.

In the current study, gross body coordination was tested using a jump rope task. The subject was asked to perform a basic jump for the first ninety seconds and then for the last thirty seconds they were to alternate between a basic jump and a criss-cross jump. In the basic jump, both feet are slightly apart and the person jumps over the rope as it passes under him/her. The criss-cross method is similar to the basic jump with the difference being that the left hand goes to the right part of the body and right hand goes to the left part of the body. The last thirty seconds was implemented to challenge the subjects and to discriminate between the upper ranges of coordination ability. To test gross body equilibrium, a different task than those listed by Fleishman and Quaintance was implemented. The task selected—a balance beam routine—was more complicated than standing on a ladder, but easier to access than walking on ice or riding a surfboard. The task was performed as follows starting from one end of the beam: (1) walk to the end of the beam, (2) perform a half-turn, (3) walk to the halfway point of the beam, (4) perform a small jump, and (5) walk to the end of the beam. The subjects were instructed to jump high enough that their feet were off the beam.

When determining how to score these tasks, it was important to have a high enough score that a differentiation between subjects was possible. The jump rope test was scored on a forty-point scale. For the first ninety seconds, one point was deducted for each time the subject tripped or stopped, with a maximum deduction of five points over fifteen seconds. For the last thirty seconds, a point was given for each complex pattern completed (basic jump, criss-cross jump). The beam task was scored on a ten-point scale, with five points given for walking along the beam, two points for the turn, and three points for the jump. Deductions were made for wobbling and for falling off the beam.

4.3.2 Subject Comfort vs. Ease of Mobility

Two different harnesses were used during this study, a sling harness for the rotations about $\mathbf{y}$ and a mountain climbing harness for rotations about $\mathbf{x}$ and $\mathbf{z}$. When testing different harnesses, it was determined that the sling harness provided the greatest stability. While providing stability, this harness also reduced the subjects' mobility. When rotations about

x were performed in the sling harness, movements were affected to such a high degree that it was not usable for these experiments. Instead, a typical mountain climbing harness was used with the suspension occurring at the natural belay hook-up, such that the subject was facing the ground. For the rotations about **z**, the subject was suspended from the natural belay hook-up, but so that they were oriented vertically (the typical configuration). Rotations about **y** were not possible with the mountain climbing harness in a comfortable manner. As the sling harness could not stably support the subject unless it impeded either the arm or leg motion, it was determined that all rotations about **y** would be performed only with the legs in the sling harness, thus providing suitable stability and comfort.

4.3.3 Fatigue

During testing subjects were given a few moments between each rotation if they so desired to readjust the harness to a more comfortable position. Even with a rest period, the subjects began to feel fatigued after a number of the rotations were performed. Initially the experiment was setup to have 24 of each rotation type, yielding 72 total rotations. Based on the pilot studies, this was determined to be too cumbersome to perform. The least fatiguing rotations were those about **z**, so all 24 of these rotations were retained. The number of rotations about **x** and **y** was reduced to 12 each. This yielded a total of 48 rotations, which provided sufficient repetitions to investigate adaptation and to determine statistical significance.

4.4 Experimental Protocol

4.4.1 Subjects

There were 20 volunteer subjects (10 male and 10 female) ranging in age from 19 to 29 with a mean age of 23.6 $\pm$ 3.5. This study adhered to MIT's Committee On the Use of Human Experimental Subjects (COUHES), and as such all subjects signed an informed consent document (Appendix C).

4.4.2 Methodology

Each subject performed a series of rotations about **x**, **y**, and **z**. The order of rotations is provided in Table 4.1. Each block consisted of an equal number of counterclockwise and clockwise rotations. All subjects performed the rotations in the same order.

Prior to beginning the experiment, subjects were given background about the research, instructions about the harnesses, and directions for the rating scales. These directions are provided in Appendix D.1. At the conclusion of each rotation, the subject was verbally prompted by the test conductor to evaluate the task using a modified Cooper-Harper rating scale, which is provided in Appendix D.2. The original Cooper-Harper rating scale was

Table 4.1: Self-rotations performed by each subject during the experiment.

Block	Symbol	Rotation Axis	Number of Trials	Rotation Magnitude (deg.)
1	Z_1	**z**	12	180
2	X_1	**x**	6	90
3	Y_1	**y**	6	90
4	Y_2	**y**	6	90
5	X_2	**x**	6	90
6	Z_2	**z**	12	180

developed to evaluate the handling qualities of aircraft [28]. The scale used in this study is a modified version obtained from NASA Johnson Space Center and ranks the motion on a 10 point scale (1 = excellent performance with no improvement needed, 10 = the task cannot be reliably performed) [42]. At the conclusion of each block, cognitive workload measures were determined using NASA-TLX, which bases workload on mental demand, physical demand, temporal demand, performance, effort, and frustration [49]. The subjects were provided with the information sheet given in Appendix D.3 so that they had a consistent definition of each of these terms and how to score them for each rotation block.

4.5 Experiment Results

4.5.1 Effect of Coordination Score

As mentioned previously, the coordination and balance of the subjects was determined using a pretest. This pretest score was then used to divide the subjects such that the average score would be the same in both groups. The validity of this pretest as a predictor can now be examined.

The first performance metric that was considered was the time to perform the task with respect to the coordination score. A linear least squares regression was implemented with the log of the performance time as the dependent variable and the coordination, group, and rotation type as independent variables. This regression found the coordination score to be statistically significant in predicting performance time for the first trial of the motion within the blocks ($p = 0.029$). When this procedure was performed for the other repetitions within the block, the significance of pretest score decreased as the number of repetitions increased. As the subjects practiced the motion, they became better at performing it until no significant difference was seen between subjects with lower and higher coordination scores.

The difference between the log of the initial performance time and the log of the final performance time is defined as $\Delta \log T$. This value can be compared between subjects since

a difference in logs is equivalent to looking at the ratio of times as

$$\Delta \log T = \log t_i - \log t_f = \log \left(\frac{t_i}{t_f} \right), \tag{4.1}$$

where the subscript i is the initial trial and f is the final trial. When a linear least squares regression is performed on this metric with respect to coordination score for the minimally trained group, the relation is statistically significant ($p = 0.031$). When this regression is performed on the data from the fully trained group the relation was not significant ($p = 0.232$). The loss of significance of the coordination score with respect to $\Delta \log T$ between groups is reasonable as the trained group had additional information to use for improving their performance, while the minimally trained group had to rely only on their innate ability.

With these results, the conclusion can be made that the pretest score gave a good indication of performance ability and was an appropriate method to balance the two groups. The average score of each group was 38 out of a possible 50 points, with standard deviations of 5.8 and 8.0 for the the minimally trained and fully trained groups, respectively.

4.5.2 Performance Times

When considering an astronaut performing an EVA in an emergency scenario, it is important to understand the difference in performance time for the first attempts of particular types of motions. Figure 4-3 shows histograms of the initial performance times about the three rotational axes for both groups. This data is summarized in Table 4.2 without the clockwise rotation about **y** for the minimally trained group as four of the ten subjects could not complete the task in the allotted 90 seconds. The **z** rotation values were calculated for nine of the ten subjects as one subject could not complete the task in the allotted time.

Table 4.2: First trial performance times for the clockwise (cl) and counterclockwise (ccl) rotations ($n = 10$ for all but the starred entries, in which $n = 9$).

		X-Rotation		Y-Rotation		Z-Rotation	
		cl	ccl	cl	ccl	cl	ccl
Minimally Trained	Mean	14.5	6.8	N/A	16.2	16.6*	22.4
	Std. Dev.	14.0	1.8	N/A	8.5	8.8*	18.1
Fully Trained	Mean	14.3	11.4	11.3	6.8	12.4	10.4
	Std. Dev.	6.5	5.1	4.7	2.3	7.2	3.9

It is clear from these data that training is helpful for **z** and **y** rotations. These results were shown to be statistically significant using the nonparametric Kruskal-Wallis test ($p = 0.027$ and $p < 0.0005$ for **z** and **y**, respectively). Had this been an emergency scenario and a rotation about **y** was necessary, an untrained astronaut would have had great difficulty in performing the task. By examining the individual subjects, it was seen that all the subjects

that had trouble with rotations about **z** also had troubles about **y**. However, there were a few subjects that had difficulty with rotations about **y** that did not have any difficulty with rotations about **z**.

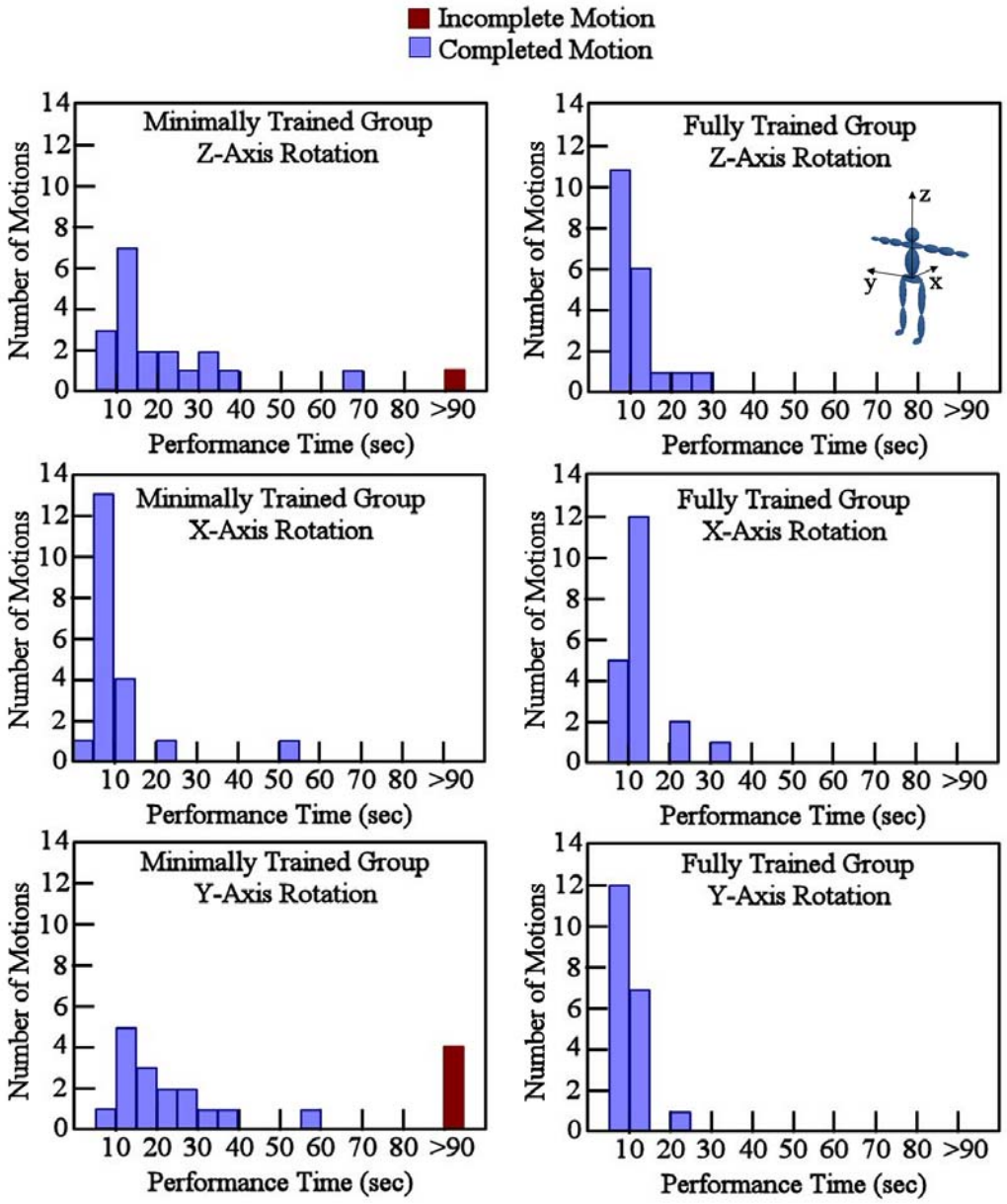

Figure 4-3: The distribution of performance times for the first trial for each axis ($n = 20$). A statistically significant difference between training groups was found for rotations about **y** and **z** ($p < 0.05$).

The lack of statistical significance between the two groups about **x** corresponds to what was observed during the experiments. The minimally trained group tended to use simple sweeping leg motions that in general created the required net rotation, but would have resulted in off-axis motions in a true microgravity environment. The trained group performed the recommended strategy that yielded planar motions, but took longer to perform, thus yielding similarities in performance time.

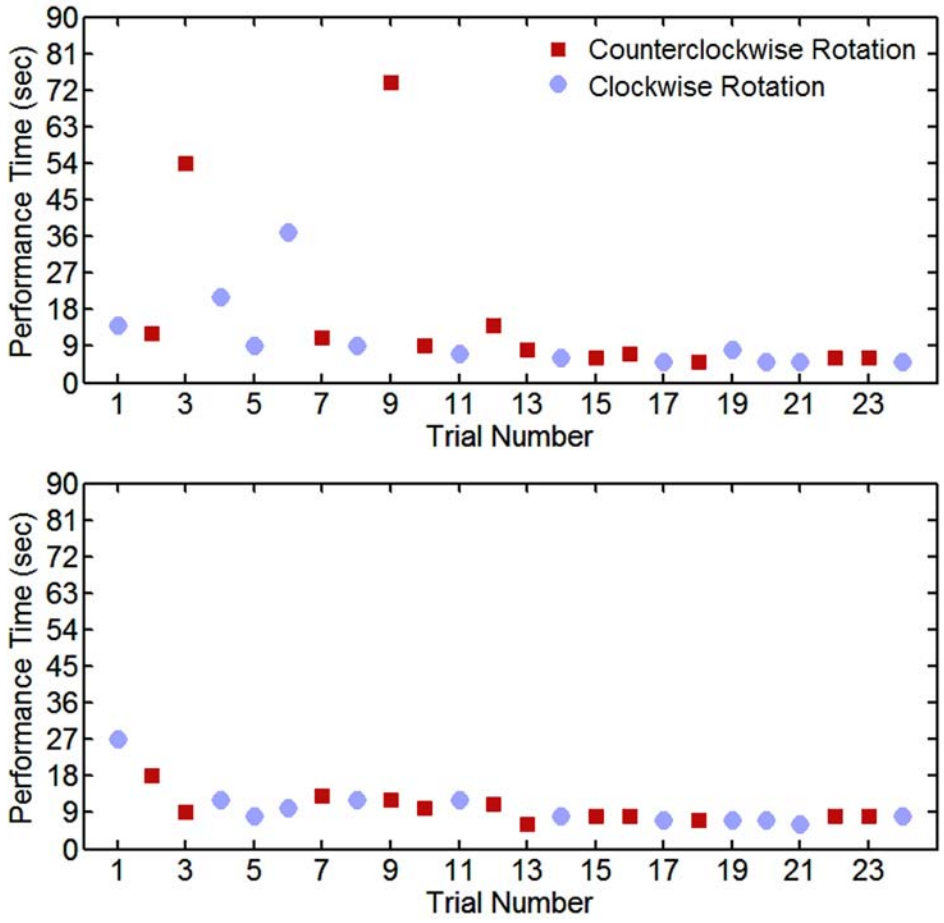

Figure 4-4: Two example learning patterns for rotations about **z**. (Top) Subject 15 shows increases in performance time with repetition and (Bottom) Subject 14 shows fewer repetitions before the steady state is achieved.

These initial data do not tell the whole story. While it seems intuitive that not all subjects have similar learning curves, there were some very different learning patterns observed between the subjects. Figure 4-4 shows two learning curves for different subjects performing rotations about **z**. The subject presented on top initially has a relatively efficient time, but with repetition of the task is shown to increase performance time in trials 3, 6, and 9. In a post-experiment interview, it was found that the subject initially tried a technique, but did not know why the technique worked. When the task was repeated the execution was slightly different causing the variance in the performance. It was not until after the fourth

repetition (the eleventh trial) that the subject understood what aspect of the performance was integral to obtaining the net motion. It is at this point the performance time reaches the steady state value. Yet certain subjects discerned the important aspect of the task with fewer repetitions. Even though the subject shown on the bottom of Figure 4-4 had a higher initial time, the steady state performance was attained after the second repetition without ever showing a dramatic increase in performance time. Of the ten minimally trained subjects, five show an increase in performance time in either the counterclockwise direction, clockwise direction, or both within the first few trials. On the other hand, only one fully trained subject showed a significant increase in performance time and this was because the subject started the trial going in the wrong direction and then corrected the mistake.

After a varying number of repetitions, a majority of the subjects obtained a steady state performance. These steady state performance times are presented in Table 4.3 and Figure 4-5, where steady state includes the trials after the subject has attempted the task five times. The steady state parameters for the clockwise rotation about **y** were calculated based on nine of the ten subjects, as one of the subjects never achieved a steady state. In Figure 4-5 box plots are shown of the steady state performance times for the various rotations, with incomplete rotations not included. The statistical significance of the differences in the steady state performance times between groups for each rotation were determined using the nonparametric Kruskal-Wallis test. A statistically significant difference was only found for the counter-clockwise performance of the **y** rotation ($p = 0.006$). The other rotations converge on average to similar performance times.

Table 4.3: Steady state performance times for the clockwise (cl) and counterclockwise (ccl) rotations ($n = 10$ for all but the starred entries, in which $n = 9$).

		X-Rotation		Y-Rotation		Z-Rotation	
		cl	ccl	cl	ccl	cl	ccl
Minimally Trained	Mean	6.9	5.1	20.2*	11.0	8.1	7.7
	Std. Dev.	3.5	1.4	26.0*	9.1	3.8	2.8
Fully Trained	Mean	8.2	6.5	7.0	5.3	6.9	6.9
	Std. Dev.	4.2	2.1	1.9	0.9	1.4	1.7

From Hypothesis 3, it was expected that there would be a greater variation in the minimally trained group than the fully trained group. An F-ratio test on the variance (Levene's test) was performed to examine this statement. The clockwise and counterclockwise rotations about both **y** and **z** showed significantly different variances ($F = 7.70$ with $p < 0.0005$ and $F = 2.87$ with $p < 0.0005$, respectively). Rotations about **x** were not seen to have significant differences in the variances ($F = 0.88$ with $p = 0.69$).

Since the subjects in the trained group were all performing the same maneuver, they converge to similar performance times regardless of their coordination score. The minimally trained group had no information about the rotation to be performed and thus each sub-

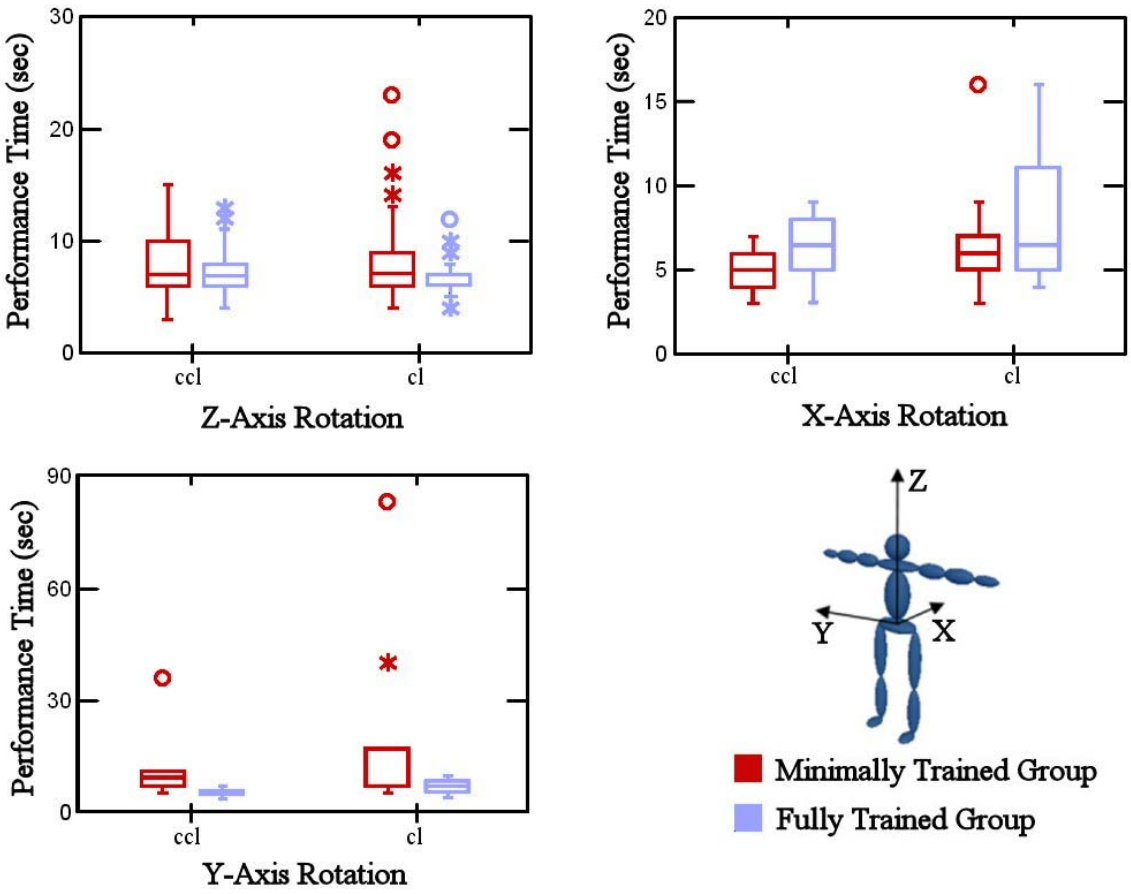

Figure 4-5: The distribution of the steady state performance times for the three rotation directions ($n = 20$ for all cases except the clockwise rotation about $\mathbf{y}$ for which $n = 19$).

ject created their own method. An increase in variation for the minimally trained group corresponds to having several different techniques evolve. The lack of significant difference seen in the variance about $\mathbf{x}$ aligns with the motion strategies performed by each group, which were described previously.

To be complete, the difference in rotation direction for a given axis was investigated. The Kruskal-Wallis test showed a significant difference in rotation direction about $\mathbf{y}$ for the fully trained group. All other cases were not significant.

4.5.3 Modified Cooper-Harper Rating Scale

Subjects rate the usability of the rotations using the modified Cooper-Harper scale (Appendix D.2). The scoring is based on three questions. Depending on whether the subject answers yes or no to these questions, different rating scales are provided. The complete scale runs from 1 to 10, where a rating of 1 is defined as a task that can be reliably performed with minimal workload and without need for improvement. A rating of 10 is defined as a

task that cannot be reliably performed. If a rotation was performed and the subject was completely unaware of the technique that produced the result, the motion would receive a 10 rating. If the motion could be reliably performed, but had too great a workload, the motion would receive a rating between 7 and 9. If the motion had a tolerable workload, but still needed improvement, it received a rating between 4 and 6. A motion that needed no improvements received a rating between 1 and 3.

Since the Cooper-Harper rating provided by the subject is based on their perception of the motion, it is not always indicative of their actual performance. For example, Figure 4-6 and Figure 4-7 show the performance time and Cooper-Harper rating for all three rotational axes for two subjects. The subject in Figure 4-6 has ratings that are indicative of the time performance for rotations about all three axes, with the longer performance times showing an increase in the Cooper-Harper rating and the lower performance times showing a decrease in rating. In Figure 4-7, the times are fairly consistent across all trials and yet the Cooper-Harper rating decreases over time. Even though this subject had similar times for each motion, the mental understanding of the motion was not complete, thus causing higher initial Cooper-Harper values. This aspect of motion usability is important to understand and discussed further in Section 4.5.4 when the workload results are presented.

Table 4.4 shows the steady state ratings for the three rotational axes for both the minimally and fully trained groups. The steady state ratings given to rotations about **z** and **x** were in a satisfactory range for both groups. However, rotations about **y** had a higher rating in the minimally trained group than seen in the fully trained group. This is consistent with the results seen in the steady state performance times, where only the rotations about **y** were seen to be statistically different.

In the development of plausibly difficult motions, it is important to understand their usability. The modified Cooper-Harper scale implemented here has been beneficial in showing trends in perceived difficulty of a motion over the trials within subject, as well as steady state usability averaged over all the subjects. The complete set of performance times and Cooper-Harper ratings are provided in Appendix E.

Table 4.4: Modified Cooper-Harper steady state ratings for both the minimally and fully trained groups about all three axes (cl, clockwise and ccl, counterclockwise).

	Fully Trained		Minimally Trained	
	cl	ccl	cl	ccl
x-Rotation	1.8	1.8	1.8	1.8
y-Rotation	1.4	1.4	4.2	2.5
z-Rotation	1.2	1.2	1.5	1.4

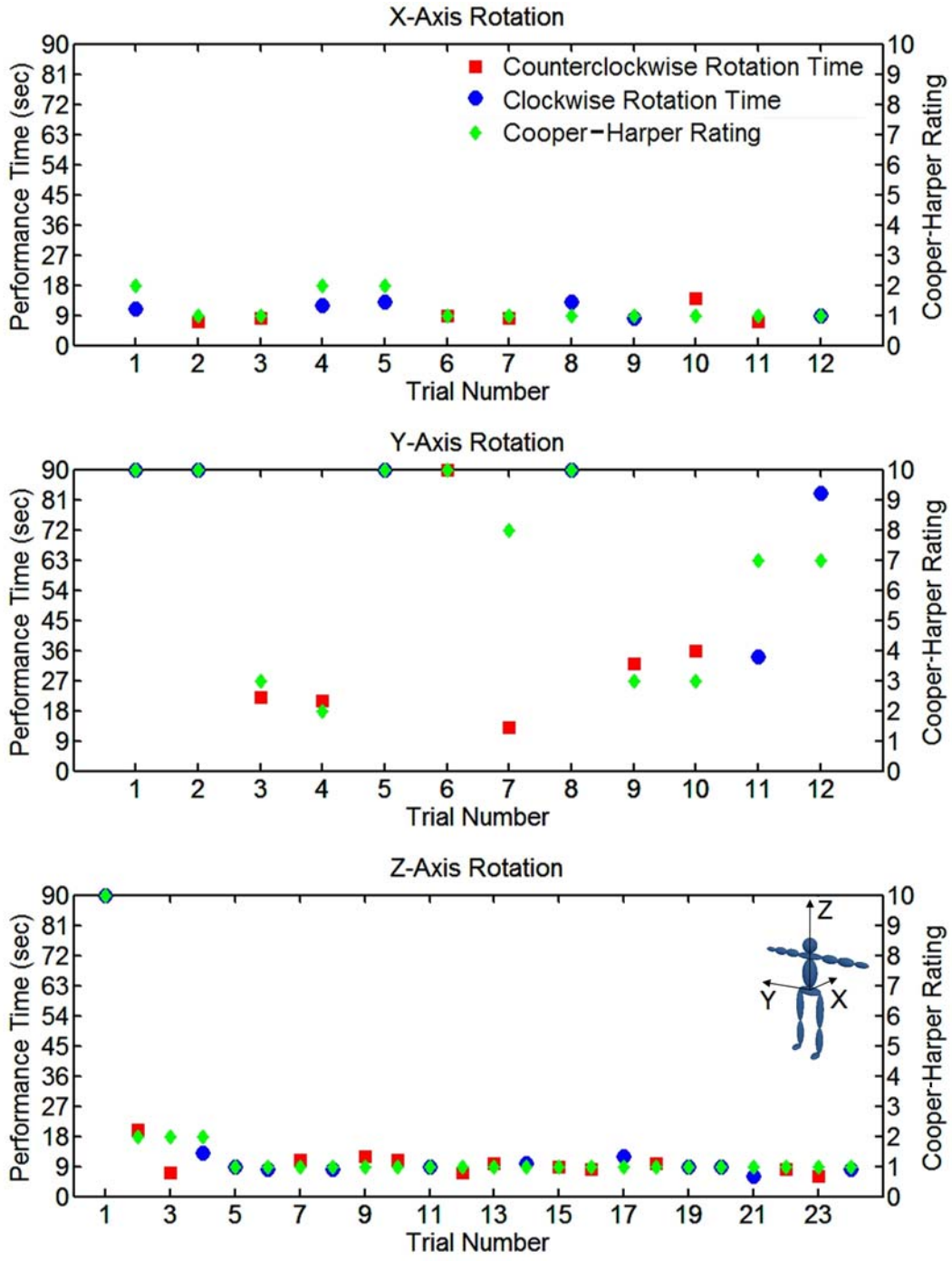

Figure 4-6: An example, Subject 12, that has Cooper-Harper ratings consistent with performance times.

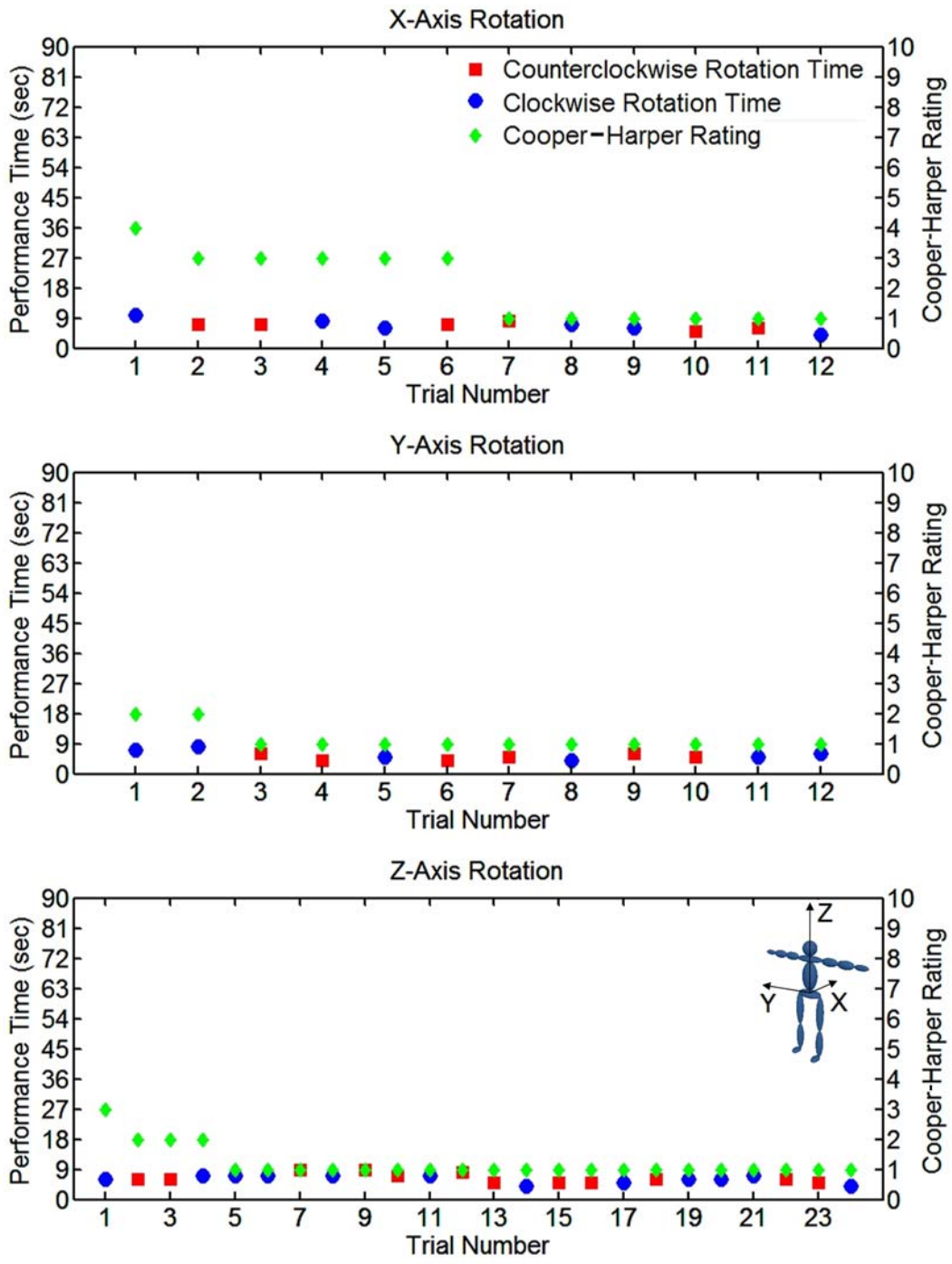

Figure 4-7: An example, Subject 11, that does not have Cooper-Harper ratings consistent with performance times.

4.5.4 Workload Assessment

The NASA Task Load Index (NASA-TLX) provides a measure of workload that incorporates perceived mental, physical, and temporal demand along with perceived effort, performance, and frustration. The NASA-TLX scores were obtained at the completion of each rotation block, as given in Table 4.1. Based on Hypothesis 2 and the performance time results, the expectation is that there will be a difference in the workloads between groups for rotations about **z** and **y**, but probably not a significant difference between rotations about **x**. In addition, the expectation is that the workload will decrease between rotational blocks as the subjects have had additional practice in performing the motions. Figure 4-8 shows the box plot of the NASA-TLX scores for each rotational block for both groups.

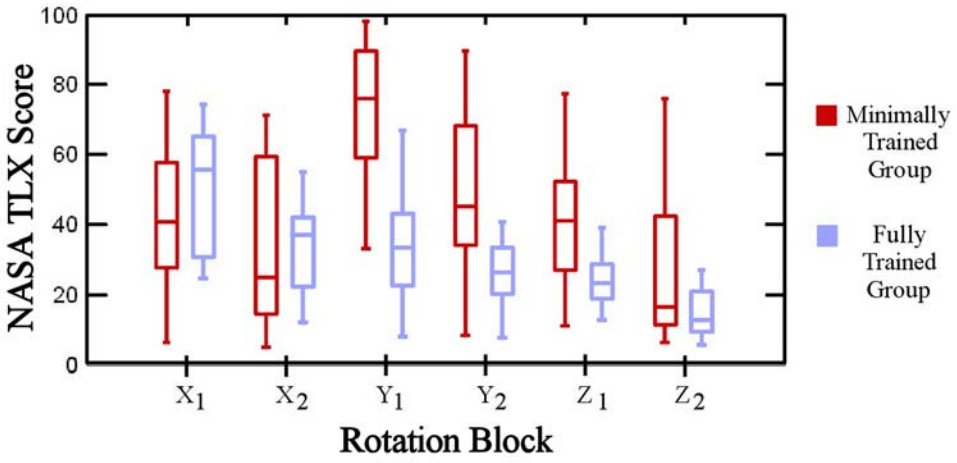

Figure 4-8: The distribution of the NASA-TLX workload scores for all subjects ($n = 20$).

The statistical significance of the differences between groups for each block was determined using the Kruskal-Wallis test. A significant difference was seen between the groups for Y_1, and Y_2, and Z_1, with p-values of 0.002, 0.023, and 0.023, respectively. The minimally trained group reported a much higher workload in each of these cases when compared to the fully trained group. For the minimally trained group the **y** rotations had the highest workload when compared to the other two axes, while for the fully trained group the **x** rotations were perceived to be the most difficult.

For each group, the perceived difficulty of the rotation decreased after the second repetition as determined by implementing a Friedman test ($p < 0.01$ for all cases). The ratio between the first and second block of each rotation axis, presented in Table 4.5, gives a numerical value of the decrease in workload and is expressed as

$$\Delta W = \frac{W_2}{W_1}, \tag{4.2}$$

where W is the workload score, 1 is after the first block of the specified rotation axis, and 2 is after the second block of the specified rotation axis. These data indicate an average

decrease of 19.7–35.1% between the first and second blocks. Similar workload decreases were seen between experimental blocks regardless of group.

Table 4.5: Average ratio between testing blocks in NASA-TLX scores for each group and rotation.

	Minimally Trained	Fully Trained
x-Rotation	0.719	0.663
y-Rotation	0.725	0.803
z-Rotation	0.692	0.649

When the steady state performance times were examined, a larger variance was seen in the minimally trained group than in the fully trained group. To see if the larger variance was expressed in the workloads as well as the times, Levene's test was again used. The variance was significantly larger for Z_1 ($F = 4.91$, $p = 0.027$), Z_2 ($F = 10.83$, $p = 0.002$), and Y_2 ($F = 6.03$, $p = 0.013$), with a nearly significant difference in X_2 ($F = 3.70$, $p = 0.065$).

In Hypothesis 2, rotations that were common in an Earth environment were expected to have lower workload scores than those that were uncommon. This is evident in comparing rotations about **y** for the fully trained and minimally trained groups. While the fully trained group was given the description of bicycle motions, the minimally trained group had no reference and instead tried to use familiar motions in an unfamiliar manner. The workloads correspond to this hypothesis as well, with the fully trained group having significantly lower workloads than the minimally trained group.

Examining rotations about **x** also support this hypothesis. Unlike the rotations about **y**, the technique provided for rotations about **x** was composed of motions that are not common in an Earth environment. Thus having higher workloads for rotations about **x** than those about **y** is consistent.

4.5.5 Motion Techniques

The motion techniques developed by the minimally trained subjects can be used to examine Hypothesis 2, along with giving a better general motion control understanding. Out of the ten minimally trained subjects, eight initially started the rotations about **z** using only their arms. The arm motions developed were generally sweeping motions, as shown in Figure 4-9. Only two subjects began the initial trial using leg motions. Once subjects modified their strategy to include their legs, they never reverted to exclusively arm motions. Seven of the ten minimally trained subjects used legs in their steady state motion. While using the legs requires more energy than the arms, due to their greater inertia and mass, the task time decreased with the added effort. These results support the idea of the motion control problem selecting a solution that balances performance time with energy expended.

During the initial performance of the rotations about **z**, two of the minimally trained subjects struggled a great deal. One spent time twisting and untwisting the upper body

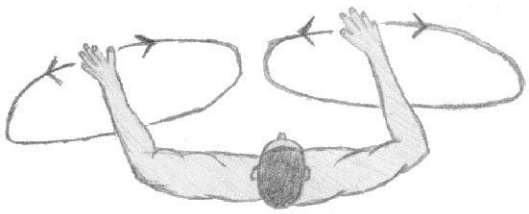

Figure 4-9: Schematic of the sweeping arm motions developed by the minimally trained group initially to rotate about **z**.

with respect to the lower body. Since no change in inertia was obtained after the initial twist, no net rotation was achieved when the subject untwisted. The other subject that experienced difficulty performed sweeping arm motions similar to the other subjects; however, the subject did not pull the arms toward the body after the sweep. Instead the arms oscillated in the same path and thus did not create any net rotation. While this conceptual information was explained to the subjects prior to the experiment, these results show that pure conceptual information is not enough for application purposes.

The suspension environment significantly affected motions developed by the minimally trained subjects for rotations about **x**. In general, large kicking motions of the leg were developed even though the instructions stated to keep the body planar. If these motions were implemented in a true microgravity environment, they would have incurred large off-axis rotations. Many subjects developed these large kicking motions since use of the legs proved to be effective in the rotations about **z**, which were performed prior to rotations about **x** for all subjects. Further, these kicking motions were similar to kicks implemented while swimming, showing that a familiar motion strategy was selected.

Rotations about **y** proved to be the hardest task for the minimally trained group, as given by the after-experiment interview and the NASA-TLX workload scores. Only one out of the ten subjects in this group began with a strategy that worked. Of the remaining nine subjects, different kicking methods were tried, including a modified freestyle, butterfly stroke, and scissor kick. At the conclusion of the experiment, only three subjects understood why their technique worked. One subject never developed a strategy for rotating clockwise, with a second able to perform the task intermittently (the subject did not understand which strategies did and did not work). The remaining subjects did not understand why their techniques worked, but could explain their strategy. In general, they had developed ways to execute their kicks such that their feet traced an elliptical trajectory in the **xz**-plane without their realization. To perform this rotation in the ways developed by the subjects was not natural and thus incurred high workload scores, which is consistent with the second hypothesis. Further, the subjects did attempt to use motions they were familiar with in new ways to achieve the desired rotation.

4.6 Summary of Hypotheses

The purpose of this study was to investigate self-rotation maneuvers in a microgravity environment. The first research hypothesis was that subjects that had motion strategy training would have a better initial performance with respect to the performance parameters than those who had not received training. By looking at the initial performance times and the subjective ratings, this hypothesis was shown to be true for rotations about **y** and **z**. No direct performance conclusions could be made for rotations about **x** with respect to this hypothesis, as the minimally trained group did not perform rotations that would work in a true microgravity scenario. The lesson learned from this rotation was that subjects will take advantage of the environment they are placed in even if they are attempting to follow the guidelines provided. Our second hypothesis stated that rotations or motions that were common in an Earth environment would yield a lower complexity score than those that were completely unfamiliar; further, in cases where no technique was provided, familiar motions would be implemented. This hypothesis was confirmed through motion observation along with the NASA-TLX scores. Our final hypothesis stated that the variation in performance of a group with less training would be greater than the variation in a group with more training. This final hypothesis was confirmed using nonparametric statistical tests on the performance time data.

Chapter 5

Conclusions

5.1 Thesis Summary

Even though astronauts undergo hundreds of hours of training, the strategies for locomotion and orientation in the unfamiliar weightless environment are not specifically prescribed. Since astronauts are not familiar with reorienting without external forces, they will most likely not develop any self-rotation techniques naturally. This research studied astronaut reorientation methods both computationally and experimentally in order to reduce astronaut adaptation time and provide for a safety countermeasure during EVA.

A multibody dynamics model was developed that is appropriate for studying human self-rotations in microgravity conditions. The model implements a modified inverse dynamics framework where the kinematics of the actuated joints are inputs and the torques and motion of the astronaut with respect to the inertial environment are the outputs. The unsuited human body parameters were calculated using GEBOD and were then augmented based on the EMU to obtain the suited parameters. The torques generated by the suit, found in previous experimental data, were also included in the model. The dynamic model determined motion feasibility of the prescribed kinematics by calculating the range of motion, possible collisions, and available torques. Several motions were analyzed to obtain a general understanding of the microgravity environment for both IVA and EVA motions.

The effects of adding the space suit were significant due to the resistance torque and limited range of motion. Since the EMU does not have hip extension, hip adduction, shoulder extension, or shoulder flexion past 180 deg., many of the easy to perform single-axis rotations could not be implemented as designed with the current spacesuit. For the rotations that could be performed suited, the motions were shown to be less effective due to the added mass on the torso. Further, it would become very tiresome to perform the self-rotations during EVA, which is why these motions are recommended for use in emergency situations when the SAFER is not working properly. However, these motions provide an easy, low-energy way to reorient during IVA. Advanced space suits will increase the efficacy of self-rotations during EVA by increasing mobility of all the joints while decreasing suit

mass [15, 55].

Reorientation trajectories were developed with two control methods—quantized control and optimal control. Since two rotations can yield any orientation, a quantization for the self-rotation planning problem was created by defining two motion primitives, which were finite time trajectories representing a rotation about a principal body axis. Given the primitives $\mathcal{A}$ and $\mathcal{B}$ about different axes, the trajectory $\mathcal{A} \circ \mathcal{B} \circ \mathcal{A}$ is sufficient to reach any orientation. The implementation of an optimal control method allowed for the development and refinement of maneuvers based on general motion parameterizations as well as optimizations of the motion primitives themselves. While it would be desirable for the optimization to provide a unique solution given a general motion parameterization, this tended to yield physically and cognitively infeasible to perform motions. With appropriate parameterizations, the optimal control method can be implemented to improve and understand the underlying maneuver characteristics.

The computational analyses provided a significant amount of data on how the rotations would vary when modifying the weightings of the penalty terms in the objective function. With the experimental data, comparisons were made between the actual methods implemented by the subjects and the simulated dynamics. The inclusion of the experimental study also allowed the effect of self-rotation training to be examined in a rigorous manner.

During the experiment, there were three main hypotheses explored: (1) Subjects that have had motion strategy training will have a better initial performance with respect to the performance parameters than those that have not received training; (2) Rotations and motions that are common in an Earth environment will yield a lower complexity score than those that are completely unfamiliar; and (3) The variation in performance of a group with less training will be greater than the variation in a group with more training. Through evaluation of the performance times and subjective ratings, these hypotheses were examined. The modified Cooper-Harper rating and the NASA-TLX implemented in this study were beneficial in showing perceived difficulty of a motion. Even when a subject had similar performance times for a rotation, the mental understanding was not always complete and higher initial Cooper-Harper values were observed. Similarly, statistically significant decreases in the NASA-TLX workload were seen after motions were repeated for both the trained and untrained groups. Based on this experiment, an untrained astronaut would have difficulty performing a rotation about $\mathbf{y}$ or $\mathbf{z}$ in an emergency scenario when compared to the trained astronaut. While there was no statistical difference between groups for rotations about $\mathbf{x}$, these rotations would have been far more difficult for the untrained group had the harness not offered extra stability.

When the experimental results for the trained group were compared with the computational optimization, it was observed that the subjects chose a balance between final time and the dynamics/kinematics penalty term. For the microgravity environment with the parameterizations analyzed, either the dynamic or kinematic penalty would have been sufficient

for predicting final times and rotational velocities.

5.2 Reassessment of Previous Literature

Previous human reorientation studies answered whether or not self-rotation was possible [56,64,89]. Kulwicki et al. [64] developed several reorientations for rotation about the body axes, with Kane [56] analyzing a few body rotations using a simple computational analysis. The current study built upon these studies by developing a higher fidelity computational model that in addition to determining the net reorientations also has the ability to quantify off-axis rotations, motion feasibility, and the necessary joint torques. These improvements help to determine motion selection by quantifying the significant characteristics.

Once the model was developed, a way to create and understand the motion strategies needed to be formed. Previous microgravity experiments showed adaptation to the environment, including decreased velocities and applied forces to the surrounding environment [6, 33, 62, 78, 80]. These adaptations would result in lower joint torques in the body. Based on this information, control strategies were investigated that incorporated these known strategies. The observation of the control of the center of mass [13, 61, 73, 90] was inherent in the formulation of the control problem as no translation of the center of mass can occur without an external torque.

The two control methods examined in this study for creating self-rotation maneuvers were quantized and optimal control. The premise behind quantized control is that the technique simplifies the control problem [14,17,40]. As self-rotation maneuvers can be highly complex, a quantization in the motion trajectory was implemented to simplify reorientation strategies. While quantization has been applied in a robotics framework, this work was one of the first applications of quantized control to a human body control problem.

The optimal control methodology can be formulated to yield motions similar to those naturally developed by the central nervous system given an appropriate objective function and constraints. Several investigators have looked at modeling the objective with dynamic and kinematic terms [36, 82, 103]. While studies could reproduce the desired motions, the environment and type of motion were important in determining what was necessary in the objective function. This research began by examining dynamic and kinematic terms, coupled with a final time penalty, to determine if appropriate microgravity motions could be predicted. This research shows that not only is the environment the motion occurs in important, but the parameterization of the motion as well.

The computational work presented in this research led to several questions that could only be answered experimentally. This research presents the first rigorous experimental analysis of microgravity reorientation. Previous simulators for microgravity motions were developed specifically for translational maneuvers, thus a new framework for simulating reorientations in microgravity was designed and built. During prior translational experi-

ments untrained subjects showed typical learning curves; that is, the highest performance time occurred for the initial trial and repeated trials show a reduction in time [33]. In the current reorientation experiment, this trend was not always observed. The underlying dynamic equations for reorientation are conservation of angular momentum, which this experiment showed to be difficult to grasp and apply when not properly trained. Further, a study that examined the control of hand-path tracking in microgravity [21] showed that complete adaptation required continuous task practice with an increase in resource allocation to the motion control task. The current study is consistent with these results as seen by the NASA-TLX and Cooper-Harper scores.

5.3 Contributions

The key contributions that resulted from this research are as follows:

1. Developed an astronaut dynamics model that is appropriate for IVA and EVA motions and incorporates constraints to ensure motion feasibility.
2. Simulated the astronaut dynamics model for several reorientation techniques and analyzed the resulting off-axis motions, necessary torques, and effects of the space suit.
3. Presented a new application of quantized control by implementing the method in a human motion problem.
4. Demonstrated that using an objective function that includes a time penalty and a kinematic or dynamic term can be used to predict human motor control strategies for the microgravity environment.
5. Designed and implemented a harness system for performing single-axis self rotations in a 1-G environment.
6. Determined that reorientation training is important for reducing the initial performance time, increasing the physical understanding of the reorientations, and reducing the perceived motion complexity.

5.4 Comments and Recommendations

The motions defined in this thesis are not the only possible rotations. Certain strategies and modifications to the methods developed by the subjects during the experiment proved very interesting. For example, instead of rotating the feet in circles for the rotation about $\mathbf{y}$ and $\mathbf{z}$, they created more of an elliptical shape that yielded larger changes in inertia than possible for a pure circle, thereby making each cycle more effective. Thus, the recommended strategies for rotating about the body axes (repeated in Figure 5-1 for clarity) based on the computational model and experimental results are:

Rotation about x: For large reorientations (greater than 45 degrees) use the concatenation method as it is a simple, effective strategy. For small reorientations, the implementation of the rotation in Definition 2.1 is not overly difficult provided one has trained with it.

Rotation about y: Regardless of reorientation amount, the bicycle maneuver described in Definition 2.2 should be performed. As one is not limited by the mechanics of a bicycle pedal, the feet no longer need to move purely about a circle, but can move in an elliptical fashion as long as the motion remains symmetric between the legs so that off-axis rotations are not generated.

Rotation about z: Regardless of reorientation amount, the cyclical motion in Definition 2.4 should be performed. Similar to the rotation about **y**, the rotation no longer needs to be circular, but can become elliptical in order to achieve a greater rotation within each cycle as long as the motion remains symmetric between the legs.

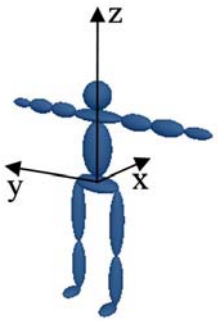

Figure 5-1: The body axes of the human model.

As self-rotations are not common in a 1-G environment it is important to provide training to the astronauts in these maneuvers so that they can become more efficient when moving in the microgravity environment. The training should occur in parabolic flight for maximum learning. If the motions are performed underwater or in simulators, then a mis-training (i.e., development of inappropriate movements) could occur and should be accounted for. For example, underwater environments cause the development of inappropriate movements due to the viscous forces of the water. Regardless of environment the training must consist of simple repeated trials such that the cognitive complexity is reduced and not just the performance time. While training in parabolic flight is the only way for the astronaut to feel the sensations of multi-axis rotations, the use of a virtual reality environment would allow the astronaut to become familiar with the rotations prior to attempting them.

During the course of this research, several assumptions were made that should be specifically addressed. First, the model uses SIMM to check feasibility of motions and only uses static muscle dynamics. In actuality the muscles are affected by the velocity at which they

lengthen and shorten. While many of the motions were performed such that this assumption held, certain noted rotations neared the limits of the available torque as predicted by SIMM. In addition, the muscle model in SIMM was not scaled based on the body parameters selected in the dynamics model. The muscle strengths and bone dimensions in SIMM were based on an average male and only compared with dynamic simulations using the average male body parameters. If a more in-depth study of the muscle interactions and muscle forces produced during movement is necessary, an integrated musculoskeletal dynamics system such as SIMM coupled with SD/FAST (Symbolic Dynamics, Inc., Mountain View, CA) or the program AnyBody [92] should be used. The development of a separate rotational-appropriate dynamics model in this thesis was performed to further understand the key dynamic principles and was not intended to be used to suggest muscle activation information.

Another simplification that was made in the current model was that joints were modeled as rigid bodies. This assumption provided a straightforward way to formulate the joints in the model while maintaining the appropriate features in the simulated rotations. In actuality joints are flexible. There is connective tissue and cartilage between the joints that can result in varying contact points between the limbs.

When implementing the SQP method, constraints can be violated temporarily to reduce the objective function value before they are brought within the appropriate limits. While some constraints can be momentarily violated, such as the final desired orientation angle, others cannot. For example, unit quaternions were used to describe the joint orientations. If equality constraints had been constructed to enforce the unit magnitudes, the dynamics model would have produced incorrect results when the constraints were violated, which would have led to an inappropriate update in the optimization. Instead of enforcing unit magnitudes of the quaternion orientations with a constraint, a normalization was performed to ensure the unit magnitudes. This is an unnecessary step if a strict enforcement of the constraint exists. However, strict enforcement methods are typically not as efficient as the SQP method.

Another limitation to using the SQP method is that the problem can become ill-conditioned, that is the Hessian of the objective function with respect to the optimization design variables can have significantly different orders of magnitude on the diagonal. When this is the case, the numerical stability of the optimization can be reduced and result in computational difficulties. While scaling the parameters to make the Hessian diagonal order one helps, large steps away from the initial scaling parameters can necessitate the recalculation of the Hessian diagonal, which is an expensive computation. Regardless of this issue, gradient-based methods still can have problems converging to global maximums and multiple initial conditions must be checked to determine if a solution is indeed global.

The results from this research have led to several areas for future work with respect to model application and development, control methods, and future experimental studies. In

the following are the key recommendations.

Model Development and Reorientation Application:

- An input to the dynamics model based on motion capture data could be developed to provide a way to couple virtual reality reorientation training with a motion simulator.
- For this research a significant amount of control was desired over the self-rotation parameterization and the equations of motions. Now that there is a framework for modeling self-rotations, the muscle forces could be analyzed in a more precise manner to better understand the muscle activations. This could be done with programs like SIMM or AnyBody.
- The current suit torques are based on a well-used space suit. As the space suits are worn, the resistance decreases. It would be very informative to run a mechanical approximation to the EMU with the ability to modify the damping and resistance to determine the effects on the necessary joint torques. In addition, it is important to test at different velocities. The torque available due to the muscles is known to be velocity dependent and it is important to determine what velocity effects are inherent with the space suit.
- The experimental suit torques are implemented in the model with a polynomial fit. An improved prediction of the necessary joint torques could be made if a hysteresis model were implemented. While there are several published versions of analytic hysteresis models, a method is needed that does not assume symmetry as the EMU does not show symmetric hysteresis.
- The design and development of EVA suits with increased ranges of motion and lower resistance torques will make astronaut locomotion easier and more efficient in all gravity environments. This will also provide astronauts with similar motion strategies during IVA or EVA, which is desirable from a cognitive and energetics standpoint.

Control Methods:

- In the current study, two common representations of a dynamic and kinematic function were examined. The results from other objectives, such as minimum metabolic energy or minimum muscle activation, should be evaluated to determine if they better represent the actual selections made experimentally.
- The multibody problem in general is highly nonlinear with nonconvex constraints. An investigation of other optimization techniques that are not gradient based, such as simulated annealing or genetic algorithms, could lead to solutions that are further from the initial condition.

- Instead of implementing the typical SQP formulation, explore methods for strict constraint enforcement.

Experimental Studies:

- In applying the quantized control method, the minimum number of reorientations necessary was implemented. However, the addition of a third rotation could simplify the motion strategy for certain scenarios. While this is a difficult problem to formulate analytically, it can be more easily explored experimentally by testing the following questions. Does the subject reduce the given set of motions to two rotations or is the third rotation implemented? If it is implemented, are there certain scenarios when it is implemented or is the choice of rotation statistically insignificant with respect to the application?

- In the current study the harness environment was seen to affect the motion strategy of the subjects. Off-axis motions generated by incorrect implementation by the trained subjects and the reorientation attempts by the untrained subjects were suppressed. The repetition of this experiment during parabolic flight would be valuable in determining how significant the training was when off-axis moments are no longer suppressed.

- During this study, several metrics pertaining to the reorientations were examined. If the experiment is repeated, the use of high-speed cameras with joint markers should be implemented in order to obtain a more detailed understanding of the joint kinematics.

- Thus far astronaut motion control has been examined in the context of rotational *or* translational motions. The actual locomotion of an astronaut involves procedures such as turns around corners that are combinations of these motion types. With the results from this research in combination with previous translational studies, methods and training for complex motion maneuvers can be developed.

5.5 Educational Outreach

While the self-rotation analyses presented in this study were designed to develop reorientation methods for astronauts in IVA and EVA scenarios, the underlying conservation equations are fundamental in most engineering disciplines. Providing undergraduates with visualizations and interactive applications can help them to conceptualize the subtleties of conservation of angular momentum. In a collaborative effort with the Office of Educational Innovation and Technology at MIT, the dynamics model developed in this research is being implemented in an Extensible 3D Graphics (X3D) environment with an astronaut modeled in Autodesk® Maya®. With this tool, undergraduates will have the ability to obtain a better grasp on a key engineering principle.

The primary concern when developing the graphical user interface was to place user interaction with the mathematical model in the visual domain. This was accomplished by having directions and information contained in colors and shapes rather than text or equations. A screen capture of the current version of the interface is shown in Figure 5-2. An icon of the body axes is presented in the lower left for the user, with the axes color-coded and direction of positive motion indicated. A motion performed using the arms is shown on the control panel with a hand and a motion performed using the legs is shown with a foot. Unlike a pre-rendered animated movie, this interactive environment can be adjusted in real-time to allow the user to see the motions from varying angles and distances. This feature enhances the user's learning of the visualized concepts.

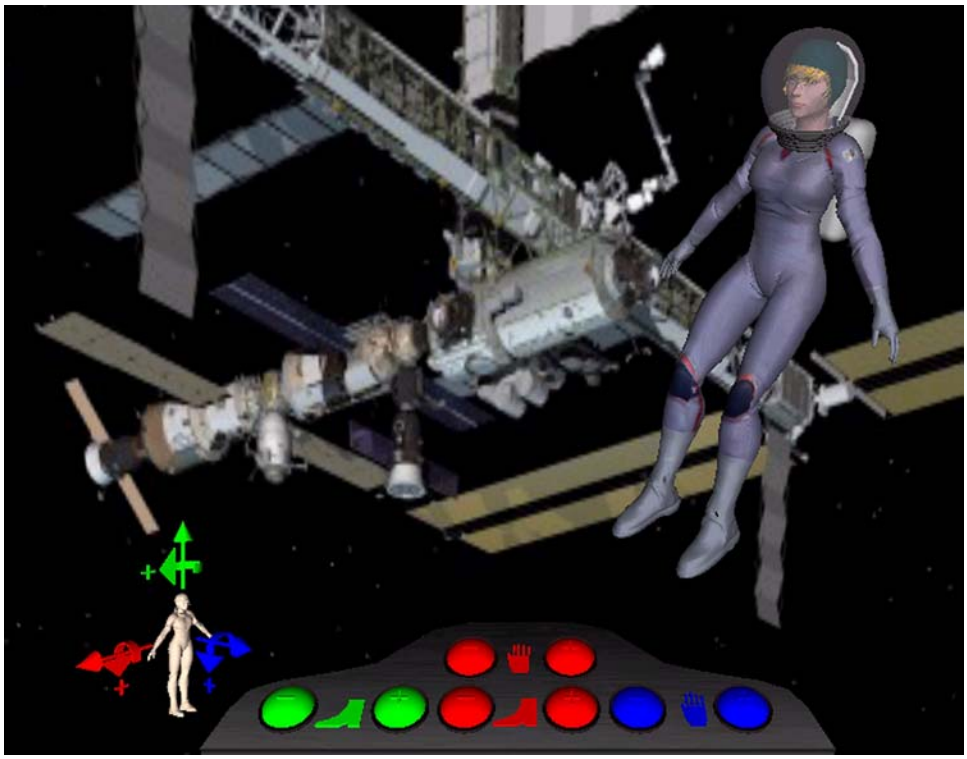

Figure 5-2: A screen capture of the graphical user interface designed for students to obtain a better understanding of conservation of angular momentum.

Appendix A

Review of Quaternions

The quaternion is composed of four parameters and can be written in several ways, including

- $\mathbf{q} = a + b\mathbf{i} + c\mathbf{j} + d\mathbf{k}$, where each parameter is identified separately and $\mathbf{i}^2 = \mathbf{j}^2 = \mathbf{k}^2 = -1$.
- $\mathbf{q} = [s\ \mathbf{v}]$, where the real part, s, is independently identified from the complex part, $\mathbf{v}$.
- $\mathbf{q} = \left[\cos\left(\frac{\theta}{2}\right)\ \sin\left(\frac{\theta}{2}\right)\mathbf{e}\right]$, where where θ is the angle of rotation about the unit vector described by $\mathbf{e} = [\mathbf{e}_1\ \mathbf{e}_2\ \mathbf{e}_3]^T$.

The norm of the quaternion is given as $|\mathbf{q}| = \sqrt{a^2 + b^2 + c^2 + d^2}$. For a unit quaternion, this norm is equivalent to one. Using the second representation, the quaternion conjugate can be defined as follows.

Definition A.1. *The conjugate of a quaternion is* $\mathbf{q}^* = [s\ -\mathbf{v}]$.

For a unit quaternion, the inverse is equivalent to the conjugate. The quaternion can also be raised to a constant coefficient. If the quaternion is expressed in the third representation, the quaternion to a constant power is defined as follows.

Definition A.2. *A quaternion raised to a constant coefficient is* $\mathbf{q}^t = [\cos(t\theta)\ \sin(t\theta)\mathbf{e}]$.

Given two quaternions, $\mathbf{q}_1 = [s_1\ \mathbf{v}_1]$ and $\mathbf{q}_2 = [s_2\ \mathbf{v}_2]$, addition and multiplication can be defined as follows.

Definition A.3. *The addition of two quaternions is defined as* $\mathbf{q}_1 + \mathbf{q}_2 = [s_1 + s_2\ \mathbf{v}_1 + \mathbf{v}_2]$.

Definition A.4. *The multiplication of two quaternions is defined as*
$\mathbf{q}_1\mathbf{q}_2 = [(s_1 s_2 - \mathbf{v}_1 \bullet \mathbf{v}_2)\ (s_1\mathbf{v}_2 + s_2\mathbf{v}_1 + \mathbf{v}_2 \times \mathbf{v}_2)]$

An interpolation from one quaternion orientation to another is not as simple as creating straight lines between the quaternions. By creating a straight line, the natural geometry of the rotation space is ignored and the motion would speed up in the middle region [100].

If the span of the unit quaternions is considered, a sphere of radius one is formed. Thus, to have a constant velocity motion, the interpolation would have to be on the great arc between the two quaternions. The formula for this spherical linear interpolation (slerp) is given as follows.

Definition A.5. *The spherical linear interpolation between* $\mathbf{q}_0$ *and* $\mathbf{q}_1$ *at the normalized time* t*, which ranges from 0 to 1, is given as* $\mathbf{q}_t = \mathbf{q}_0 \left(\mathbf{q}_0^{-1}\mathbf{q}_1\right)^t$.

While the quaternion has many useful applications, it is sometimes necessary to use other representations, such as a matrix representation or Euler angle representation. The quaternion can be converted to a rotation matrix with the following equation.

$$R = \begin{bmatrix} 2a^2 + 2b^2 - 1 & 2bc + 2ad & 2bd - 2ac \\ 2bc - 2ad & 2a^2 + 2c^2 - 1 & 2cd + 2ab \\ 2bd + 2ac & 2cd - 2ab & 2a^2 + 2d^2 - 1 \end{bmatrix}.$$

The pitch (Θ), yaw (Ψ), and roll (Φ) of the body can be defined as rotations about the $\mathbf{y}$, $\mathbf{z}$, and $\mathbf{x}$, respectively, and are determined from the quaternion orientations as

$$\begin{aligned} \Theta &= \sin^{-1}\left(-2\left(bd - ac\right)\right), \\ \Psi &= \tan^{-1}\left(\frac{2\left(bc + ad\right)}{a^2 + b^2 - c^2 - d^2}\right), \\ \Phi &= \tan^{-1}\left(\frac{2\left(cd + ab\right)}{a^2 - b^2 - c^2 + d^2}\right). \end{aligned}$$

If the quaternion representation is desired from the Euler angles, then the individual quaternions for each angle,

$$\begin{aligned} q_{\text{pitch}} &= \left[\cos\left(\frac{\Theta}{2}\right), 0, \sin\left(\frac{\Theta}{2}\right), 0\right], \\ q_{\text{yaw}} &= \left[\cos\left(\frac{\Psi}{2}\right), 0, 0, \sin\left(\frac{\Psi}{2}\right)\right], \\ q_{\text{roll}} &= \left[\cos\left(\frac{\Phi}{2}\right), \sin\left(\frac{\Phi}{2}\right), 0, 0\right], \end{aligned}$$

can be multiplied together appropriately as

$$\mathbf{q} = \mathbf{q}_{\text{yaw}}\mathbf{q}_{\text{pitch}}\mathbf{q}_{\text{roll}},$$

assuming a standard Euler angle representation.

Appendix B

Extravehicular Mobility Unit Joint Torques

Figures B-1 through B-7 show the measured torques and implemented polynomial fit. The measured data were from experiments performed by Schmidt [96] and Frazer [39].

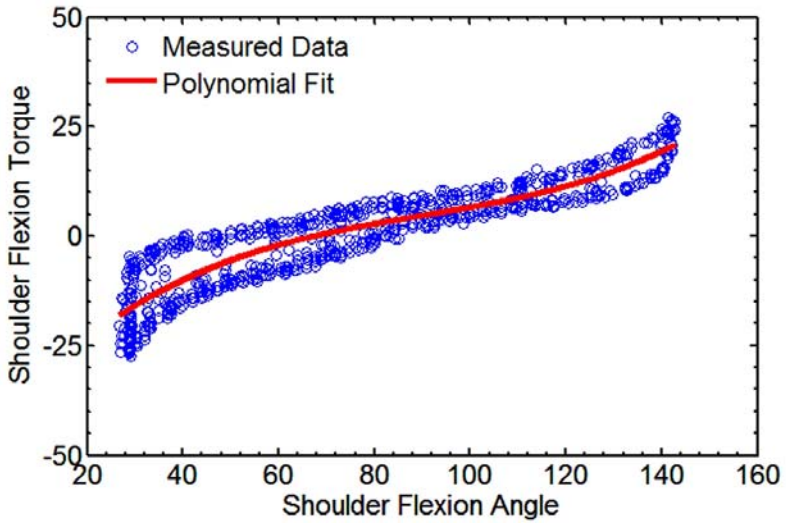

Figure B-1: The measured data and implemented polynomial fit for the shoulder flexion. Writing the shoulder flexion torque as τ and the shoulder flexion angle as θ, the polynomial fit is expressed as $\tau = 4.4 \times 10^{-5}\theta^3 - 0.01\theta^2 + 1.26\theta - 44.0$.

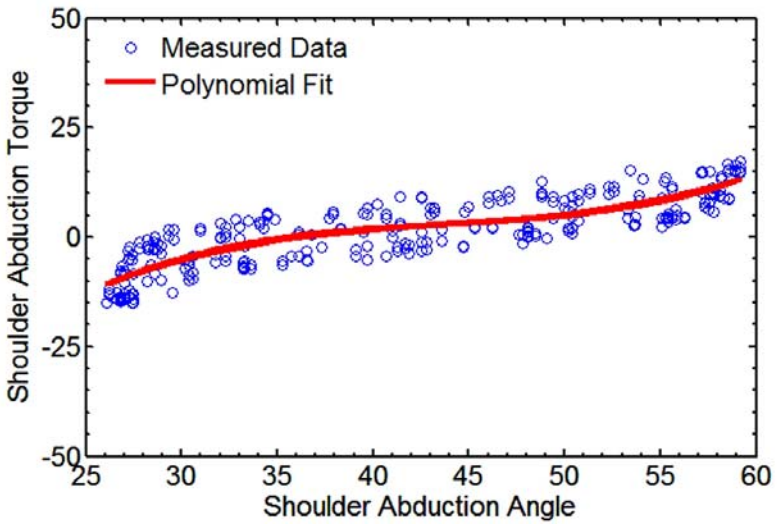

Figure B-2: The measured data and implemented polynomial fit for the shoulder abduction. Writing the shoulder abduction torque as τ and the shoulder abduction angle as θ, the polynomial fit is expressed as $\tau = 1.8 \times 10^{-3}\theta^3 - 0.24\theta^2 + 10.5\theta - 156.5$.

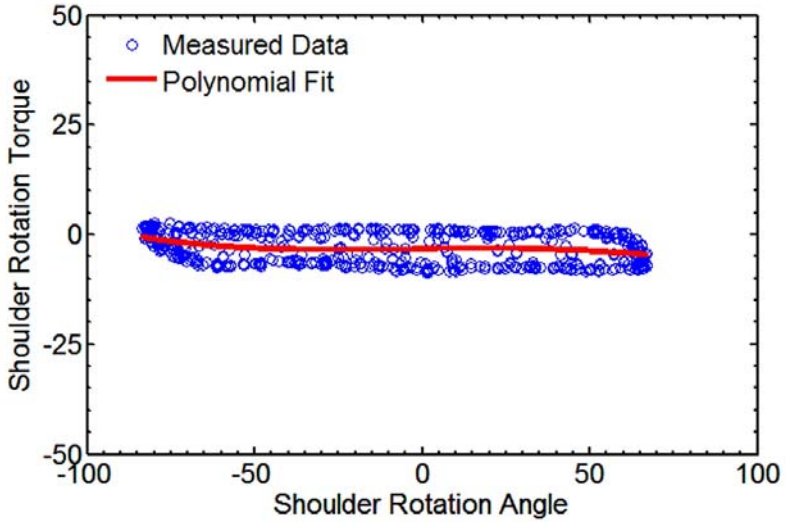

Figure B-3: The measured data and implemented polynomial fit for the shoulder rotation. Writing the shoulder rotation torque as τ and the shoulder rotation angle as θ, the polynomial fit is expressed as $\tau = -6.1 \times 10^{-6}\theta^3 - 6.3 \times 10^{-6}\theta^2 + 9.1 \times 10^{-3}\theta - 3.3$.

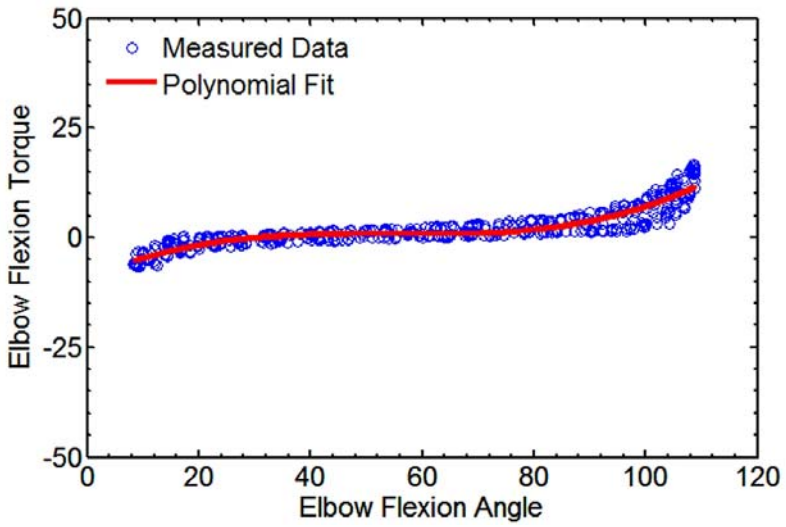

Figure B-4: The measured data and implemented polynomial fit for the elbow flexion. Writing the elbow flexion torque as τ and the elbow flexion angle as θ, the polynomial fit is expressed as $\tau = 6.8 \times 10^{-5}\theta^3 - 0.01\theta^2 + 0.59\theta - 9.5$.

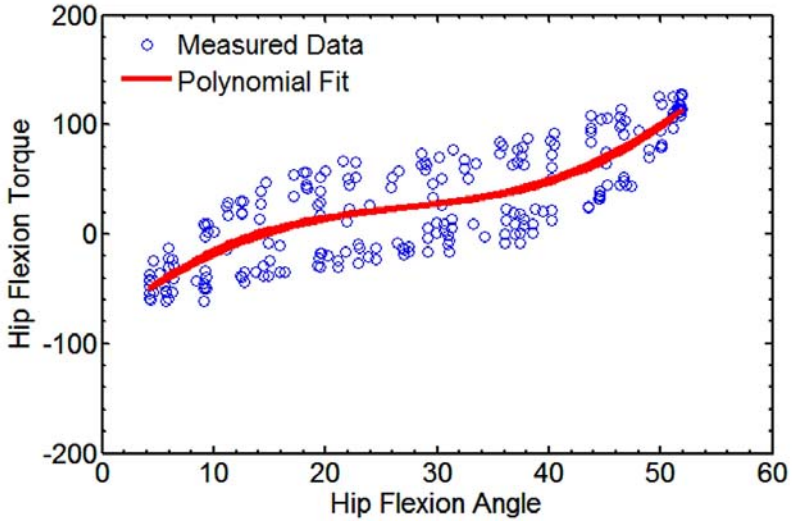

Figure B-5: The measured data and implemented polynomial fit for the hip flexion. Writing the hip flexion torque as τ and the hip flexion angle as θ, the polynomial fit is expressed as $\tau = 4.2 \times 10^{-3}\theta^3 - 0.35\theta^2 + 10.4\theta - 87.5$.

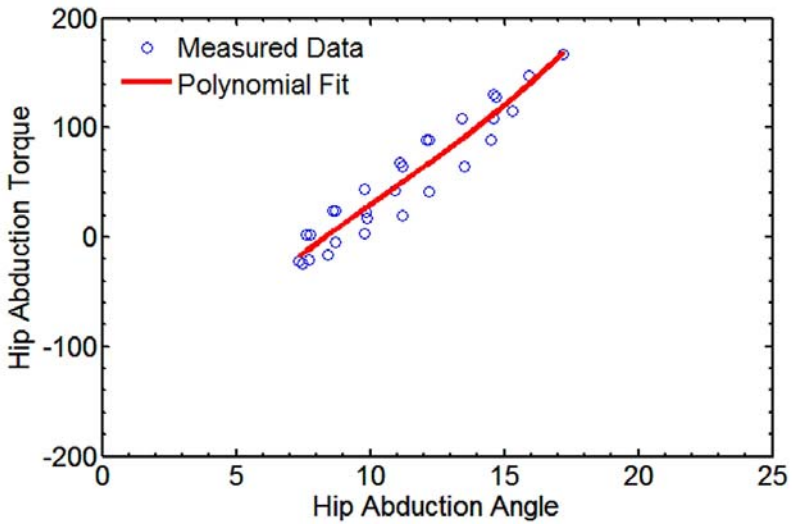

Figure B-6: The measured data and implemented polynomial fit for the hip abduction. Writing the hip abduction torque as τ and the hip abduction angle as θ, the polynomial fit is expressed as $\tau = 4.8 \times 10^{-2}\theta^3 - 1.5\theta^2 + 33.1\theta - 198.3$.

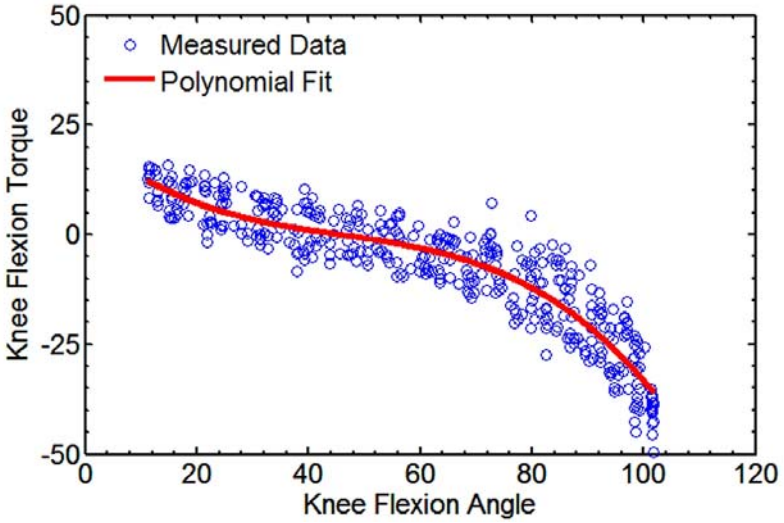

Figure B-7: The measured data and implemented polynomial fit for the knee flexion. Writing the knee flexion torque as τ and the knee flexion angle as θ, the polynomial fit is expressed as $\tau = -1.5 \times 10^{-4}\theta^3 + 0.02\theta^2 - 1.1\theta + 22.4$.

Appendix C

COUHES Informed Consent Form

Prior to reading the consent form, subjects were informed that they would only be participating in the pulley system portion of the study.

You are asked to participate in a research study conducted by Professor Dava Newman, PhD, and Leia Stirling, SM, from the department of Aeronautics and Astronautics at the Massachusetts Institute of Technology (M.I.T.). You have been asked to participate in this study because you have been identified as a member of the M.I.T. community who might be interested in such a research program. If you agree to take part in this study, you will be one of about 10 to 20 other subjects. You should read the information below and ask questions about anything you do not understand before deciding whether or not to participate.

PARTICIPATION AND WITHDRAWAL

Your participation in this study is completely voluntary and you are free to choose whether to be in it or not. If you choose to be in this study, you may subsequently withdraw from it at any time without penalty or consequences of any kind. The investigator may withdraw you from this research if circumstances arise which warrant doing so. If at any time during this study, any investigator feels that your safety is at risk, the investigators may terminate your participation in this study.

PURPOSE OF THE STUDY

The purpose of this study is to identify the control strategies used by humans to move their body from one location to another in the absence of gravity. Future space exploration missions will require astronauts to spend long periods of time in a microgravity environment and then be expected to perform tasks in full or partial gravity. Understanding the mechanisms by which humans adapt their control strategies to differing gravity environments may lead to the development

of new astronaut countermeasures. These countermeasures would be designed to accelerate astronauts' adaptation to a new gravity environment and reduce the risk of injuries associated with falls.

When weighted properly underwater, humans experience a weightless sensation similar to that experienced by astronauts in space. Humans can also experience a similar weightlessness feeling when rolling on a smooth floor in one plane. Thus, part of this experiment will be carried out both underwater and rolling on a smooth floor to simulate a zero-gravity, space environment. Ths study will be paired with another separate study (COUHES #2718) which investigates control strategies adopted during parabolic flight on NASA's KC-135 microgravity aircraft. Control strategies from the underwater experiments and the KC-135 experiments will be compared and techniques for underwater adaptation will be evaluated based on subjects performance.

PROCEDURES

If you volunteer to participate in this study, we would ask you to do the following things:

For subjects participating in the 1-G "rolling" portion of the study:

Preparation:

- You will lie on a rolling platform, similar to a "mechanic's creeper" and will be lightly strapped down.
- You will be instructed where the sensors are that you will be interacting with.

Acclimation:

- You will be given the opportunity to move yourself around using your arms and legs to push and pull yourself around while you get used to moving on the rolling platform.

Experiment:

- You will be asked to move your body along a small course made up of 3–4 sensors. You will use the sensors as restraints to pull and push yourself from one sensor to the next.
- The course will be repeated approximately 5–10 times.
- After completion of the course trials, you will be asked to perform a series of prescribed body motions including push-offs and landings.

For subjects participating in the underwater portion of the study:

Preparation:

- You will be briefed on all risks associated with SCUBA diving.
- The investigators will review emergency procedures.
- You will don a SCUBA mask, weight belt, ankle weights and small inflatable snorkeling vest.
- You will put a SCUBA regulator in your mouth from a tank sitting on the pool deck (this setup is known as a "hookah").
- You will next enter the water with 2 investigators. The investigators will work with you to adjust the weights on the weight belt and on your ankles to make you neutrally buoyant (neutrally buoyant means that you neither sink nor float).

Acclimation:

- You will be given the opportunity to swim at the bottom of the pool while using the hookah.
- You will be given as much time as you need to feel comfortable with ear equalization and breathing using the hookah.

Experiment:

- You will be asked to move your body along a small course made up of 3–4 sensors. You will use the sensors as restraints to pull and push yourself from one sensor to the next.
- The course will be repeated approximately 5–10 times.
- After completion of the course trials, you will be asked to perform a series of prescribed body motions including body twists, limb extensions and push-offs and landings.

For subjects participating in the pulley system portion of the study:

Preparation:

- You will be in two different harnesses depending on the rotation you will be performing. In the upright harness, you will be strapped in and lifted a few inches off the ground such that you cannot reach the floor with your feet. In the sling harness, you will lie down inside the harness and will be lifted such that you cannot reach the floor with your hands or feet.
- You will be instructed where the cameras are that will be recording your position.

Acclimation:

- You will be given the opportunity to make yourself comfortable in each harness before the experiment begins.

Experiment:

- You will be asked to reorient your body around your three body axes in a clockwise and counterclockwise manner.
- The rotations will be repeated approximately 5–10 times.

All underwater experiment operations will take place at either the Alumni pool or the Z-center pool at M.I.T. All other experiments will take place in Building 37 or in one of the M.I.T. gyms. The entire experiment will take approximately 2 hours to complete.

POTENTIAL RISKS AND DISCOMFORTS

The only risks involved in this study are those associated with SCUBA diving in shallow (less than 15 feet) water. There are no risks or discomforts associated with the sensor hardware. In any SCUBA diving environment, divers are exposed to risks and discomforts relating to pressure differentials. Subjects may feel discomfort when descending due to blockages in their inner ears. In extreme conditions, subjects may rupture an eardrum if the blockage is severe. When working underwater, there is always a risk of drowning if subjects inhale sufficient amounts of water. While this study will be carried out in less than 15 feet of water, there is still a small risk of subjects incurring over-expansion injuries. These can occur if a subject is breathing regulated (high pressure) air underwater, holds his/her breath and quickly swims to the surface. As a safety precaution, two fully trained SCUBA divers will accompany the subject during the experiment. Each SCUBA diver will have a spare breathing regulator and will be ready to assist the subject in the event of an emergency. If at any time during the study any investigator feels that the subject has become uncomfortable underwater to the point where the subject's safety is in jeopardy, the investigators may terminate the subject's participation in this study.

For subjects performing only the 1-G "rolling" study, there are no inherent risks.

For subjects performing the pulley system portion of the study, slight discomfort occurs for some people when wearing the upright harness. You will be allotted breaks in order to minimize any discomfort. The height you will be lifted above the ground is small, but in order to be completely safe, mats will be provided underneath the pulley configuration.

POTENTIAL BENEFITS

Other than accumulating SCUBA experience, subjects are NOT anticipated to benefit directly from participating in this study. Understanding the control strategies of astronauts is central to the development of countermeasures that will allow humans to conduct extended space exploration missions. This study is designed to reveal the typical control strategies that humans adopt in a 0-G setting and will hopefully lead to new countermeasure development.

PAYMENT FOR PARTICIPATION

Subjects will NOT be paid for participating in this study.

CONFIDENTIALITY

Any information that is obtained in connection with this study and that can be identified with you will remain confidential and will be disclosed only with your permission or as required by law.

Video taping will be only used to back out joint angles. Several video cameras will record the subject's motions and custom software will be used to extract the joint angles. If possible, the cameras will be set up to exclude the subjects' faces from the video. Furthermore, all subjects will be wearing SCUBA masks and regulators, so subject recognition will be extremely difficult, even if video cameras happen to capture subjects faces. In the event that a subject is recognizable, the video will be altered to obscure the identity. The anonymity of the subjects will be fully preserved.

Following the experiment, force and joint angle data will be stored on lab hard drives and on CD/DVDs. All video from which subjects can be recognized will be destroyed.

IDENTIFICATION OF INVESTIGATORS

If you have any questions or concerns about the research, please feel free to contact:

Principal Investigator	Professor Dava Newman dnewman@mit.edu 617-258-8799
Co-Investigator	Leia Stirling leia@mit.edu 617-452-4040

EMERGENCY CARE AND COMPENSATION FOR INJURY

In the unlikely event of physical injury resulting from participation in this research you may receive medical treatment from the M.I.T. Medical Department, including emergency treatment and follow-up care as needed. Your insurance carrier may be billed for the cost of such treatment. M.I.T. does not provide any other form of compensation for injury. Moreover, neither the offer to provide medical assistance nor the actual provision of medical services shall be construed as an admission of negligence or acceptance of liability. Questions regarding this policy may be directed to M.I.T.'s Insurance Office, (617) 253-2823.

RIGHTS OF RESEARCH SUBJECTS

You are not waiving any legal claims, rights or remedies because of your participation in this research study. If you feel you have been treated unfairly, or you have questions regarding your rights as a research subject, you may contact the Chairman of the Committee on the Use of Humans as Experimental Subjects, M.I.T., Room E25-143B, 77 Massachusetts Ave, Cambridge, MA 02139, phone 1-617-253 6787.

SIGNATURE OF RESEARCH SUBJECT OR LEGAL REPRESENTATIVE

I understand the procedures described above. My questions have been answered to my satisfaction, and I agree to participate in this study. I have been given a copy of this form.

_____

Name of Subject

_____

Name of Legal Representative (if applicable)

_____

Signature of Subject or Legal Representative Date

SIGNATURE OF INVESTIGATOR

In my judgment the subject is voluntarily and knowingly giving informed consent and possesses the legal capacity to give informed consent to participate in this research study.

_____

Signature of Investigator Date

Appendix D

Added Human Rotation Experiment Information

D.1 Background and Directions for the Subjects

The following background and directions were read to each subject regardless of group.

> In this study I am looking at self-rotation of astronauts. By self-rotation I mean the ability for one to rotate without any external torques. Explicit self-rotation, while helpful for intravehicular activity (IVA), is essential for extravehicular activity (EVA). Consider an astronaut performing an EVA and during this period, the astronaut becomes separated from the spacecraft and the thruster backpack incurs a partial failure. If the astronaut has trained with a simple reorientation methodology, a maneuver can be performed such that the remaining thruster will direct the astronaut back to the spacecraft. While astronauts have experimented with methods for rotating about their body axes, no universally adopted methods exist. Further, no training is provided to assist in learning any motion strategies.
>
> In this experiment you will be placed into two different types of harnesses: (1) a sling harness, in which you can rotate about your y-axis (when on your side) and (2) a climbing harness, in which you can rotate about your z and x-axes. The figure of the definition of the axes will be provided for you in your training document. During this test you will be asked to rotate clockwise and counterclockwise about the various axes. Each rotation will be repeated several times. When performing the motions, please perform them at a comfortable operating speed. If at any time you feel uncomfortable and need to rest, please let me know. There are a few scheduled breaks during this experiment.
>
> Please do not hold onto the harness when performing motions about the z and x-axes. For each of these rotations you may use your arms and/or legs. For

rotations about the y-axis, you may only use your legs to achieve the rotation. You may use your arms to hold the harness in support of your body.

D.2 Modified Cooper-Harper Rating Scale

The questions given by the test coordinator are based on the handling qualities rating scale shown in Figure D-1. This scale was originally developed to rate the aircraft handling qualities of an aircraft by test pilots [28].

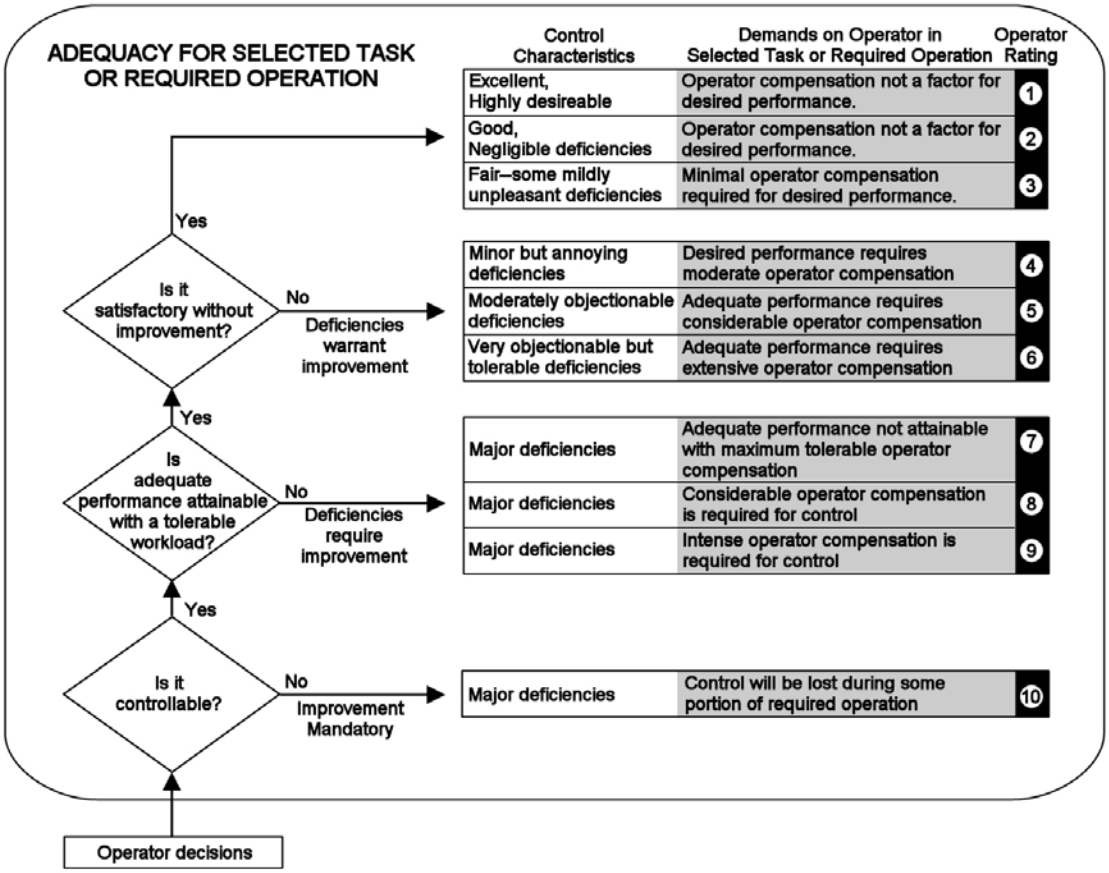

Figure D-1: Cooper-Harper handling quality scale.

The test conductor guides the subject Cooper-Harper Rating evaluation with the following questions:

Question 1. Can the task be reliably performed?

- If yes, go to question 2.
- If no, assign a rating of 10.

Question 2. Is adequate task performance attainable with a tolerable workload (i.e. if deficiencies require improvement)?

- If yes, go to question 3.
- If no, prompt subject for a rating between 7-9.

Question 3. Is task performance adequate without improvement?

- If yes, prompt subject for a rating between 1-3.
- If no, prompt subject for a rating of 4-6.

D.3 NASA Task Load Index (TLX)

The information sheet provided for the subjects to guide them through the NASA-TLX is as follows:

> **Mental Demand:** How much mental and perceptual activity was required (e.g., thinking, deciding, calculating, remembering, looking, searching, etc.)? Was the task easy or demanding, simple or complex, exacting or forgiving?
>
> **Physical Demand:** How much physical activity that was required (e.g., pushing, pulling, turning control, activating, etc.)? Was the task easy or demanding, slow or brisk, slack or strenuous, restful or laborious?
>
> **Temporal Demand:** How much time pressure did you feel due to the rate or pace at which the tasks or task elements occurred? Was the task slow and leisurely or rapid and frantic?
>
> **Performance:** How successful you think you were in accomplishing the goals of the task set by the experimenter? How satisfied were you with your performance in accomplishing these goals?
>
> **Effort:** How hard did you have to work (mentally and physically) to accomplish your level of performance?
>
> **Frustration:** How insecure, discouraged, irritated, stressed and annoyed versus secure, gratified, content, relaxed and complacent did you feel during the task?
>
> **Try to remember how you feel when you are determining your scoring for your first trial and use the same scaling for future trials.**

The NASA-TLX was administered on a computer. Screen captures of the questionnaire are shown in Figure D-2. Part one of the questionnaire had the subject rate the magnitude of each component of the workload in the task performed. Part two had the subject perform 15 pairwise comparisons of the workload factors to obtain relative weightings.

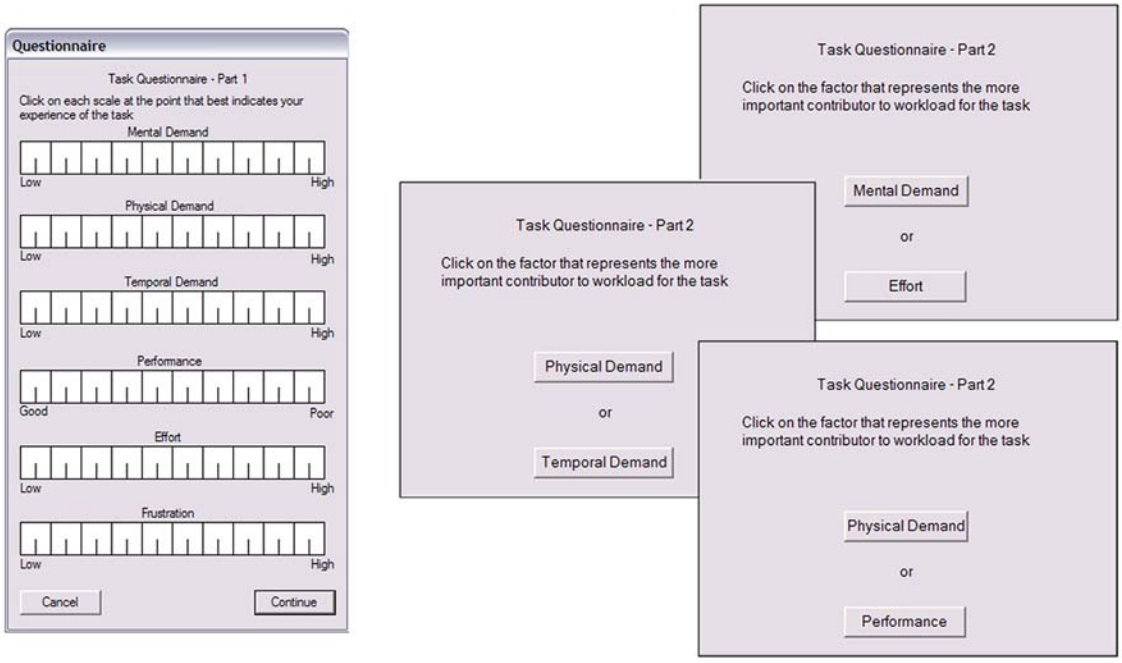

Figure D-2: Screen captures from the NASA-TLX questionnaire. On the left is part one, where the subject rated the magnitudes of each workload component. On the right are three of the fifteen comparisons that the subject made for part two.

Appendix E

Individual Subject Data from Experiments

Figures E-1 through E-20 show the performance times and modified Cooper-Harper rating for all twenty subjects.

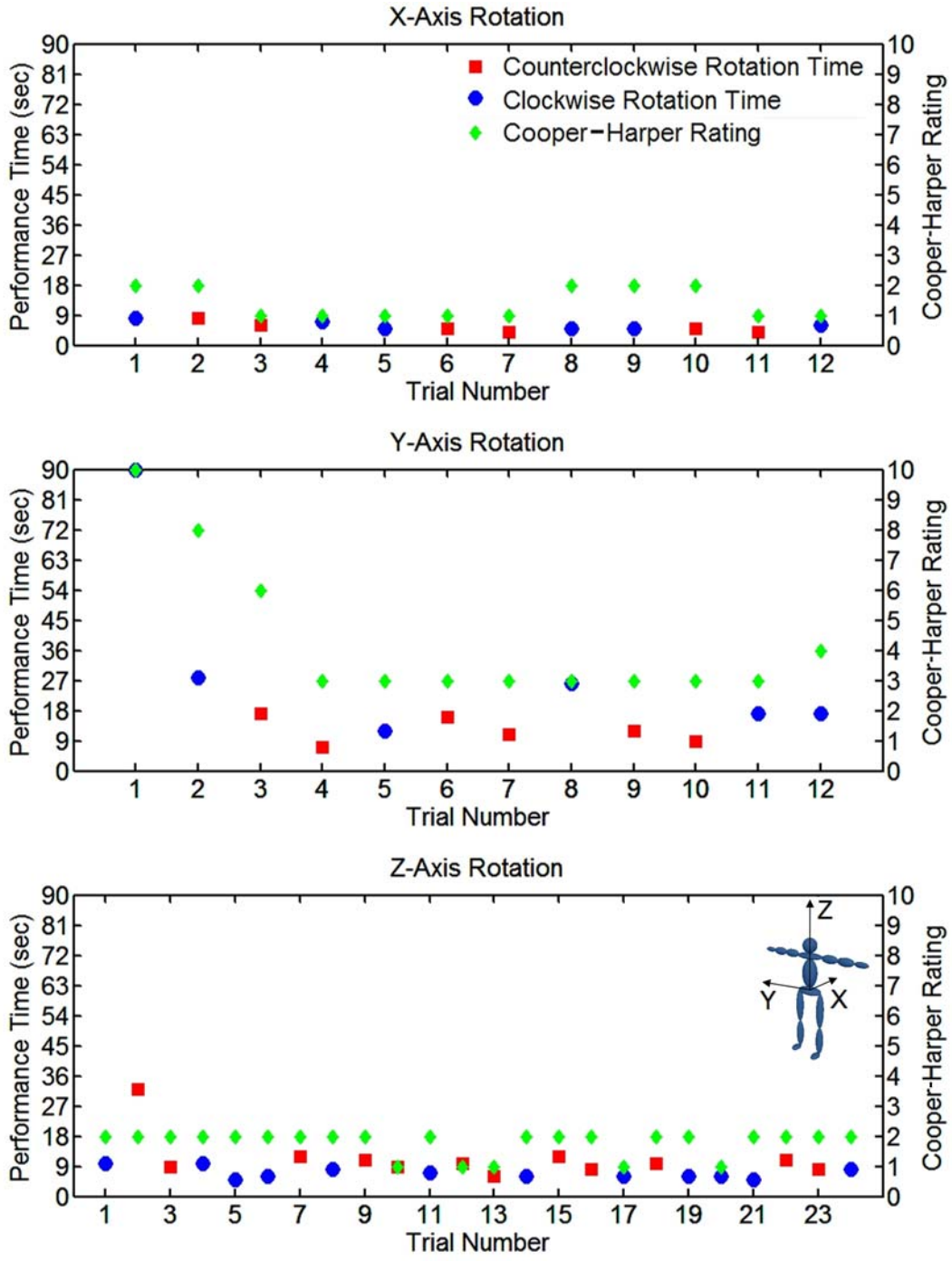

Figure E-1: Performance times and modified Cooper-Harper rating for Subject 1.

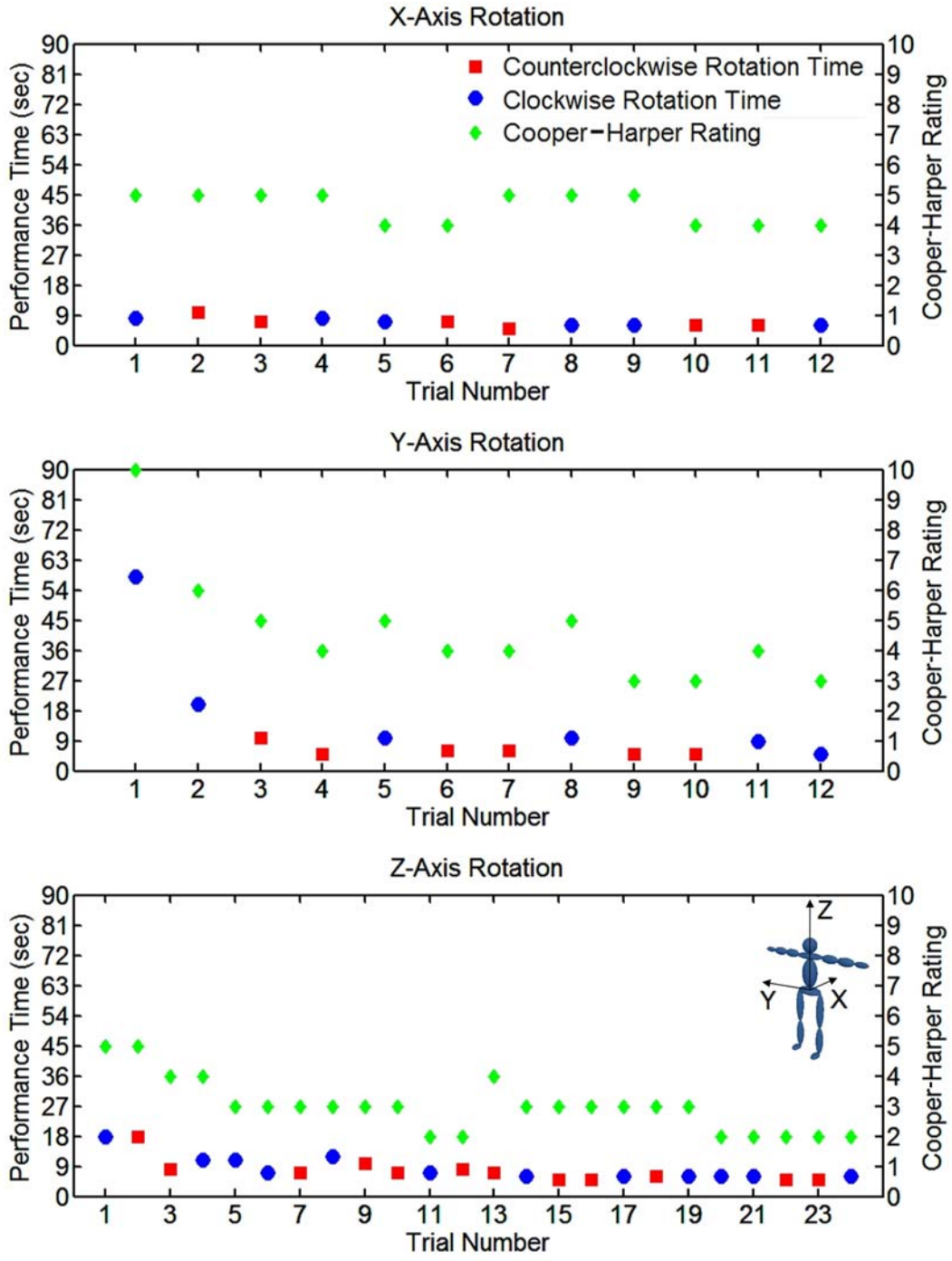

Figure E-2: Performance times and modified Cooper-Harper rating for Subject 2.

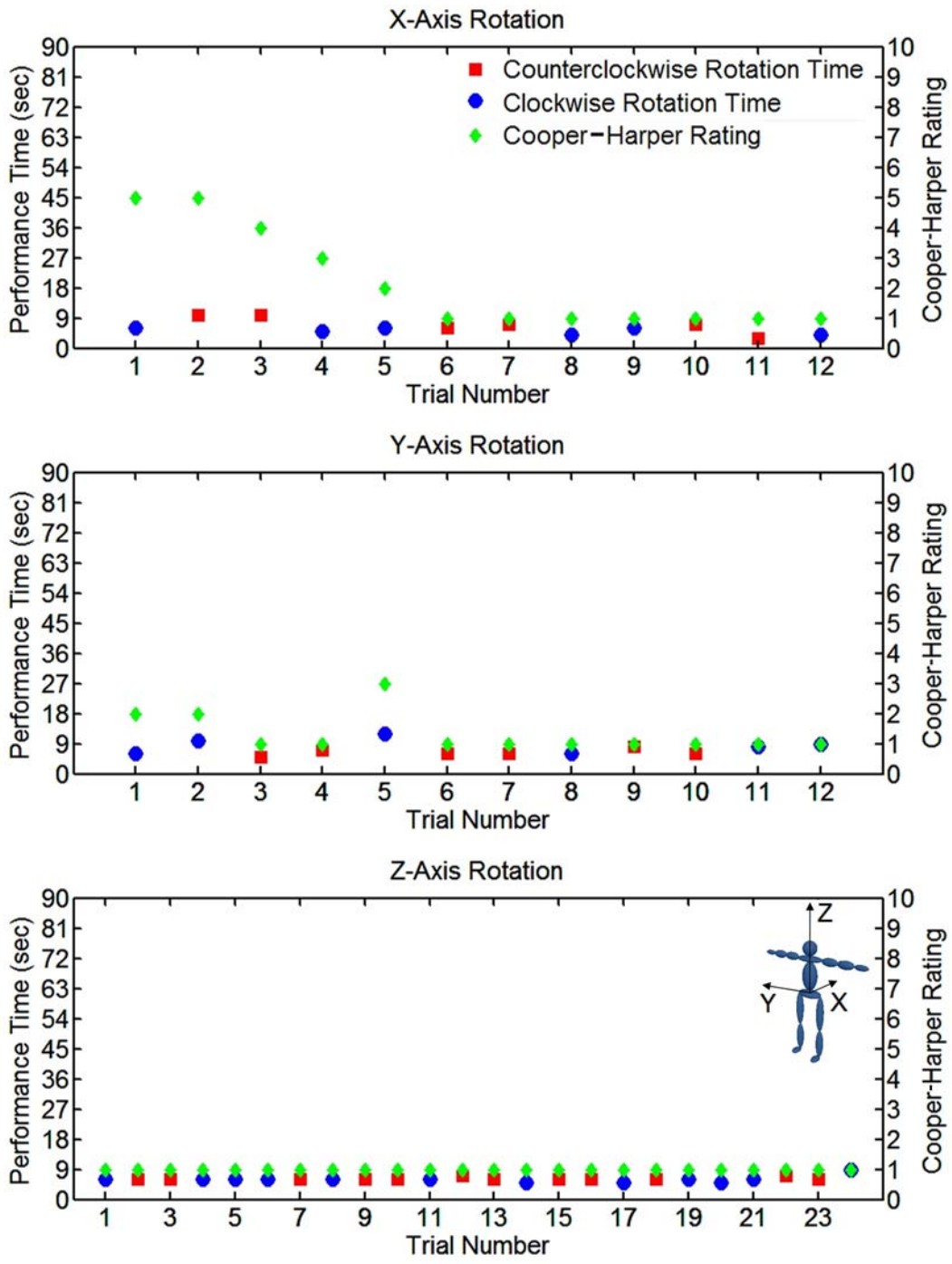

Figure E-3: Performance times and modified Cooper-Harper rating for Subject 3.

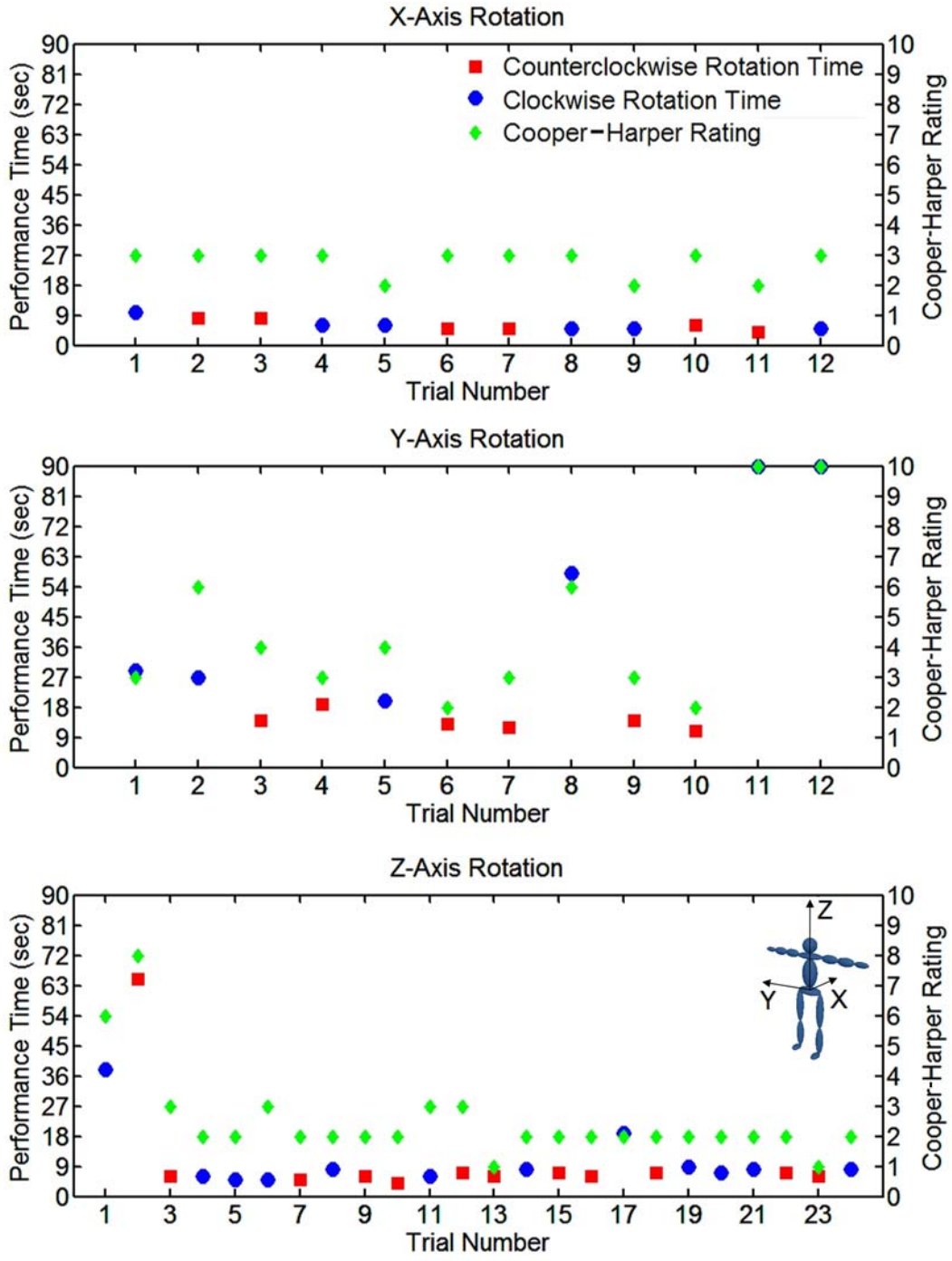

Figure E-4: Performance times and modified Cooper-Harper rating for Subject 4.

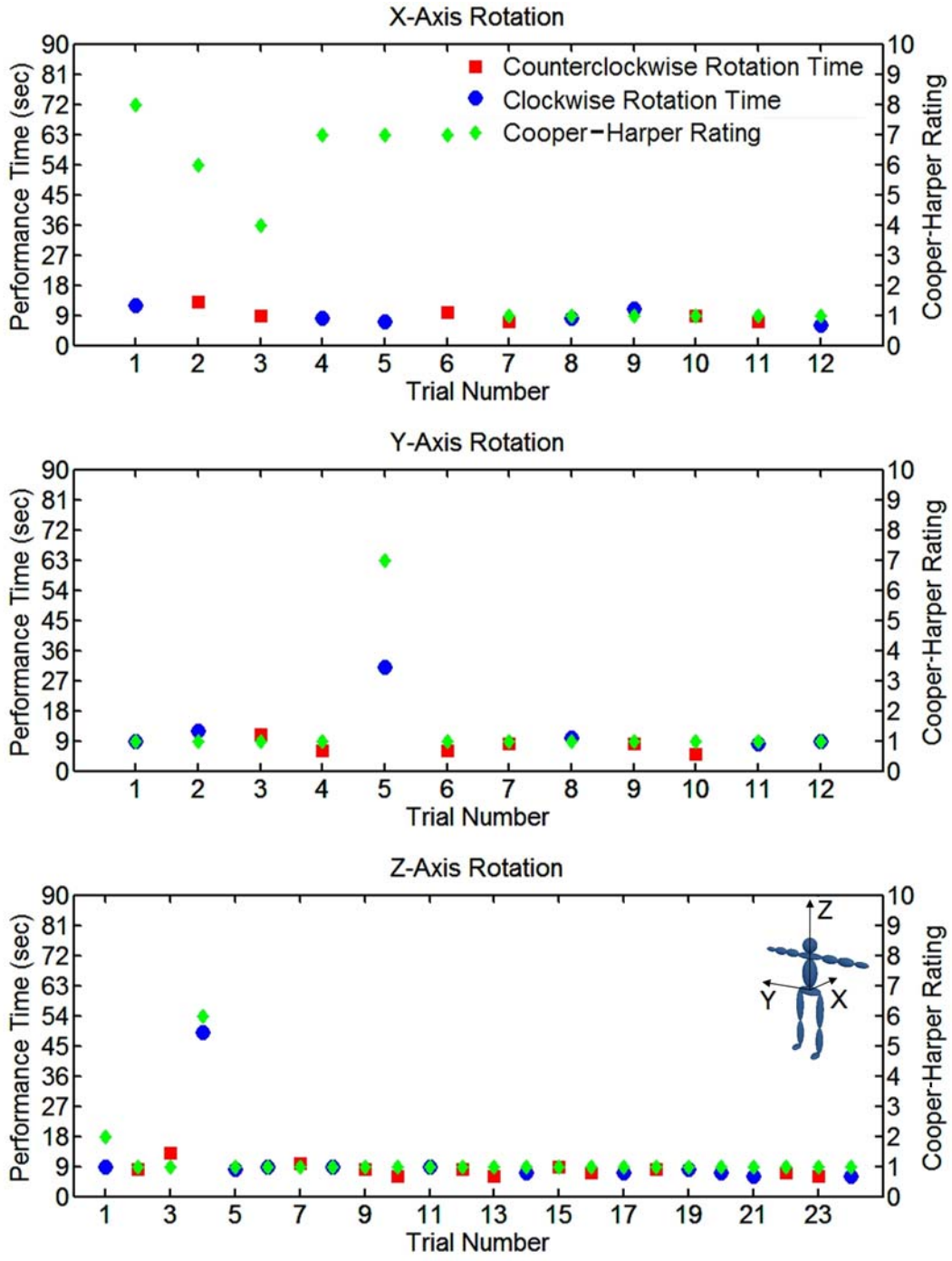

Figure E-5: Performance times and modified Cooper-Harper rating for Subject 5.

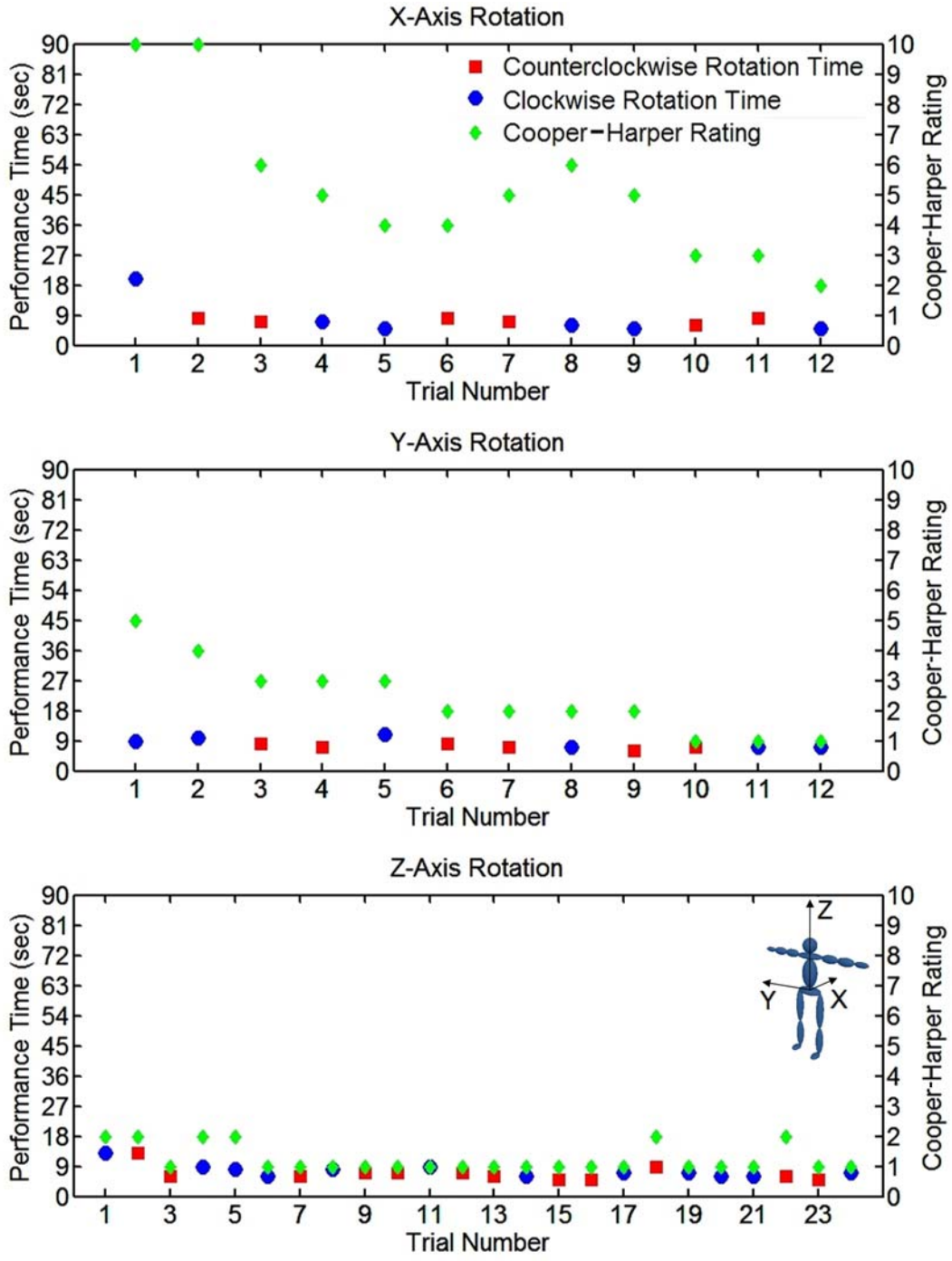

Figure E-6: Performance times and modified Cooper-Harper rating for Subject 6.

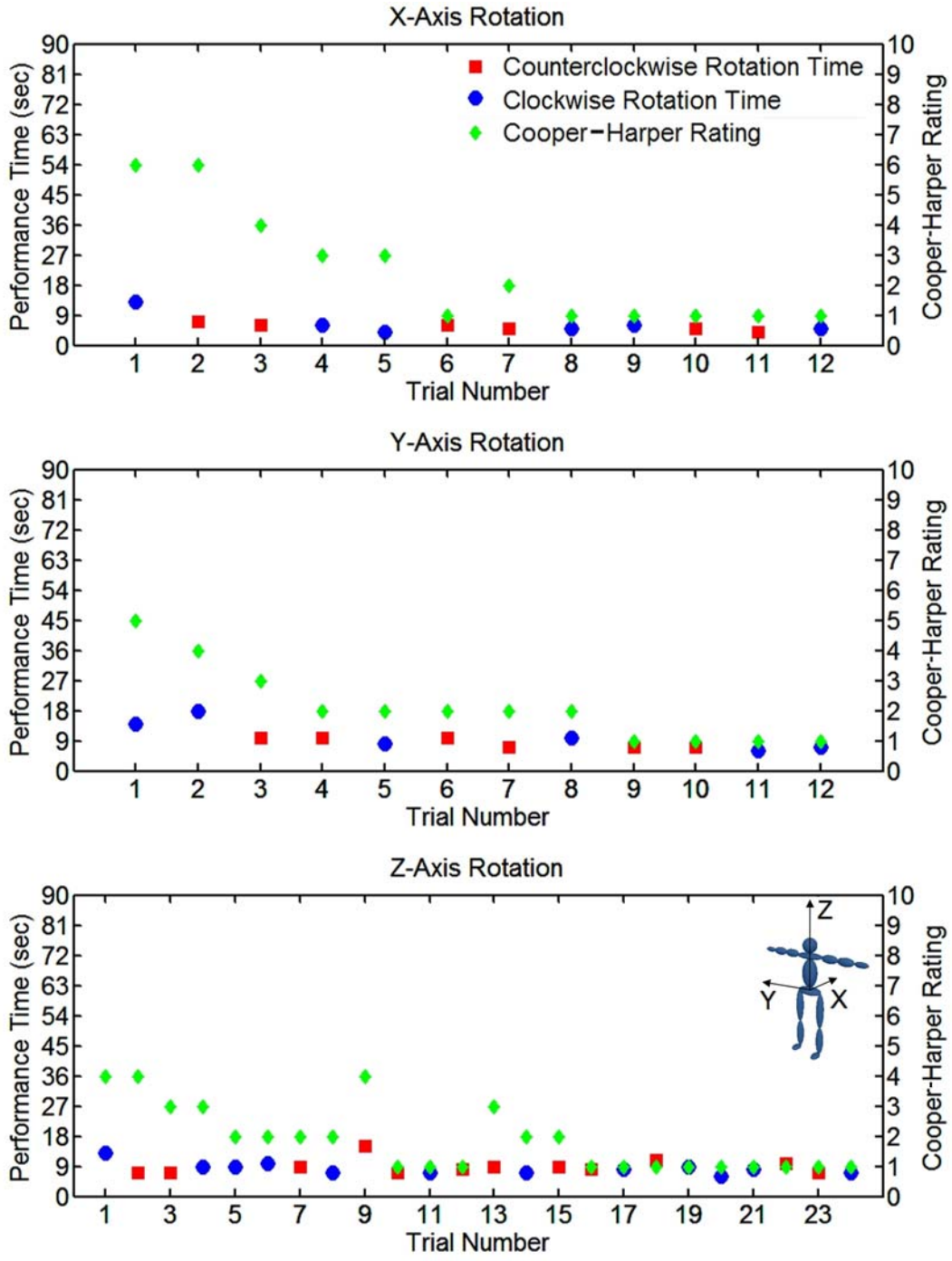

Figure E-7: Performance times and modified Cooper-Harper rating for Subject 7.

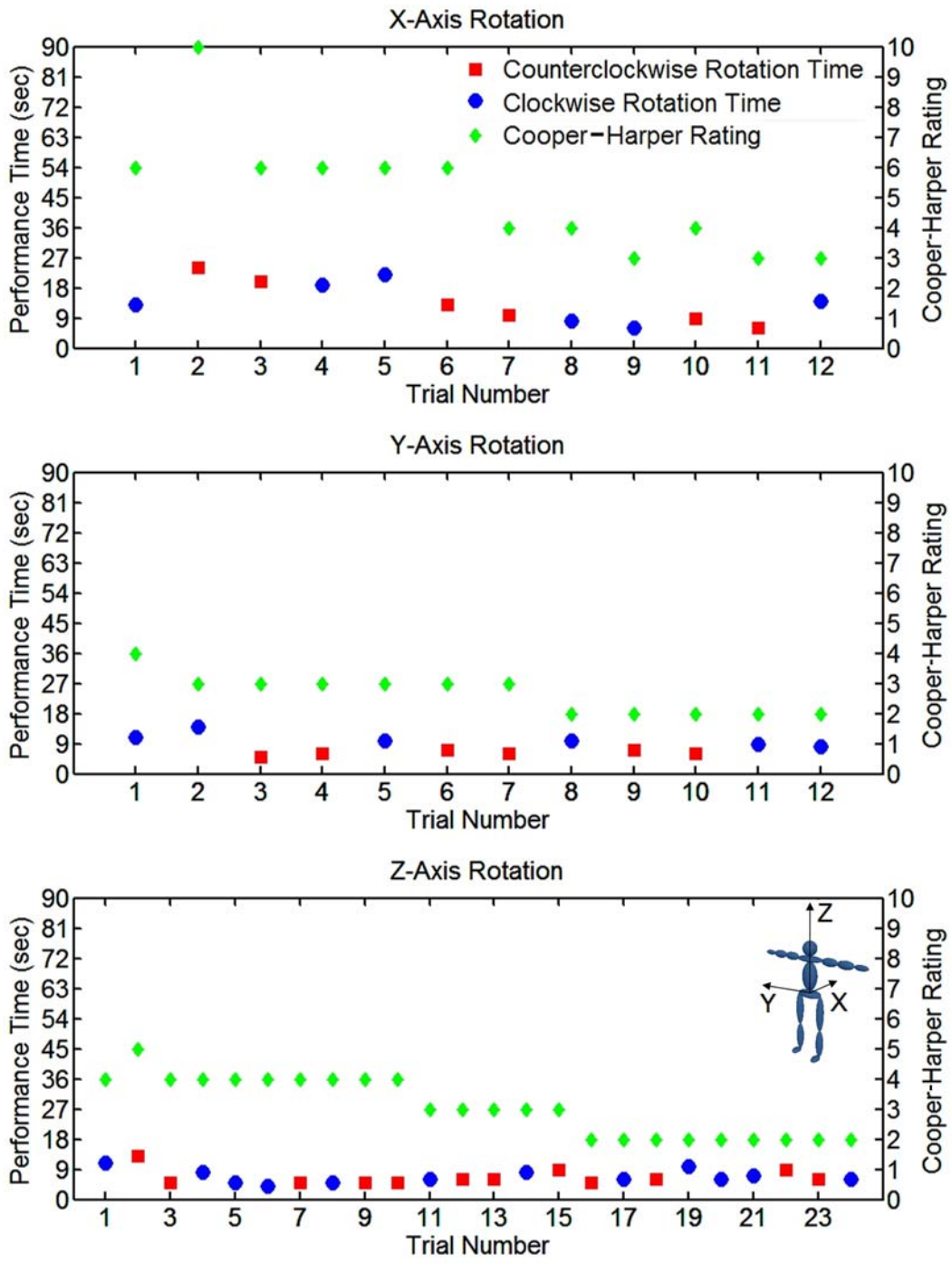

Figure E-8: Performance times and modified Cooper-Harper rating for Subject 8.

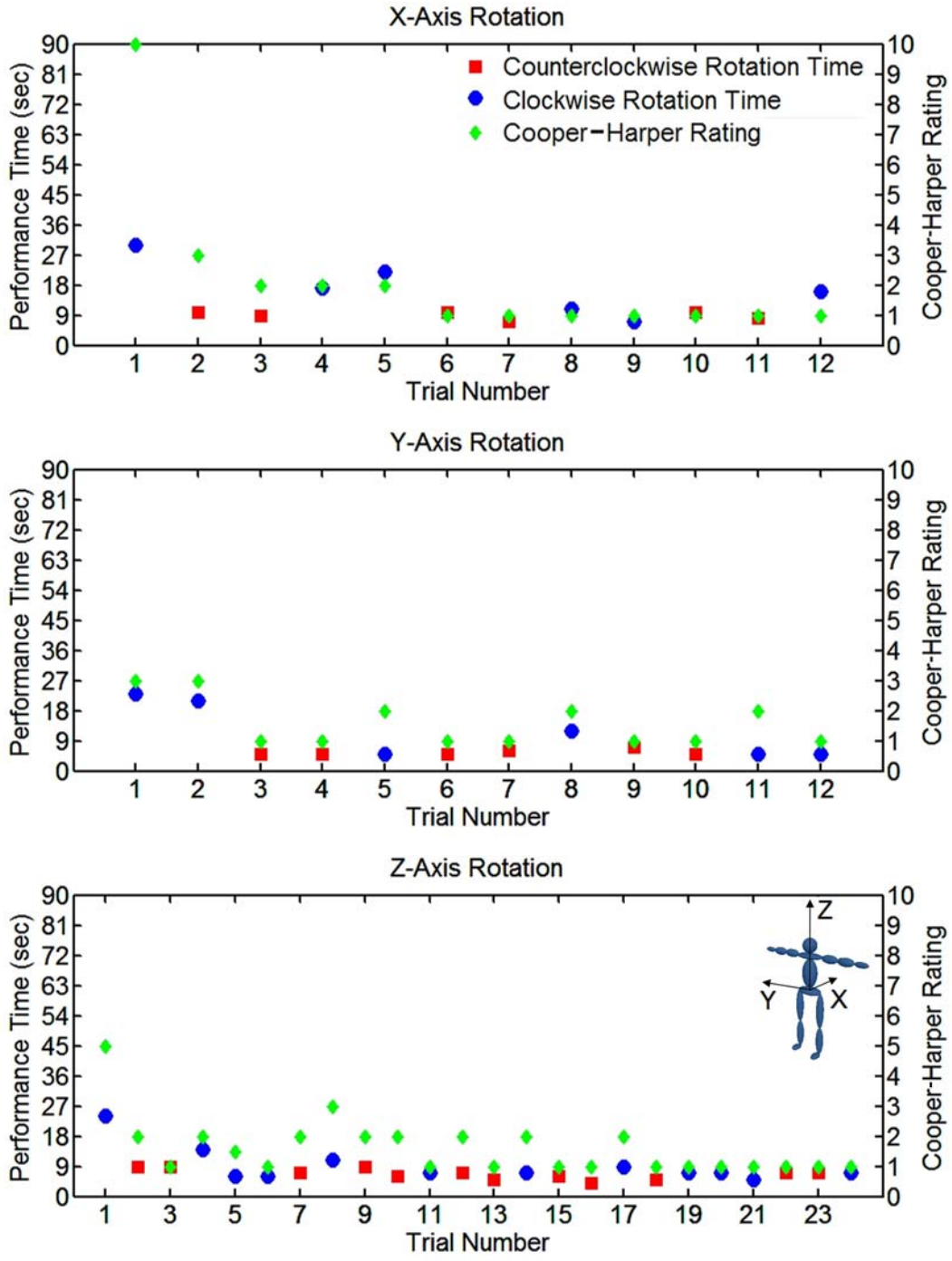

Figure E-9: Performance times and modified Cooper-Harper rating for Subject 9.

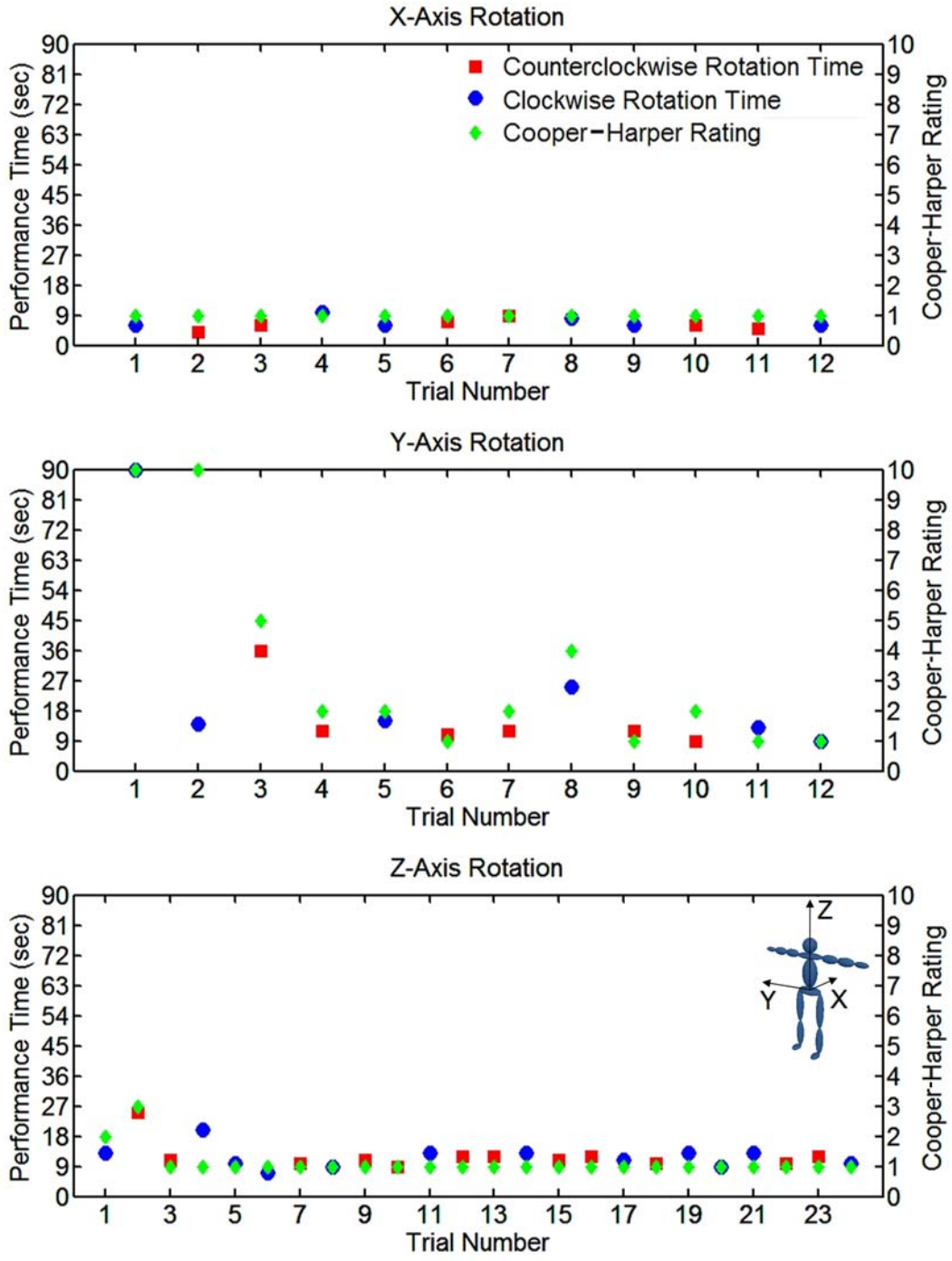

Figure E-10: Performance times and modified Cooper-Harper rating for Subject 10.

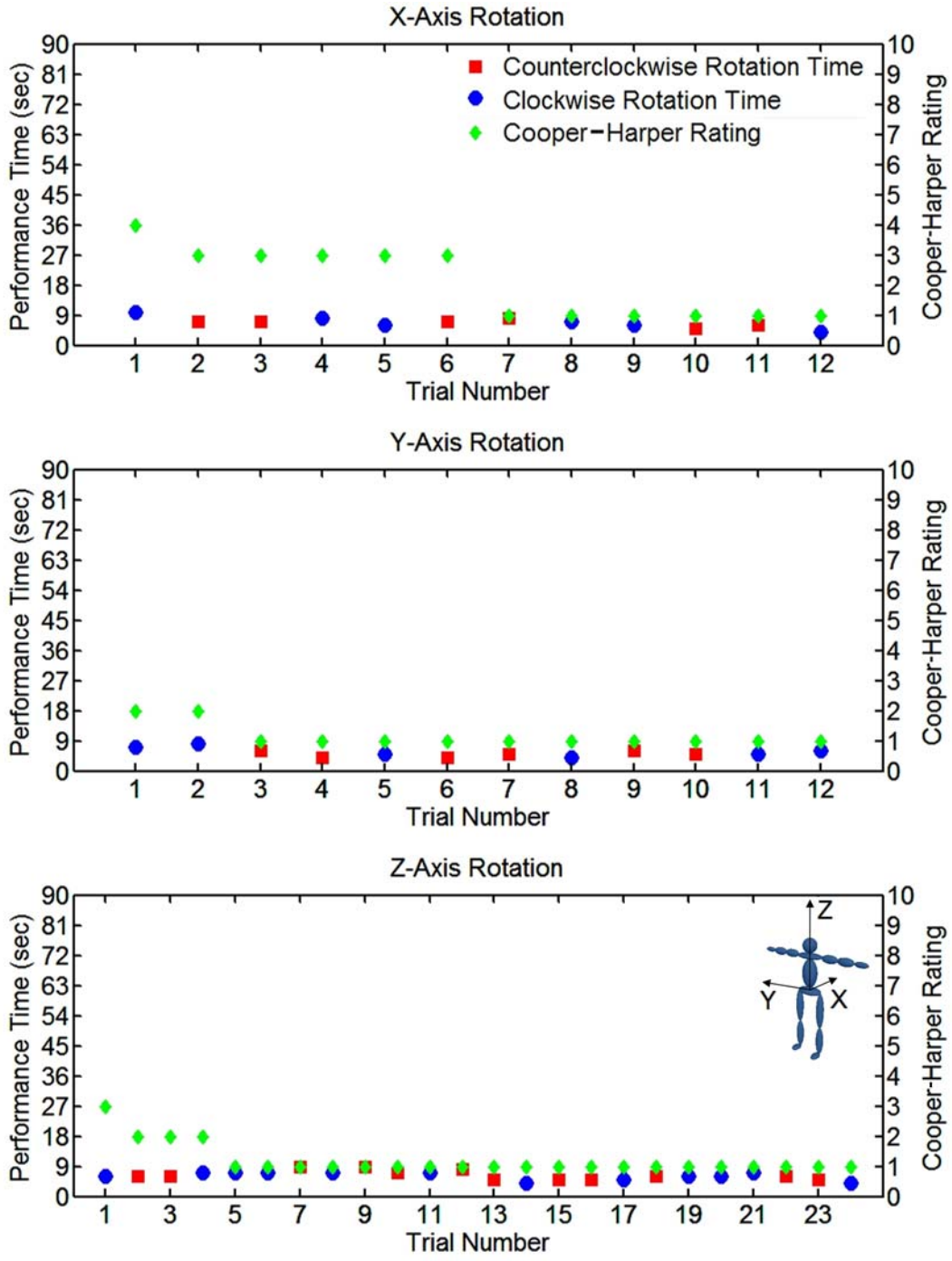

Figure E-11: Performance times and modified Cooper-Harper rating for Subject 11.

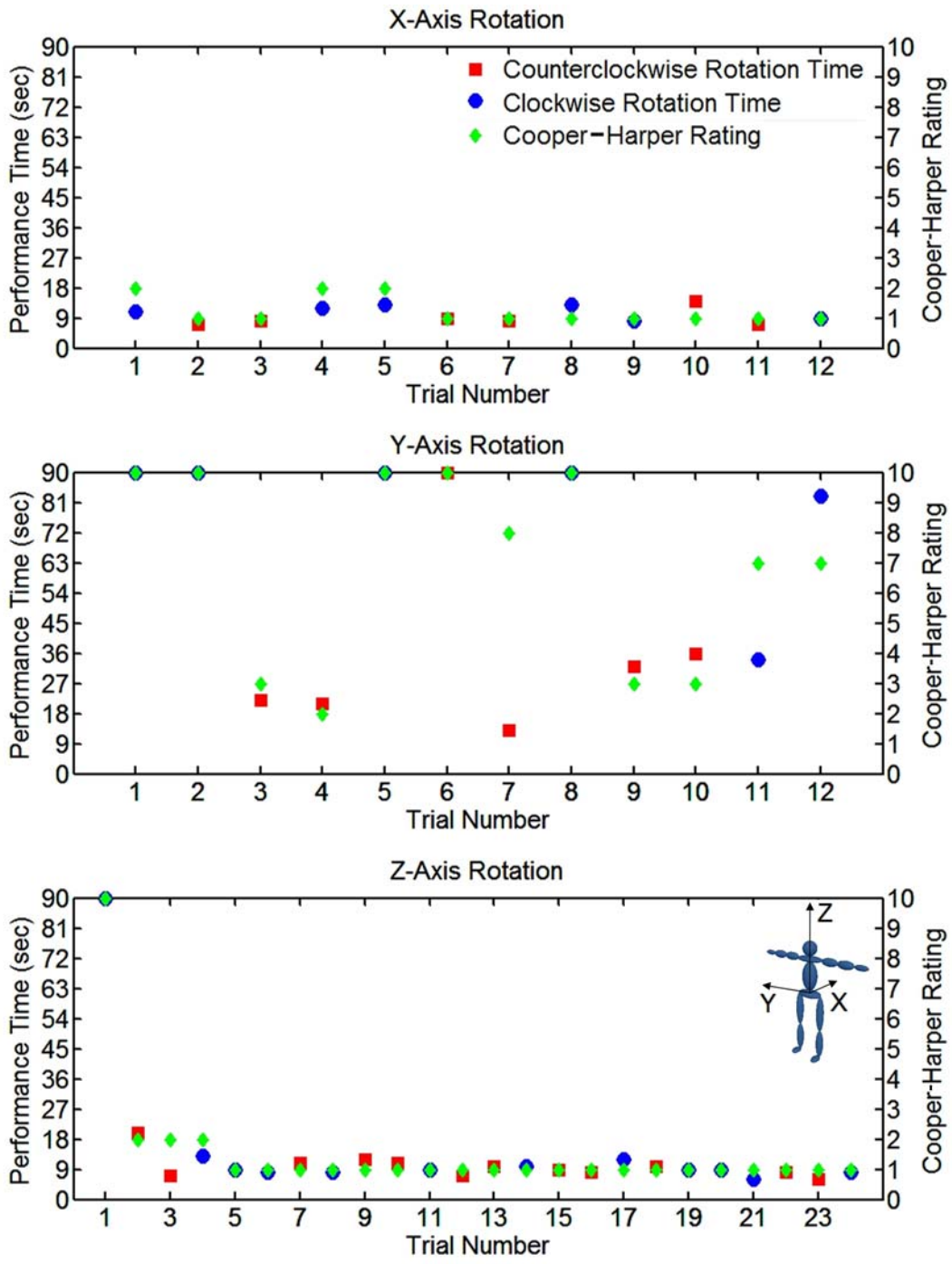

Figure E-12: Performance times and modified Cooper-Harper rating for Subject 12.

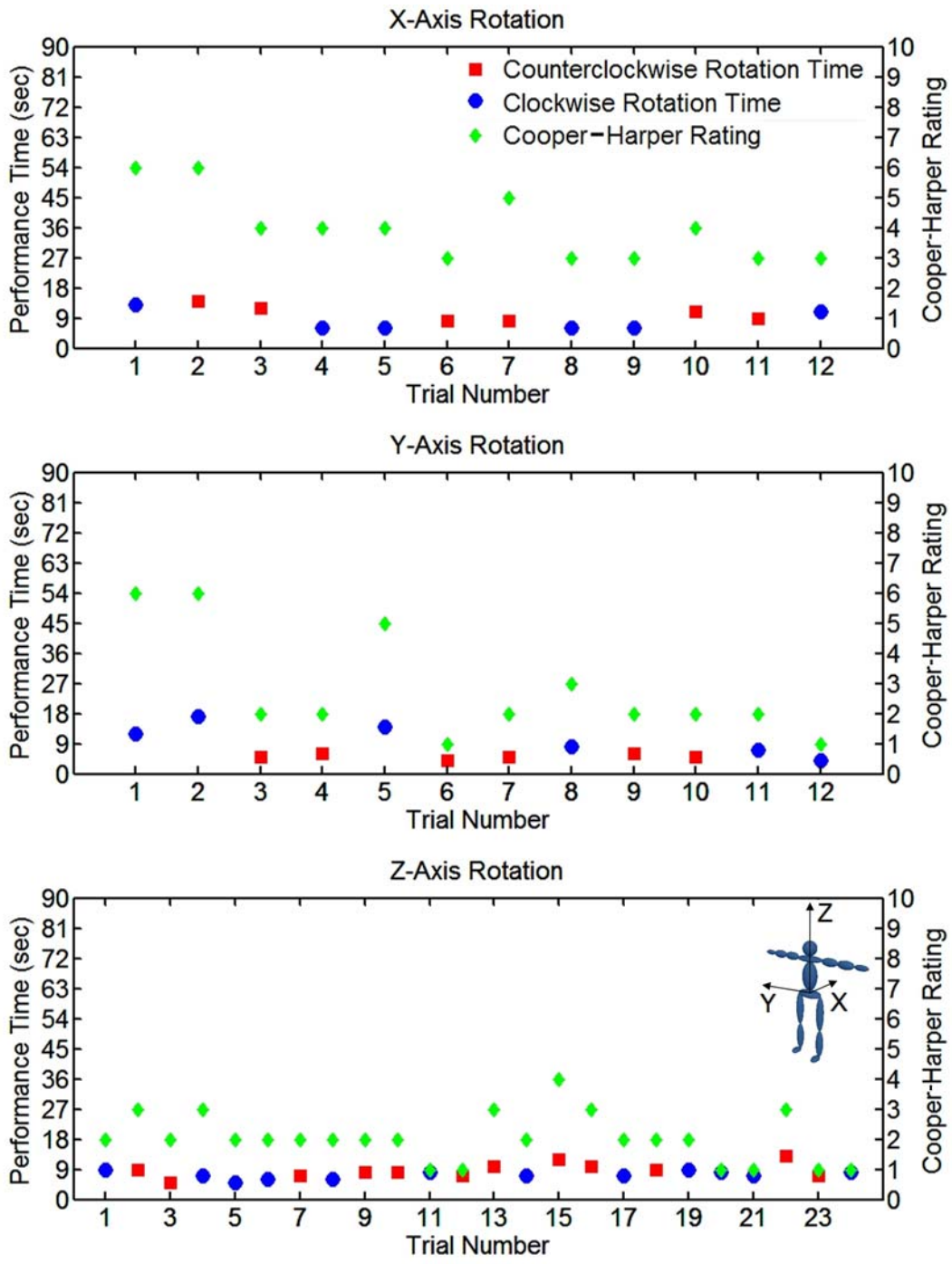

Figure E-13: Performance times and modified Cooper-Harper rating for Subject 13.

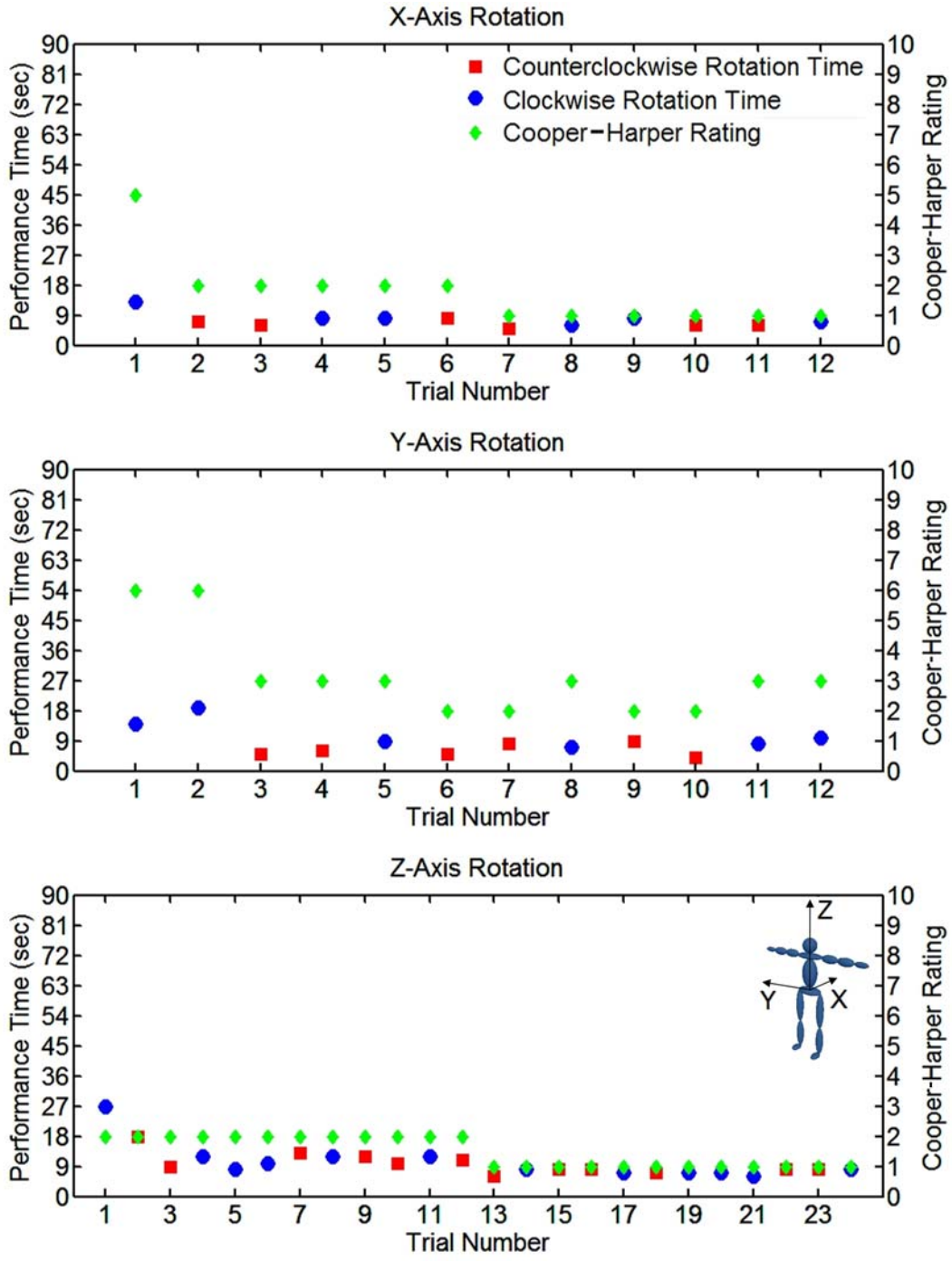

Figure E-14: Performance times and modified Cooper-Harper rating for Subject 14.

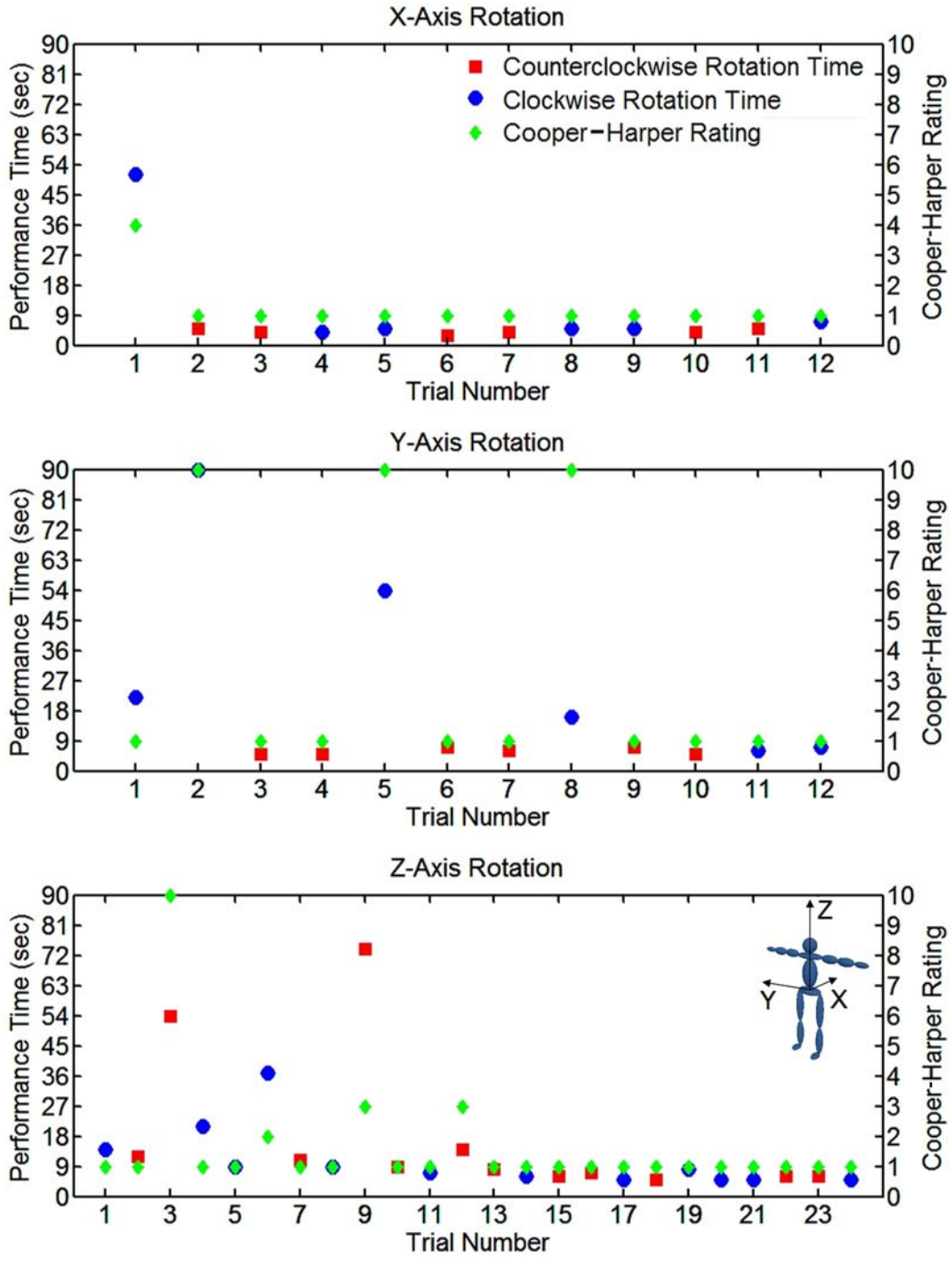

Figure E-15: Performance times and modified Cooper-Harper rating for Subject 15.

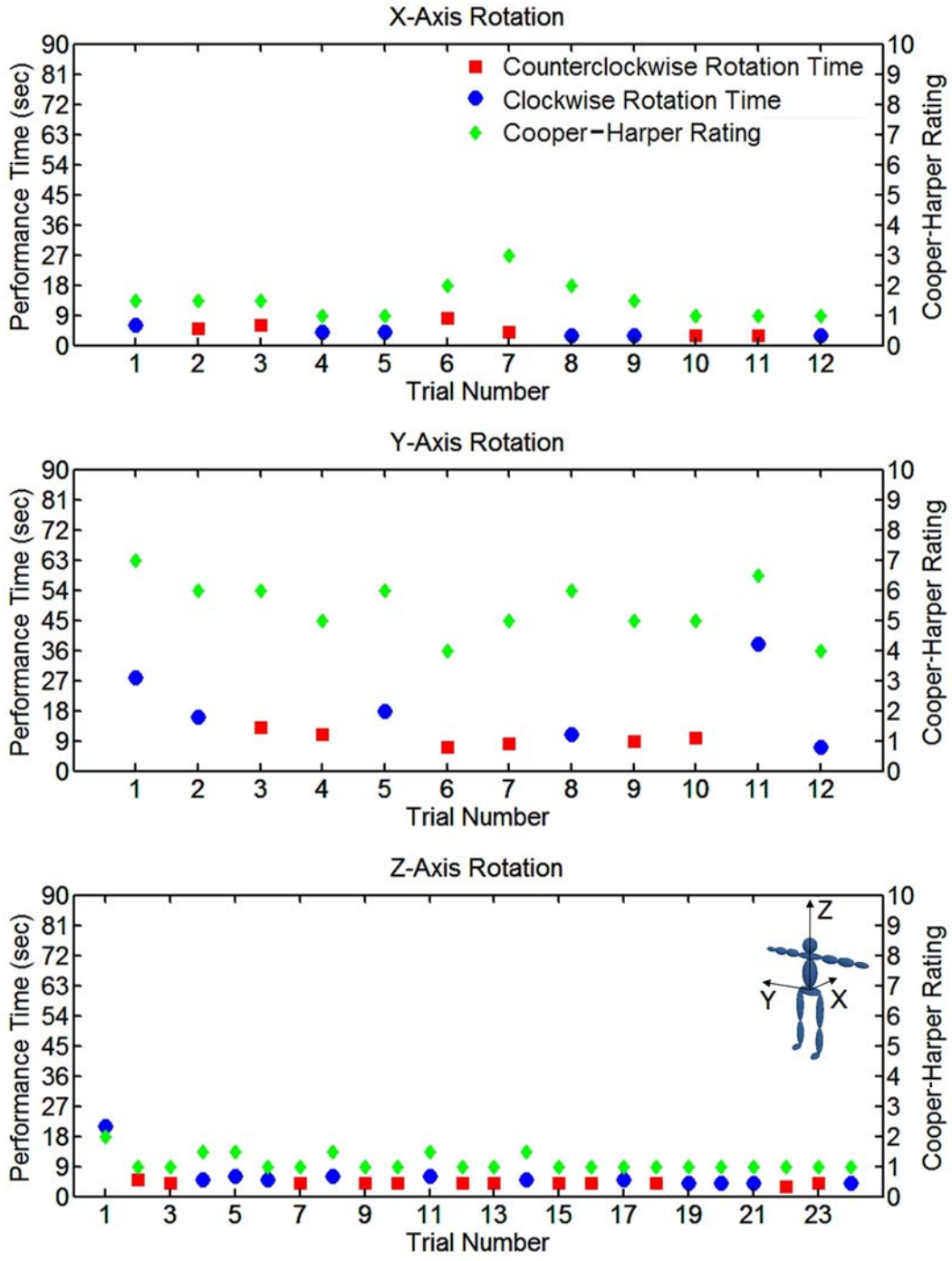

Figure E-16: Performance times and modified Cooper-Harper rating for Subject 16.

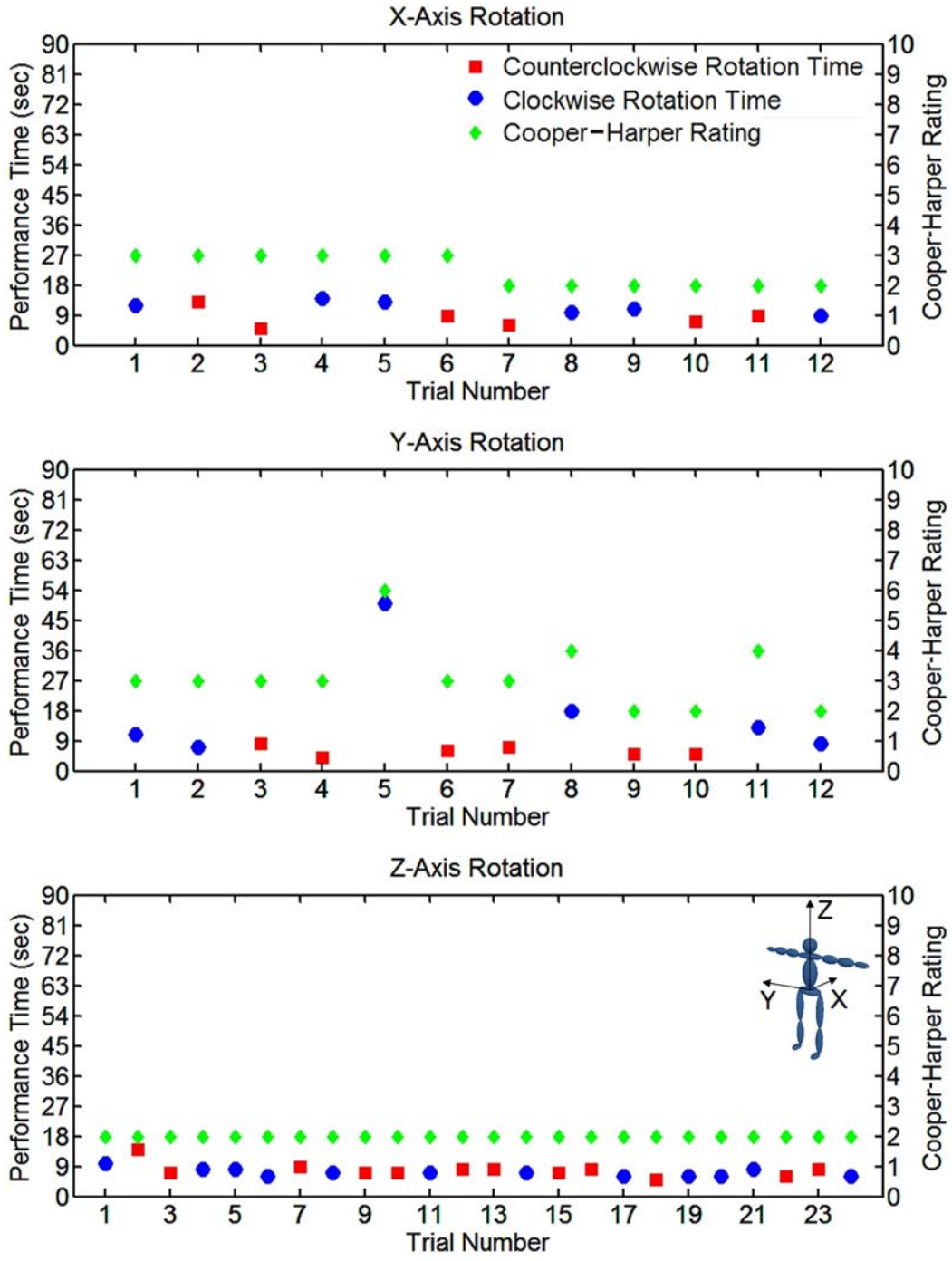

Figure E-17: Performance times and modified Cooper-Harper rating for Subject 17.

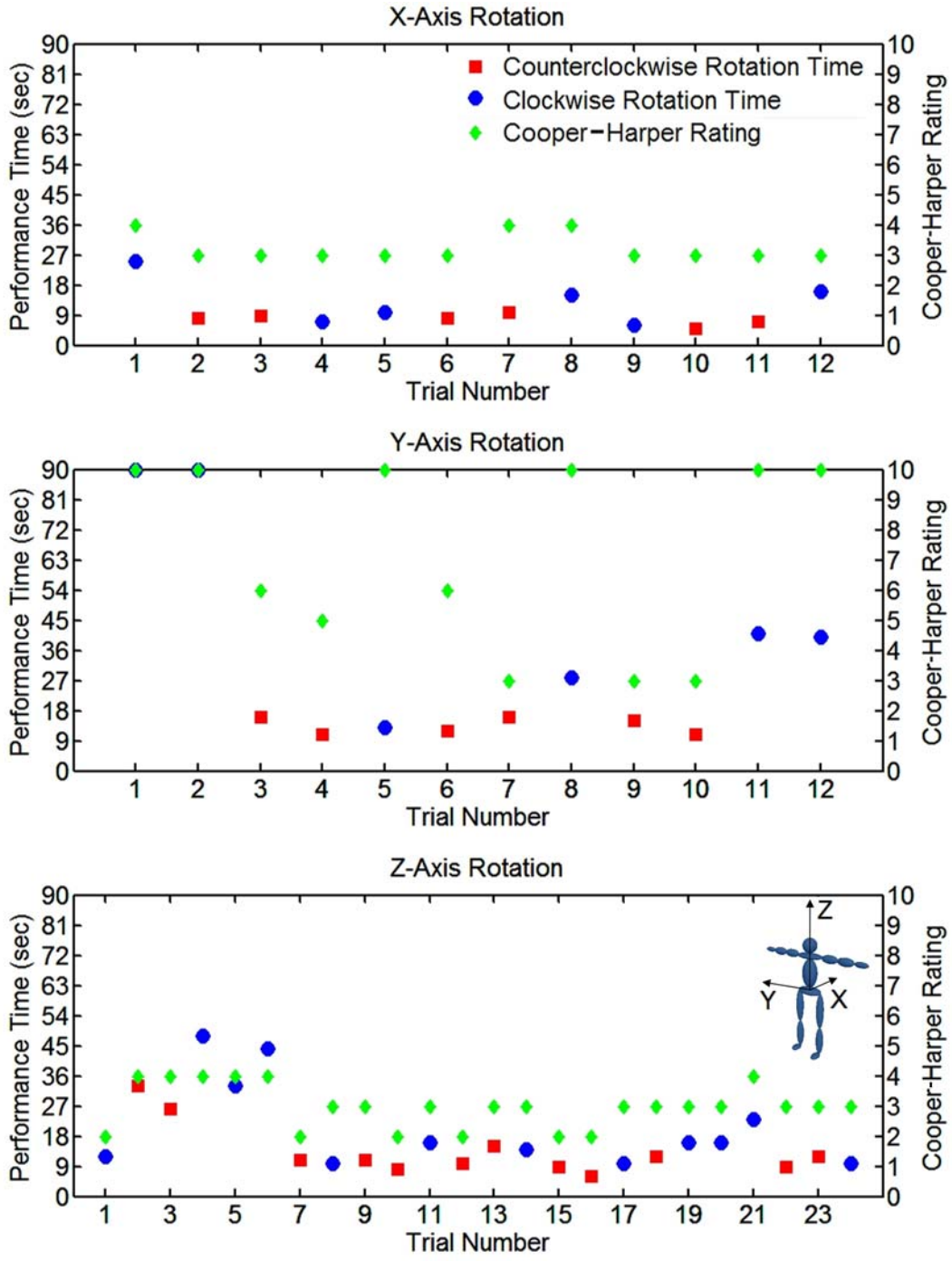

Figure E-18: Performance times and modified Cooper-Harper rating for Subject 18.

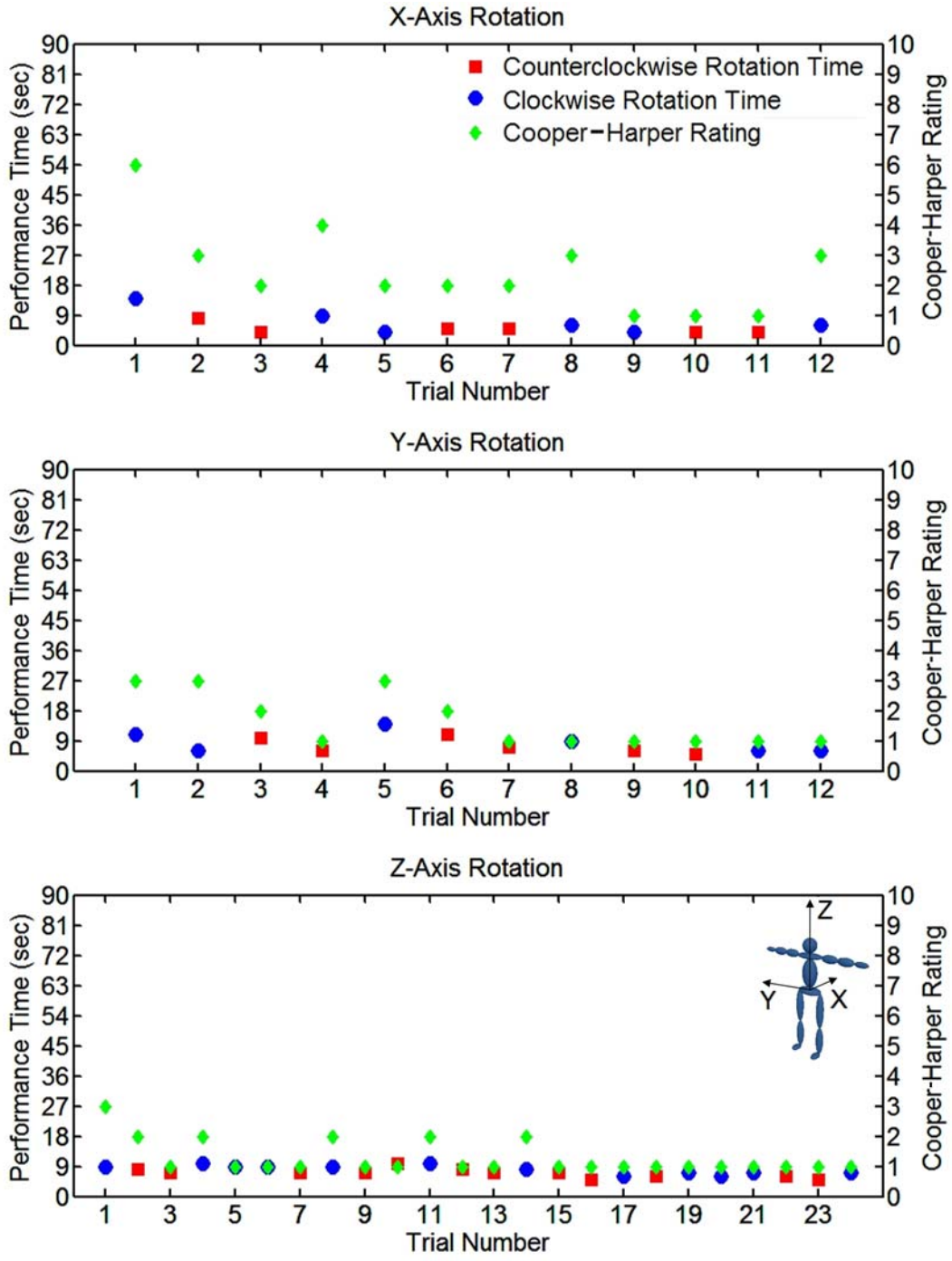

Figure E-19: Performance times and modified Cooper-Harper rating for Subject 19.

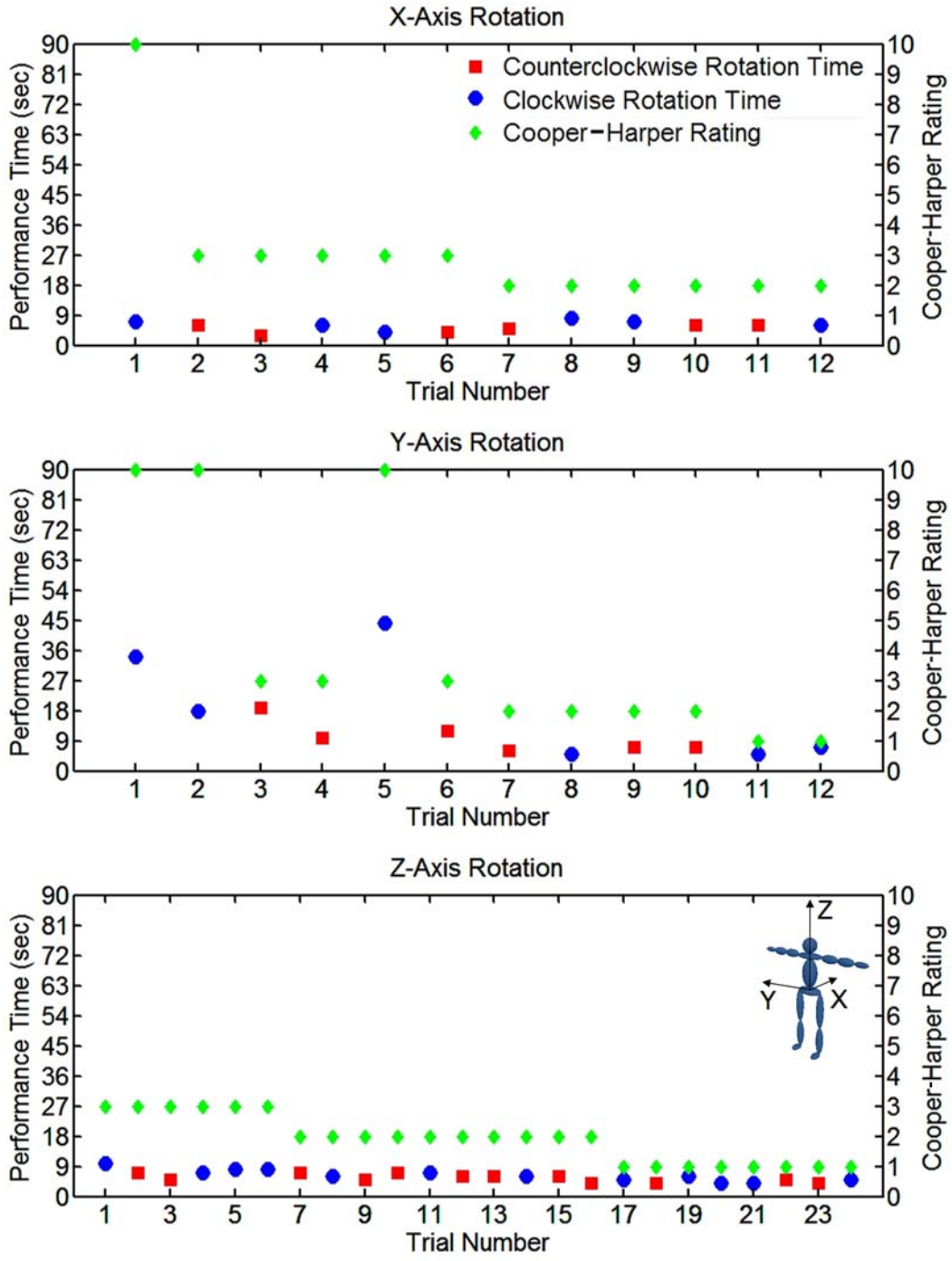

Figure E-20: Performance times and modified Cooper-Harper rating for Subject 20.

Bibliography

[1] SIMM 4.0: Software for interactive musculoskeletal modeling user's manual. June, 2004.

[2] Man-systems integration standards. NASA-STD-3000, 1995.

[3] NASA extravehicular mobility unit (EMU) LSS/SSA data book, rev. D. Hamilton Standard, a United Technologies Company, 1997.

[4] Constellation program human-system integration requirements. NASA Document No. CxP 70024, 2006.

[5] I. Abramov, A. Stoklitsky, A. Barer, and S. Filipenkov. Essential aspects of space suit operating pressure trade-off. In Proceedings of the International Conference on Environmental Systems, Society of Automotive Engineers, 1994.

[6] A. Amir and D. Newman. Research into the effects of astronaut motion on the spacecraft: A review. *Acta Astronautica*, 47(12):859–869, 2000.

[7] F. Anderson and M. Pandy. Dynamic optimization of human walking. *Journal of Biomechanical Engineering*, 123:381–390, 2001.

[8] A. Arsie and E. Frazzoli. Motion planning for a quantized control system on $SO(3)$. In Proceedings of the 46th Conference on Decision and Control, New Orleans, 12–14 December, 2007.

[9] H. Asada and J.-J. Slotine. *Robot Analysis and Control*. John Wiley & Sons, 1986.

[10] C. Atkeson and J. Hollerbach. Kinematic features of unrestrained vertical arm movements. *Journal of Neuroscience*, 5(9):2318–2330, 1985.

[11] P. Baerlocher and R. Boulic. *Deformable Avatars*, chapter Parametrization and Range of Motion of the Ball-and-Socket Joint, pages 180–190. Kluwer Academic Publishers, 2001.

[12] G. Baroni, G. Ferrigno, A. Anolli, G. Andreoni, and A. Pedotti. Quantitative analysis of motion control in long term μgravity. *Acta Astronautica*, 43:131–151, 1998.

[13] G. Baroni, A. Pedrocchi, G. Ferrigno, J. Massion, and A. Pedotti. Motor coordination in weightless conditions revealed by long-term microgravity adaptation. *Acta Astronautica*, 49:199–213, 2001.

[14] C. Belta, A. Bicchi, M. Egerstedt, E. Frazzoli, E. Klavins, and G. Pappas. Symbolic planning and control of robot motion. *IEEE Robotics & Automation Magazine*, 14(1):61–70, 2007.

[15] K. Bethke. The second skin approach: Skin strain field analysis and mechanical counter pressure prototyping for advanced spacesuit design. Master's thesis, Massachusetts Institute of Technology, 2005.

[16] N. Bhushan and R. Shadmehr. Computational nature of human adaptive control during learning of reaching movements in force fields. *Biological Cybernetics*, 81:39–60, 1999.

[17] A. Bicchi, A. Marigo, and B. Piccoli. On the reachability of quantized control systems. *IEEE Transactions on Automatic Control*, 47(4):546–563, 2002.

[18] E. Bizzi, V. Cheung, A. d'Avella, P. Saltiel, and M. Tresch. Combining modules for movement. *Brain Research Reviews*, 57:125–133, 2008.

[19] E. Bizzi and F. Mussa-Ivaldi. Neural basis of motor control and its cognitive implications. *Trends in Cognitive Sciences*, 2(3):97–102, 1998.

[20] A. Bloch, P. Krishnaprasad, J. Marsden, and R. Murray. Nonholonomic mechanical systems with symmetry. *Archive for Rational Mechanics and Analysis*, 136(1):21–99, 1996.

[21] O. Bock, S. Abeele, and U. Eversheim. Sensorimotor performance and computational demand during short-term exposure to microgravity. *Aviation, Space, and Environmental Medicine*, 74(12):1256–1262, 2003.

[22] O. Bock, I. Howard, K. Money, and K. Arnold. Accuracy of aimed arm movements in changed gravity. *Aviation, Space, and Environmental Medicine*, 63:994–998, 1992.

[23] D. Boone and S. Azen. Normal range of motion of joints in male subjects. *Journal of Bone and Joint Surgery*, 61:756–759, 1979.

[24] A. Brody, R. Jacoby, and S. Ellis. Extravehicular activity self-rescue using a hand-held thruster. *Journal of Spacecraft and Rockets*, 29(6):842–848, 1992.

[25] H. Cheng, L. Obergefell, and A. Rizer. Generator of body data (GEBOD) manual. AL/CF-TR-1994-0051, Human Systems Center, Wright-Patterson Air Force Base, Ohio, 1994.

[26] C. Clauser, P. Tucker, J. McConville, E. Churchill, L. Laubach, and J. Reardon. Anthropometry of air force women. AMRL-TR-70-5, Aerospace Medical Research Laboratory, Wright-Patterson Air Force Base, Ohio, 1972.

[27] F. Coffield, D. Moseley, E. Hall, and K. Ecclestone. *Learning Styles and Pedagogy in Post-16 Learners: A Systematic and Critical Review.* Learning and Skills Research Center, 2004.

[28] G. Cooper and R. Harper. The use of pilot rating in the evaluation of aircraft handling qualities. NASA TN D-5153, April 1969.

[29] S. Delp. *Surgery Simulation: A Computer Graphics System to Analyze and Design Musculoskeletal Reconstructions of the Lower Limb*. PhD thesis, Stanford University, 2000.

[30] D. DelVecchio, R. Murray, and P. Perona. Decomposition of human motion into dynamics-based primitives with application to drawing tasks. *Automatica*, 39(12):2085–2098, 2003.

[31] L. DiPietro, N. Hogan, H. Krebs, and B. Volpe. Submovements underlie voluntary human arm movements: evidence from emg. In Proceedings of the Annual Meeting of the Society of Neuroscience, 2005.

[32] E. Drumwright, O. Jenkins, and M. Matarić. Exemplar-based primitives for humanoid movement classification and control. Proceedings of the International Conference on Robotics and Automation, New Orleans, LA, 2004.

[33] P. Ferguson. *Quantifying and Modeling Adaptive Astronaut Movement: Motion Strategies for Long-Duration Spaceflight Missions*. PhD thesis, Massachusetts Institute of Technology, 2006.

[34] J. Fisk, J. Lackner, and P. DiZio. Gravitoinertial force level influences arm movement control. *Journal of Neurophysiology*, 69(2):504–511, 1993.

[35] T. Flash. The control of hand equilibrium trajectories in multi-joint arm movements. *Biological Cybernetics*, 57:257–274, 1987.

[36] T. Flash and N. Hogan. The coordination of arm movements: An experimentally confirmed mathematical model. *Journal of Neuroscience*, 5(7):1688–1703, 1985.

[37] E. Fleishman and M. Quaintance. *Taxonomies of Human Performance: The Description of Human Tasks*. Academic Press, Inc., 1984.

[38] D. Franklin, R. Osu, E. Burdet, M. Kawato, and T. Millner. Adaptation to stable and unstable dynamics achieved by combined impedance control and inverse dynamics model. *Journal of Neurophysiology*, 90:3270–3282, 2003.

[39] A. Frazer. Modeling human-spacesuit interactions. Master's thesis, Massachusetts Institute of Technology, 2003.

[40] E. Frazzoli, M. Dahleh, and E. Feron. Maneuver-based motion planning for nonlinear systems with symmetries. *IEEE Transactions on Robotics*, 21(6):1077–1091, December 2005.

[41] C. Frohlich. The physics of somersaulting and twisting. *Scientific American*, 242(3):154–164, 1980.

[42] M. Gernhardt. Private Communications with the EVA Physiology, Systems, & Performance (EPSP) Project, 2007.

[43] P. Gill, W. Murray, and M. Wright. *Practical Optimization*. Academic Press, 1986.

[44] S. Gottschalk. *Collision Queries Using Oriented Bounding Boxes*. PhD thesis, University of North Carolina, Chapel Hill, 2000.

[45] H. Grunhofer and G. Kroh. A review of anthropometric data on german air force and united states air force flying personnel 1967–1968. AGARD-AG-205 (AD A010 674), Advisory Group for Aerospace Research and Development, Neuilly Sur Seine, France, 1975.

[46] B. Hall. *Lie Groups, Lie Algebras, and Representations: An Elementary Introduction*. Springer-Verlag, 2003.

[47] M. Hardt. *Multibody Dynamical Algorithms, Numerical Optical Control, with Detailed Studies in the Control of Jet Engine Compressors and Biped Walking*. PhD thesis, University of California, San Diego, 1999.

[48] G. Harris. *The Origins and Technology of the Advanced Extravehicular Space Suit*. American Astronautical Society, 2001.

[49] S. Hart and L. Staveland. *Development of NASA-TLX (Task Load Index): Results of Empirical and Theoretical Research*, pages 239–250. Human Mental Workload. North Holland Press, Amsterdam, 1988.

[50] A. Hofmann. *Robust Execution of Bipedal Walking Tasks from Biomechanical Principles*. PhD thesis, Massachusetts Institute of Technology, Cambridge, 2006.

[51] N. Hogan. An organizing principle for a class of voluntary movements. *Journal of Neuroscience*, 4(11):2745–2754, 1984.

[52] K. Holzbaur, W. Murray, and S. Delp. A model of the upper extremity for simulating musculoskeletal surgery and analyzing neuromuscular control. *Annals of Biomedical Engineering*, 33(6):829–840, June 2005.

[53] N. Hussain and T. Kane. Optimal detumbling of multibody systems. *Advances in the Astronautical Sciences*, 82:1329–1343, 1993.

[54] N. Hussain and T. Kane. Three-dimensional reorientation of a system of interconnected rigid bodies. *Journal of the Astronautical Sciences*, 42(1):1–25, 1994.

[55] D. Judnick, D. Newman, and J. Hoffman. Modeling and testing of a mechanical counterpressure bio-suit system. In Proceedings of the International Conference on Environmental Systems, Chicago, IL, 2007.

[56] T. Kane. Self-rotation of astronauts by means of limb movements. Transactions of the Second National Conference on Space Maintenance and Extra Vehicular Activities, 1968.

[57] T. Kane and D. Levinson. Multibody dynamics. *The Journal of Applied Mechanics*, 50:1071–1078, 1983.

[58] T. Kane and D. Levinson. The use of Kane's dynamical equations in robotics. *The International Journal of Robotics Research*, 2(3):3–21, 1983.

[59] O. Khatib, L. Sentis, J. Park, and J. Warren. Whole-body dynamic behavior and control of human-like robots. *International Journal of Humanoid Robotics*, 1(1):29–43, 2004.

[60] O. Khatib, J. Warren, V. de Sapio, and L. Sentis. Human-like motion from physiologically-based potential energies. In J. Lenarcic and C. Galletti, editors, *On Advances in Robot Kinematics*, pages 167–178. Kluwer Academic Publishers, 2004.

[61] I. Kingma, H. Toussaint, D. Commissaris, and G. Savelsbergh. Adaptation of center of mass control under microgravity in a whole-body lifting task. *Experimental Brain Research*, 125:35–42, 1999.

[62] G. Klute. Pilot investigation: Nominal crew induced forces in zero-g. SAE Technical Paper 921155, 1992.

[63] H. Krebs, N. Hogan, M. Aisen, and B. Volpe. Quantization of continuous arm movements in humans with brain injury. *Proceedings of the National Academy of Sciences*, 96:4645–4649, 1999.

[64] P. Kulwicki, E. Schlei, and P. Vergamini. Weightless man: Self-rotation techniques. Technical Documentary Report No. AMRL-TDR-62-129, 1962.

[65] S. Kumar. Isolated planar trunk strengths measurement in normals: Part iii—results and database. *International Journal of Industrial Ergonomics*, 17:103–111, 1996.

[66] J. Lackner and P. DiZio. Human orientation and movement control in weightless and artificial gravity environments. *Experimental Brain Research*, 130:2–26, 2000.

[67] F. Lacquaniti, J. Soechting, and C. Terzuolo. Some factors pertinent to the organization and control of arm movements. *Brain Research*, 252(2):394–397, 1982.

[68] K. Liu, A. Hertzman, and Z. Popovič. Learning physics-based motion style with nonlinear inverse optimization. In Proceedings of SIGGRAPH, 2005.

[69] K. Liu and Z. Popovič. Synthesis of complex dynamic character motion from simple animations. In Proceedings of SIGGRAPH, 2002.

[70] R. Longman, J. Li, M. Steinbach, and H. Bock. Issues in the implementation of time-optimal robot path planning. 35th AIAA Aerospace Sciences Meeting & Exhibit, Reno, NV, 6–9 Jan., 1997.

[71] J. Luh, M. Walker, and R. Paul. On-line computational scheme for mechanical manipulators. *A.S.M.E. Journal of Dynamic Systems, Measurement, and Control*, 102, 1980.

[72] D. Manzey, B. Lorenz, A. Schiewe, G. Finell, and G. Theile. Behavioral aspects of human adaptation to space: Analyses of cognitive and psychomotor performance in space during an 8-day space mission. *Clinical Investigator*, 71:725–731, 1993.

[73] J. Massion. Movement, posture, and equilibrium: Interaction and coordination. *Progress in Neurobiology*, 38:35–56, 1992.

[74] J. Massion, K. Popov, J. Fabre, and P. Rage. Is the erect posture in microgravity based on the control of trunk orientation or center of mass position. *Experimental Brain Research*, 114:384–389, 1997.

[75] J. McConville, T. Churchill, I. Kaleps, C. Clauser, and J. Cuzzi. Anthropometric relationships of body and body segment moment of inertia. AMRL-TR-80-119 (AD A097 238), Aerospace Medical Research Laboratory, Wright-Patterson Air Force Base, Ohio, 1980.

[76] M. Millard, J. McPhee, and E. Kubica. Multi-step forward dynamic gait simulation. Proceedings of the ECCOMAS Thematic Conference, Multibody Dynamics 2007, Milan, Italy, 25–28 June, 2007.

[77] F. Mussa-Ivaldi and S. Solla. Neural primitives for motion control. *IEEE Journal of Oceanic Engineering*, 29(3):640–650, 2004.

[78] D. Newman, A. Amir, and S. Beck. Astronaut-induced disturbances to the microgravity environment of the *Mir* space station. *Journal of Spacecraft and Rockets*, 38(4):578–583, 2001.

[79] D. Newman, S. Beck, A. Amir, G. Baroni, G. Ferrigno, and A. Pedotti. Measuring astronaut performance in microgravity: Loads and modeling. In Proceedings of the First Biennial Space Biomedical Investigators Workshop, League City, TX, January 1999.

[80] D. Newman, M. Tryfonidis, and M. van Schoor. Astronaut-induced disturbances in microgravity. *Journal of Spacecraft and Rockets*, 34:252–254, 1997.

[81] K. Novak, L. Miller, and J. Houk. The use of overlapping submovements in the control of rapid hand movements. *Experimental Brain Research*, 144:351–364, 2002.

[82] K. Ohta, M. Svinin, Z. Luo, S. Hosoe, and R. Laboissière. Optimal trajectory formation of constrained human arm reaching movements. *Biological Cybernetics*, 91:23–36, 2004.

[83] R. Osu, N. Kamimura, H. Iwasaki, E. Nakano, C. Harris, Y. Wada, and M. Kawato. Optimal impedance control for task achievement in the presence of signal-dependent noise. *Journal of Neurophysiology*, 92:1199–1215, 2004.

[84] E. Papadopoulos. *On the Dynamics and Control of Space Manipulators*. PhD thesis, Massachusetts Institute of Technology, 1990.

[85] P. Papalambros and D. Wilde. *Principles of Optimal Design: Modeling and Computation, 2nd Ed.* Cambridge University Press, 2000.

[86] C. Papaxanthis, T. Pozzo, and J. McIntyre. Kinematic and dynamic processes for the control of pointing movements in humans revealed by short-term exposure to microgravity. *Neuroscience*, 135:371–383, 2005.

[87] C. Papaxanthis, T. Pozzo, K. Popov, and J. McIntyre. Hand trajectories of vertical arm movements in one-g and zero-g environments. *Experimental Brain Research*, 120:496–502, 1998.

[88] C. Papaxanthis, T. Pozzo, K. Popov, and M. Schieppati. Trajectories of arm pointing movements on the sagittal plane vary with both direction and speed. *Experimental Brain Research*, 148:498–503, 2003.

[89] V. Parin and O. Gazenko. Weightlessness (medical and biological research). NASA TT F-16105, translation of "Nevesmost (Mediko-Biologicheskiye Issledovaniye)," Moscow, Meditsina Press, 1975.

[90] J. Patron, P. Stapley, and T. Pozzo. Human whole-body reaching in normal gravity and microgravity reveals a strong temporal coordination between postural and focal task components. *Experimental Brain Research*, 165:84–96, 2005.

[91] R. Playter. *Passive Dynamics in the Control of Gymnastic Maneuvers*. PhD thesis, Massachusetts Institute of Technology, 1994.

[92] J. Rasmussen, V. Vondrak, M. Damsgaard, M. deZee, and S. Christensen. The AnyBody project—Computer analysis of the human body. In Proceedings of Computer Analysis of the Human Body, Biomechanics of Man, 13–15 November, 2002.

[93] S. Redon. Continuous collision detection for rigid and articulated bodies. SIGGRAPH 2004 course notes, 2004.

[94] G. Schaffner. Private Communications with the NASA Anthropometry and Biomechanics Facility, 2007.

[95] M. Scher and T. Kane. Pitch and yaw motions of a human being in free fall. NASA-CR-97902, 1968.

[96] P. Schmidt. *An Investigation of Space Suit Mobility with Applications to EVA Operation*. PhD thesis, Massachusetts Institute of Technology, 2001.

[97] H. Schmitt and D. Reid. Anecdotal information on space adaptation syndrome. Space Adaptation Syndrome Drug Workshop, National Space Biomedical Research Institute, 1985.

[98] L. Sentis and O. Khatib. Control of free-floating humanoid robots through task prioritization. In Proceedings of the IEEE International Conference on Robotics and Automation, Barcelona, Spain, 2005.

[99] R. Shadmehr and F. Mussa-Ivaldi. Adaptive representation of dynamics during learning of a motor task. *Journal of Neuroscience*, 14(5):3208–3224, 1994.

[100] K. Shoemake. Animating rotation with quaternion curves. *SIGGRAPH*, 19(3):245–254, 1985.

[101] N. Stubbs, J. Fernandex, and W. Glenn. Normative data on joint ranges of motion of 25- to 54-year-old males. *International Journal of Industrial Ergonomics*, 12:265–272, 1993.

[102] A. Sulejmanpašič and J. Popovič. Adaptation of performed ballistic motion. *ACM Transactions on Graphics*, 24(1):165–179, 2005.

[103] M. Tagliabue, A. Pedrocchi, G. Baroni, A. Pedotti, and G. Ferrigno. Evaluation of theories of complex movement planning in different levels of gravity. *Acta Astronautica*, 56:900–910, 2005.

[104] P. Tsang and M. Vidulich. *Principles and Practice of Aviation Psychology*. Lawrence Erlbaum Associates, Mahwah, NJ, 2003.

[105] G. Walsh and S. Sastry. On reorienting linked rigid bodies using internal motions. *IEEE Transactions on Robotics and Automation*, 11(1):139–146, 1995.

[106] R. Woodworth. The accuracy of voluntary movement. *Psychological Review*, 3:350–359, 1899.

[107] M. Yeadon. The simulation of aerial movement—ii. a mathematical inertia model of the human body. *Journal of Biomechanics*, 23(1):67–74, 1990.

[108] J. Young, R. Chandler, C. Snow, K. Robinette, G. Zehner, and M. Lofberg. Anthropometric and mass distribution characteristics of the adult female. FAA-AM-83-16, Civil Aeromedical Institute, Federal Aviation Administration, Oklahoma City, Oklahoma, 1983.

[109] J. Zhao, M. Diehl, R. Longman, H. Bock, and J. Schlöder. Nonlinear model predictive control of robots using real-time optimization. AIAA/AAS Astrodynamics Specialist Conference and Exhibit, Providence, RI, Aug. 16–19, 2004.

[110] J. Zhao, R. Longman, H. Bock, and M. Diehl. Inverse dynamics approach to real time optimal control of robots. *Advances in the Astronautical Sciences*, 120:1023–1042, 2005.